NTNU
Innovation and Creativity

Multimodal Volume to Volume Registration between Ultrasound and MRI

Tommy Ryen

Master of Science in Computer Science
Submission date: June 2006
Supervisor: Richard E. Blake, IDI
Co-supervisor: Frank Lindseth, SINTEF

Norwegian University of Science and Technology
Department of Computer and Information Science

Problem Description

The use of medical images for diagnostics, treatment planning and surgical guidance is constantly increasing. A wide range of 3D imaging modalities is now available, e.g. Ultrasound, MRI, CT, PET and SPECT. Often, two or more imaging modalities are used to acquire volume data from the same object or scene. In order to better be able to compare all the information contained in such image volumes they have to be brought into spatial correspondence with each other. That way both similarities and differences can be detected. Differences can be caused by several factors, including varying characteristics of the imaging modalities used and spatial differences because of tissue growth, aneurisms and movements. The process of finding this spatial correspondence between two images is known as registration, and can be performed iteratively, transforming one image, while keeping the other image in a fixed position. A similarity measure is used to measure the spatial correspondence between the images, and will change from iteration to iteration. An optimizer will also have to be employed in order to guide the transformations in the direction of greatest similarity. The process halts when the optimizer is unable to find a transformation that increases the similarity measure any more.

The student will in this project develop a software module that makes it possible to register preoperative MRI data to intraoperative 3D ultrasound images. This module will be integrated with CustusX, a software system for image guided surgery developed at SINTEF. In order to optimize the spatial correspondence between them, various similarity measures and optimization schemes will be investigated as well. The registration procedure should be fully automated, i.e. not employ carefully selected marker points in the images. However, a manual translation into a good starting position may be acceptable. Finally, to ensure a stabile and reliable system the registration module will have to be tested thoroughly and the results obtained from the module must be validated.

Assignment given: 20. January 2006
Supervisor: Richard E. Blake, IDI

Abstract

This master-thesis considers implementation of automated multimodal volume-to-volume registration of images, in order to provide neurosurgeons with valuable information for planning and intraoperative guidance. Focus has been on medical images from magnetic resonance (MR) and ultrasound (US) for use in surgical guidance. Prototype implementations for MRI-to-US registration have been proposed, and tested, using registration methods available in the Insight Toolkit (ITK). Mattes' Mutual Information has been the similarity metric, based on angio-graphic volumes that have not been preprocessed from both modalities. Only rigid transformations have been studied, and both types of Gradient Descent and Evolutionary optimizers have been examined.

The applications have been tested on clinical data from relevant surgical operations. The best results were obtained using an evolutional (1+1) optimizer for translational transformations only. This application was both fast and accurate. The other applications, using types of Gradient Descent optimizers, has proved to be significantly slower, inaccurate and more difficult to parameterize.

It has been experienced that registration of angio-graphic volumes are easier to accomplish than registration of volumes of other weightings, due to their more similar characteristics. Angio-graphic images are also readily evaluated using volume renderings, but other methods should be constructed to provide a less subjective measure of success for the registration procedures.

The obtained results indicate that automatic volume-to-volume registration of angio-graphic images from MRI and US, using Mattes' Mutual Information and an Evolutionary Optimizer, should be feasible for the neuronavigational system considered here, with sufficient accuracy. Further development include parameter-tuning of the applications, to possibly achieve increased accuracy. Additionally, a non-rigid registration application should be developed, to account for local deformations during surgery. Development of additional tools for performing accurate validation of registration results should be developed as well.

Preface

This report is part of the master thesis of the course of *Master of Science of Computer Science (Sivilingeniør i Datateknikk)* at the Norwegian University of Science and Technology (Norges Teknisk Naturvitenskaplige Universitet, NTNU).

The overall goal of the project is to propose suitable methods for, and implement a fully set of fully automated volume-to-volume registration algorithms for use in neurosurgical guidance. The registration methods should enable registration of different preoperative MRI volumes with various intraoperative ultrasound volumes. Focus will be on implementation and evaluation of different methods for solving this problem. Erik Harg, a former master student, did a similar study last year. I will both try to enhance his methods, as well as proposing other possible approaches.

The work with this report has been done both at NTNU and SINTEF Health Research, department of Medical technology (MedTech). I would like to thank Richard Blake at IDI, NTNU, for presenting me to the MedTech group at SINTEF. I would like to thank my supervisor Frank Lindseth at SINTEF for guiding my work. I would also like to thank Erik Harg for giving me valuable comments and supplying me with necessary sources for reading. Last, but not least, I would like to thank my parents and brothers for always being there for me and supporting me.

Contents

List of Figures

List of Tables

Part I

Introduction

The work in this thesis builds upon the work done last semester in the course TDT 4725, Image Processing - Depth study, where I studied the current state-of-the-art in volume-to-volume registration. The emphasis for that thesis was on useful concepts and methods in multimodal registration of medical images used both for planning and during neurosurgery.

In the first part I will at first describe the overall goal of the project. In chapters 2 to 4 I sum up the main findings from my survey on the current state of the art in medical imaging registration. This will also lead to an outline of the rest of the work in this project. This part is not meant as a complete survey, merely a short introduction to the key issues in the field. For a more thorough presentation of the field of medical image registration, please see my in-depth-study report (available from SINTEF Med Tech), or the literature listed in the *References section*. This part will also present the methods that, in my in-depth-study, was found suitable for solving the problem definition, which will be presented shortly.

1 Problem Definition

Before a typical neurosurgical operation, MRI volumes of the patient's head are acquired in different *modes*. Different modes of MRI emphasize different aspects of the physiological and anatomical nature of the patient, in order to reveal as much information as possible. These images have to be combined mentally by the neurosurgeon in the process of planning an optimal surgical procedure. The most significant MRI data set is selected as a *master*, and used as a basis for subsequent surgical guidance.

During surgery, but before the *dura mater*[1] is opened, a free-hand US scan of the brain is performed, and the scan is resampled and compounded into a 3D image data set. This procedure is repeated after opening the dura, and may be performed several times during surgery, generating a series of 3D data sets. These data sets contain updated information on the structures of the brain, in the areas reached by the US scan, which may help the neurosurgeon in monitoring and optimizing the surgical procedure.

In order to provide the neurosurgeon with as much information as possible in planning the surgical operation, the different preoperative MRI volumes should be registered, resulting in multi-informational MRI volumes. When the planning is finished, and the surgical procedure starts, it is still advantageous to extract information from several sources. In order to combine the information from the preoperative master MRI volume with the subsequent intraoperative US volume, a registration procedure of the volumes should be performed. The resulting volume from this procedure is a pseudo-MRI volume, incorporating information of spatial deformations observed from the US volumes. The registration procedure for the preoperative MRI volumes and the registration procedure for the master MRI volume (or pseudo MRI volume later on) with the subsequent US volumes, may differ substantially, as there usually is no good single algorithm for all registration problems. Note that the registration of the subsequent US volumes may or may not be a multimodal registration step, according to whether the US volume is registered directly to the pseudo MRI volume or to the preceding US volume, respectively. If the latter is the case, the resulting transformation of the registration process should be applied to the MRI volume later on as well.

The overall goal of this project is to propose, and implement, a set of fully automated volume-to-volume registration algorithms that will perform step number two (2) of the following registration system: 1)Registration of different preoperative MRI volumes, 2)registration of a selected preoperative master MRI volume to the initial US volume, and 3)registration of each of the subsequent US volumes with the pseudo MRI volume, which may include registration of the last obtained US volume to the preceding US volume.

The last step, or the last two, should enable a set of subsequent warpings to the master MRI volume. Harg had the exact same problem definition for his assignment last year. I therefore adopt his easily understood schematic description of the registration steps in Figure 1 [8][9].

[1] A tough membrane surrounding and protecting the brain.

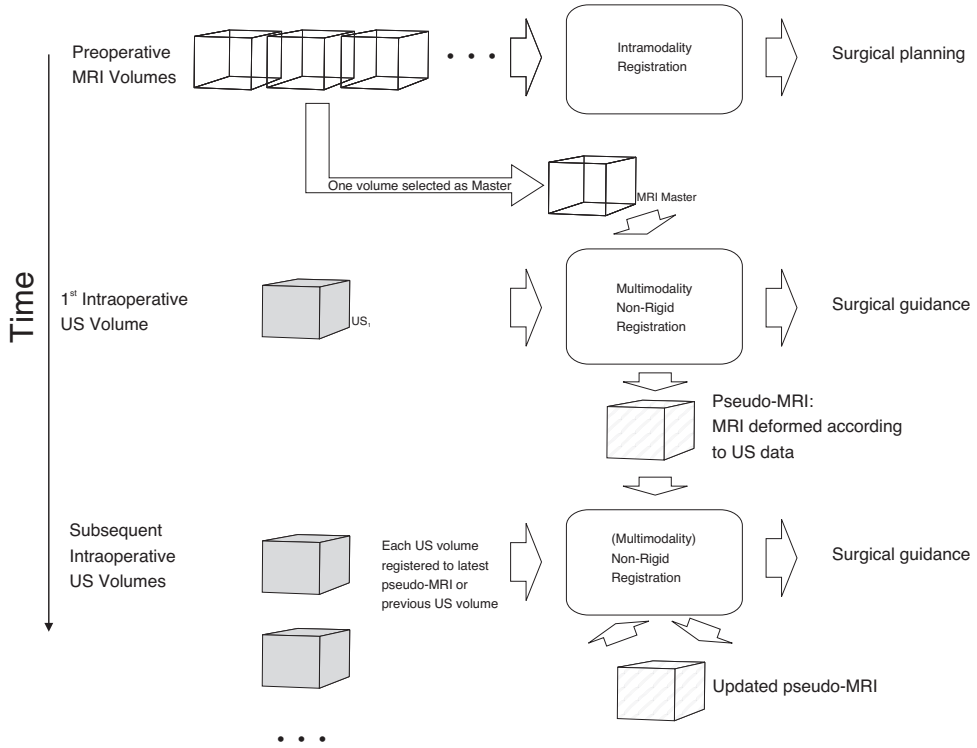

Figure 1: **Schematic representation of the registration process. Images are firstly acquired, then they are registered according to the problem definition. In the end the surgeon utilizes the images for planning and surgical guidance.** (Figure adapted from [8][9].)

2 Background

This chapter starts out, presenting the history and development of the field of registration, before a more thorough description of the registration system defined in chapter 1 is given in chapter 2.2. This chapter will briefly discuss the three separate steps of the registration system, as well as point out the main differences of the two imaging-modalities that should be registered.

2.1 The Field of Registration

The last decades have seen remarkable development in medical imaging technology. Numerous imaging modalities are currently available, and images obtained from these provide useful information in planning and guidance of surgical procedures. Utilization of medical images has opened up new areas of applications, and new methods are continuously developed. Especially in neurosurgery, accurate and up-to-date information is critical, so methods for extracting important information from multiple images, combining this information, and finally presenting the results to the surgeon is of significant importance.

Huge investments within universities and industry have been made in order to invent and develop the technology needed to acquire images from multiple imaging modalities. The use of medical images in healthcare is constantly increasing, and a wide range of imaging modalities is now available, including CT, MRI, US, PET and SPECT. A substantial amount of computing is needed in order to present the images in preferable ways for diagnosis, treatment planning and surgical guidance. After processing the images from raw signals to 2D or 3D images, a variety of enhancement and processing techniques can be applied to the images to emphasize and present useful information to doctors and specialists. This includes segmentation of special tissues of interest, such as cancerous tissues and aneurisms[2], and presenting them to an interpreter for analysis. Sometimes however, we have two images of the same scene and want to find a spatial correspondence of them. This will give us most information out of both images, detecting both similarities and differences. Differences can be caused by several factors, including varying characteristics of different imaging modalities and spatial differences because of tissue growth and movement. The process of finding this spatial correspondence between two images is known as *registration*.

For diagnosis and preoperative planning it has been common to use a high resolution imaging modality, such as X-ray computed tomography (CT) or magnetic resonance imaging (MRI). This way the surgeon gets a good view and understanding of the internal structures and anatomy, enabling him or her to find the best possible approach for a given surgical procedure. This reduces the possibility of failure during operation which can be fatal for the patient [12]. *Preoperative* image volumes can also be used during surgery. By aligning an image to the patient in physical space, surgical tools can be overlaid to the image using stereotactic systems employing tracker tools. This way, the surgical tools can be positioned relative to the image volume within a navigation system, giving the surgeon a 3D quasi-real-time view of the operation [2]. As indicated, this is a truth with modifications, as the preoperative image does not provide information of the actual spatial relationship of the tissues. During neurosurgical intervention, the brain tissues will shift and warp with respect to the skull, mainly due to tumor resection, cerebrospinal fluid drainage, hemorrhage or even the use of diuretics [27] [24] [22]. The use of stereotactic systems based on preoperative images certainly enable previously inhibiting procedures [34], but the

[2]Swelling or ballooning of a blood vessel

real-time feeling can as indicated be quite misleading. Because of the inaccuracy of utilization of preoperative images for surgical guidance, the need for more updated imagery arises.

Updated images can be obtained using some sort of *intraoperative* imaging modality, and both CT [21], MRI [22] and Ultrasound (US) [7] [18] has been proposed. The two former provide the best image quality, but sadly, they suffer from the biggest drawbacks as well. Intraoperative use of CT will expose both the patient, but especially the clinical personnel, for large doses of radiation, possibly causing serious illness on a long-term basis. MRI however does not suffer from this drawback, but will on the other hand involve large investments as specially equipped operating rooms would be necessary. These rooms would require a sterile draped magnet, in which the surgeon could perform operations. Also the cost of running such an operation room would be significant [7] [17]. Expectations regarding MRI-based neuronavigation systems are significant, but such a system will not be common and widespread until prices become more reasonable. US has not been dedicated much attention until recently, probably owing to a historical common perception of limited image quality. The SonoWand system developed by Gronningsaeter et al. [7] [14] is a notable exception, as it uses US data *directly*, as opposed to updating an image with better resolution, for surgical guidance.

US has also been used for surgical guidance *indirectly*, updating a preoperative image (CT or MRI), by using its data to accommodate for brain shifts during surgery. This way both initial anatomical information and the updated structural data from the US images is incorporated in a common virtual image. This was done by Bucholz et al. [1], however, only in two dimensions (2D). Peters et al. [25][4][5][6] developed a similar 3D navigation system, but had to settle with a semi-automatic solution using manually selected homologous points in the image volumes for alignment. Their application includes real-time compounding and updating of an intraoperative US volume, subsequently registered with the preoperative MRI volume. The latter system is the most promising system in the area today, as a similar fully automatic system has not been reported. A fully automatic MRI-US system would be preferable, but requires much research still. Such a system would require what is known as a multimodal non-rigid registration procedure, which is quite complex and has many degrees of freedom, at least for MRI-US registration.

Algorithms for a complete registration procedure are needed. Successfully implemented, these algorithms will result in better utilization of the broad range of medical images available in planning and guidance of surgery today.

2.2 The Registration System

As indicated in chapter 1 the registration problem can be separated into three different parts:

1. Registration of different preoperative MRI volumes
2. Registration of a selected preoperative master MRI volume to the initial US volume
3. Registration of each of the subsequent US volumes with the pseudo MRI volume, which may include registration of the last obtained US volume to the preceding US volume.

The last two steps will produce "pseudo-MRI" volume that contains information of both the master MRI volume and subsequent US volumes. It will still have the characteristics of a MRI volume, as the most recent US volume information is extracted and used to alter the MRI volume to account for changes during surgery.

Even though the three steps are closely related to each other, they are most easily handled separately. The different MRI weightings such as T1, T2 and MR Angio have notable differences, but they are of similar resolution, visual quality and visualize nearly the same amount of information. Images of corresponding slices from two different MRI volumes can be seen in figure 2. The first step is the most straight-forward step, and was actually solved satisfactory by Harg last year [9]. For that reason, I will not present algorithms for this step in this report.

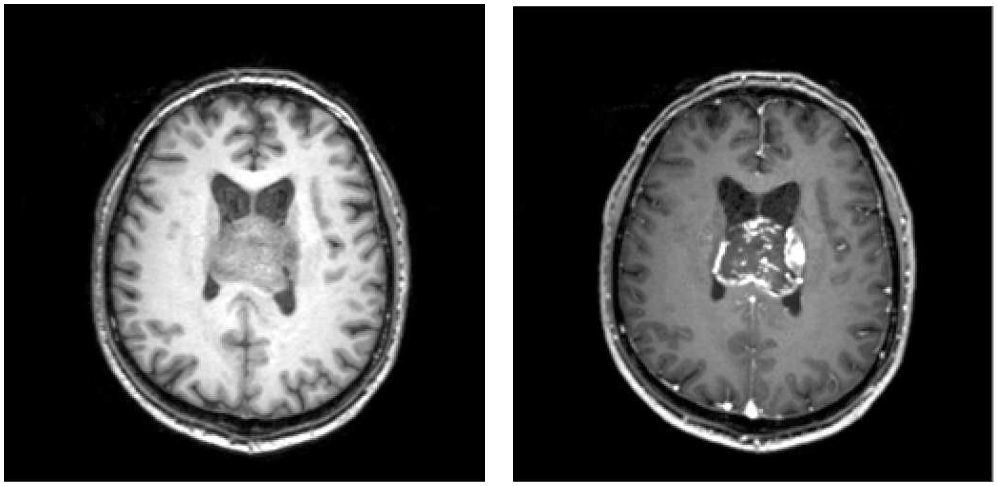

(a) Normal T1 weighted MRI. (b) T1 weighted MRI with contrast fluid.

Figure 2: **Corresponding slices from two MRI volumes of the same patient. Contrast fluid is used to highlight the tumor in the center of the image** (Courtesy of SINTEF MedTech)

Step two of the registration system is probably the most difficult step of the three. The registration of MRI and US volumes face several difficulties not present in the first step. Being a multimodal registration step, an integration of two different imaging technologies is needed. Ultrasound has a lower spatial resolution than MRI, is burdened with more noise, and has a drastically reduced field of view (figure 3). Additionally the information available in US visualize mainly tissue boundaries, whereas MRI mainly contains information about tissue types. In the case of *angio*-graphic images from the two modalities, the mentioned differences are less pronounced. Such images contain information of the walls of the blood vessels, which appear in a similar manner in both modalities. However, US Angio images still suffer from a limited field-of-view, lower signal-to-noise ratio and a lower spatial resolution. The blood vessels also appear "thicker" in the ultrasound image than in MRI, which is also a characteristic due to the image acquisition process. This can also be seen in figure 3. Step two may for the mentioned reasons be most easily solved using angio-graphic images. This assumption is also utilized in my methods later on in the report.

The result of step two is an MRI volume which is aligned with the first ultrasound volume, obtained before surgery. Step three can be performed, either by registering each subsequent US volume to the most current pseudo-MRI, like step two including a non-rigid transformation to account for local perturbations cause by surgery, or by registering each US volume to the previous one. This second method is beneficial, because the pseudo-MRI may be successively

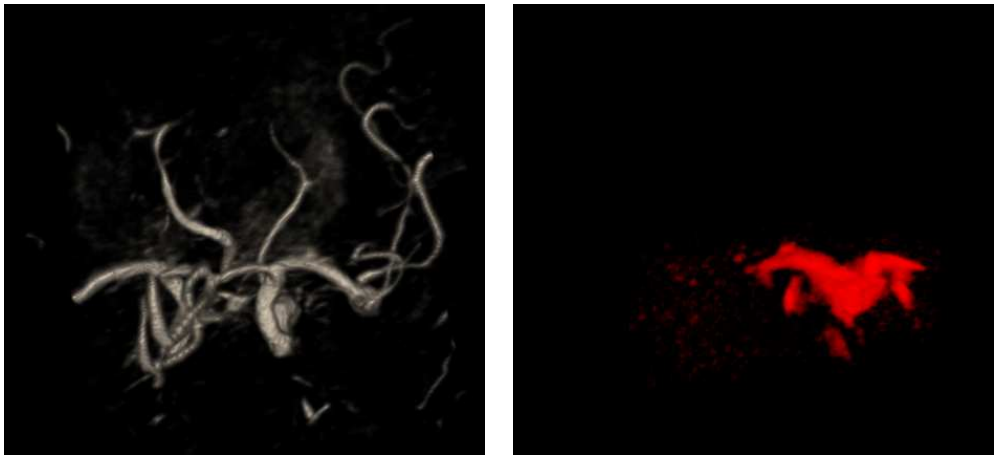

(a) MR Angio. (b) US Angio.

Figure 3: **3D renderings of angio-graphic volumes. Both the different field of view, and thickness is evident.** (Courtesy of SINTEF MedTech)

updated with the resulting transformation from the non-rigid US to US registration. This approach will also require an additional registration application for this last transformation. However, unimodal registration of US volumes is more likely to succeed than successive non-rigid multimodal registration steps.

3 Registration Components

The goal of any registration application is to find a spatial correspondence of two images; i.e. we search for a "transformation" that transforms the *moving image* as close as possible into, and with respect to, the *fixed image*. A registration application consists of several building blocks, working together to produce this transformation. I will now present a brief introduction of those crucial design choices that will have to be made: *Type of transform*, *similarity basis* and *metric*, *optimization scheme* and *interpolation method*. A schematic description of a typical registration system can be seen in figure 4.

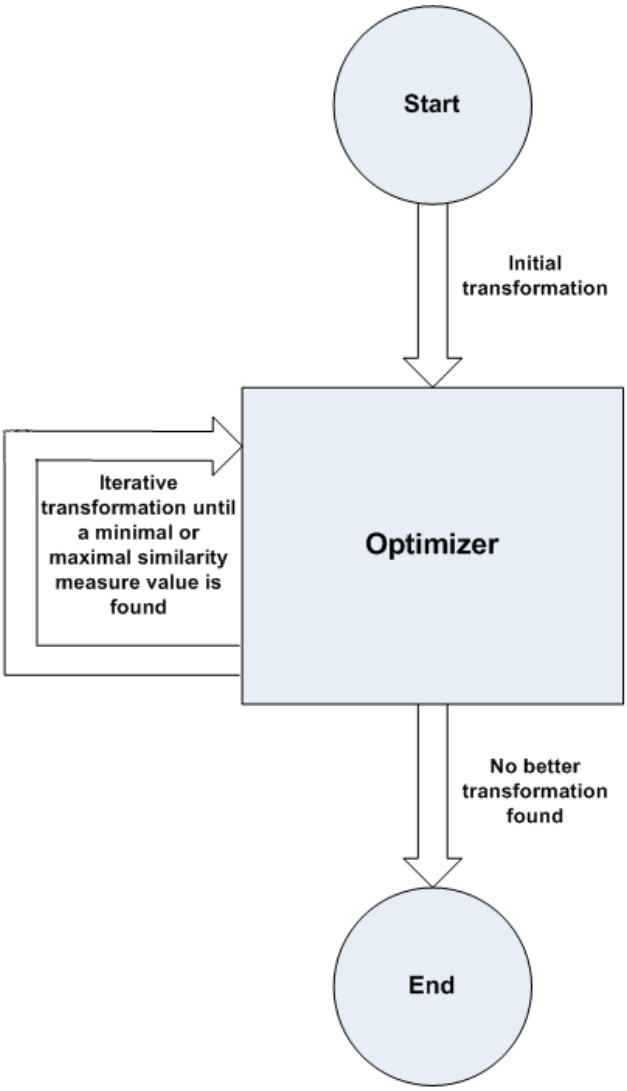

Figure 4: **Schematic description of a traditional registration procedure.**

3.1 Transform

The transformation of the moving image is a transformation using a transformation matrix. The nature of this matrix itself will therefore have significant impact on the result, and thus on how we should be searching for it. What type of matrix we want to employ depends on the application, especially on the complexity and differences of the images we want to register. The choice also depends on the desired accuracy of the application, as more degrees of freedom are needed for more accurate transformations.

The types of transformations can be divided in two broad categories: *Rigid* and Non-Rigid. For rigid transformations the same matrix is applied to all pixels in an image. This most often include translation and rotation, but can also include scaling and shear-transformations for what is known as affine transforms, and the resulting image will look very similar to the starting image.

However, if the registration process involves local deformation, we will have to employ a non-rigid transformation to find a deformation model that likely resembles the natural deformation of tissues. This generally involves a higher degree of freedom, which corresponds to the number of elements in the resulting transformation matrix, or deformation field. A higher degree of freedom implies more parameters to be found, generally making the process more time-consuming. The non-rigid registration process is also more susceptible to noise. A lessen the noise impact on the deformation field, and ensure a smooth changing transformation, dampening schemes are usually employed. A common way to smooth the deformation field is to describe it in terms of parametric cubic curves, such as B-splines or NURBS, or more precisely, their control points. Other useful non-rigid transforms include the use of mechanically, optical or elastic based models for the stretching of the deformation field.

Rigid transforms will probably perform well on registration problems where nearly no deformation on the image volumes exists. Such convenience is not always the situation in real life. Actually, most tissues are far from rigid and can deform considerably. For brain images, the skull will usually keep the tissues *in place*, but when the dura mater is opened the deformation will occur for brain images as well. The advantages of rigid transforms however, are that they are easy to understand and usually computationally inexpensive. As mentioned, non-rigid transformation models all seek to measure or compensate for a *smooth deformation* of the depicted tissues, by constraining the allowable transformation according to a predefined model.

It is not uncommon to employ an approach using both rigid and non-rigid transforms in a sequence. Rigid transforms will often be better at finding a good general alignment of the two images, using a small amount of time, and can consequently be used to align the two images globally before employing a non-rigid approach. Both classes of registration transforms will therefore be interesting in any registration problem.

3.2 Similarity Measure

In order to find the right transformation parameters, we have to have a way to measure similarity between the two images that we perform registration on. First of all we have to choose which information to measure on. The most obvious property is the voxel intensity values. Other features can be extracted from the voxel intensity values, and examples are edges and ridges of structures in the image. Voxel intensity values or features extracted from these, are denoted as

the *similarity basis*, while the choice of how to use the information is defined as the *similarity metrics*. Metrics are therefore algorithms that measure the degree of spatial correspondence of different images, with respect to the similarity basis. The performance of the metrics, and hence the choice of which metric to employ, heavily depends on the basis. A possible solution to a registration problem can be to use both voxel intensities and features together as a basis, in order to utilize as much information as possible. Segmentation can also be employed to find physical objects, such as various tissues or blood vessels, and do a registration to align the segmented parts.

Voxel intensity-based similarity measures range from plain and simple to fairly complex. Most of these measures will work best in a unimodal environment, as most of them try to map intensities on a one-to-one basis. If we want to register images from different modalities, a more intricate approach often has to be considered; imaging modalities tend to represent structures in different ways and with different intensities. Several different metrics exist, and many of them can handle unimodal registration. However, complex methods like correlation ratio (CR) and mutual information (MI), has a greater potential in multimodal registration, as they on the other hand try to find the best statistical intensity-to-intensity ratio. Also by extracting features a multimodal registration procedure is most likely to be successful, as we can try to extract information to make the basis of the two images more similar.

3.3 Optimizer

The similarity measures discussed above compute a measure of degree of spatial correspondence between two images. This measure is used as a *cost function* in an optimization procedure, in order to *minimize* or *maximize* the similarity measure of two images. An optimization algorithm is an *iterative* process taking a series of guesses on how to alter transformation parameters, starting from an initial position. Progression towards an optimal registration is then achieved by seeking transformations that decreases the cost function until the cost function converges into an optimal minimal value. For a given current estimate of the cost function the optimization algorithm then makes another estimate of the transformation, evaluates the cost function again, and continues until no transformation can be found that results in a better estimate of the cost function. The starting position however, has to be sufficiently close the optimal solution for the algorithm to converge to the optimal solution; the starting position has to be within what is known as the *capture range*. The starting position is optimally retrieved automatically, but can also be specified with simple user interaction [10] [11].

A problem for optimization algorithms is that they can converge into an incorrect solution, called a *local optimum*. An optimization procedure has as many degrees of freedom as the transformation in the registration procedure. This can be seen as a hyper- or parameter-space containing all possible values for the cost function. The dimensionality of the parameter-space can range from six dimensions for rigid body registration to hundreds or thousands for free-form deformation transformations. If we think of this parameter-space as a multi-dimensional landscape, the lowest point in a valley will correspond to a (possible local) optimal solution of the registration problem. The job for the optimizer now consists in finding the parameters for a transformation to this position. The only way of overcoming incorrect solutions is to initialize the algorithm close enough to the correct solution, thus avoiding getting stuck in a non-correct minimum[11]. Additionally, searching through the entire parameter-space is tremendously time-consuming, reinforcing the importance of a good initial estimate of the registration process [11] [3].

The categories of optimizers is parted into optimization techniques that base their choices on cost values only, and those which also incorporate cost value derivatives into computation [3] [26]. Additionally, all optimization schemes employ some sort of voxel *interpolation technique*, which will be discussed in chapter 3.4. Choosing the best optimization scheme is a somewhat *empirically* based decision; one should use what gives the best results for the current application, as different optimizers could work better than others, depending on given situations [20].

3.4 Interpolation

When the optimizer computes transformation parameters, and transforms an image accordingly, this implies some sort of interpolation of the image; the transform will rarely map the voxel locations of one grid directly onto that of the other. This will cause a *smoothening* of the image. Interpolation can also *introduce small minima* in parameter-space, hence affecting the performance of the optimizer.

The most simple interpolation algorithm is nearest neighbor interpolation (NN), which simply uses the intensity value from the voxel closest to the new position. This interpolation technique is very fast, but also very inaccurate. It also has a tendency to introduce small local minima in parameter-space, altering the conditions for subsequent optimization [26]. Trilinear interpolation (TLI) makes use of intensity values from the nearest eight voxels, linearly interpolating between the nearest two voxels in all directions, thus calculating a weighted intensity value. This interpolation technique reduces aliasing effects, hence giving smoother transitions than NN. Trilinear interpolation is considered both accurate and fast enough in most registration procedures [26] [31]. Tricubic interpolation (TCI) makes use of intensity values from as much as the 64 closest voxels, each contributing to the intensity value for the new point. The weighting for this method is controlled by a cubic polynomial function of the distance to the voxels. This interpolation technique reduces aliasing effects in an even higher degree than trilinear interpolation. Tricubic interpolation is therefore the most accurate interpolation technique, but suffers from being very slow as intensities from 64 voxels have to be considered [26]. It is also possible to use trilinear and tricubic interpolation in combination, in the way that the former is used for computing similarity measures, while the latter is used for the actual transformation of the moving image [26].

A possible way of overcoming the smoothening of the image and introduction of artifacts caused by interpolation is a hierarchical approach. The images are therefore subsampled to a pyramid-set of images before the procedure starts. The process then starts by performing a registration on the images at the lowest resolution. The transformation solution obtained at this resolution, is then used as the starting estimate for registration at the next higher resolution. [32] This step is repeated until we reach the highest resolution. This approach is currently considered standard in medical image registration [11] [15]. Example images for a multi-resolution approach can be seen in Figure 5.

Choosing the best interpolation method remains, however, a balancing act between computational cost and correctness. The choice of interpolation technique should be considered thoroughly, in order to avoid perturbing the parameter-space while doing so within reasonable time.

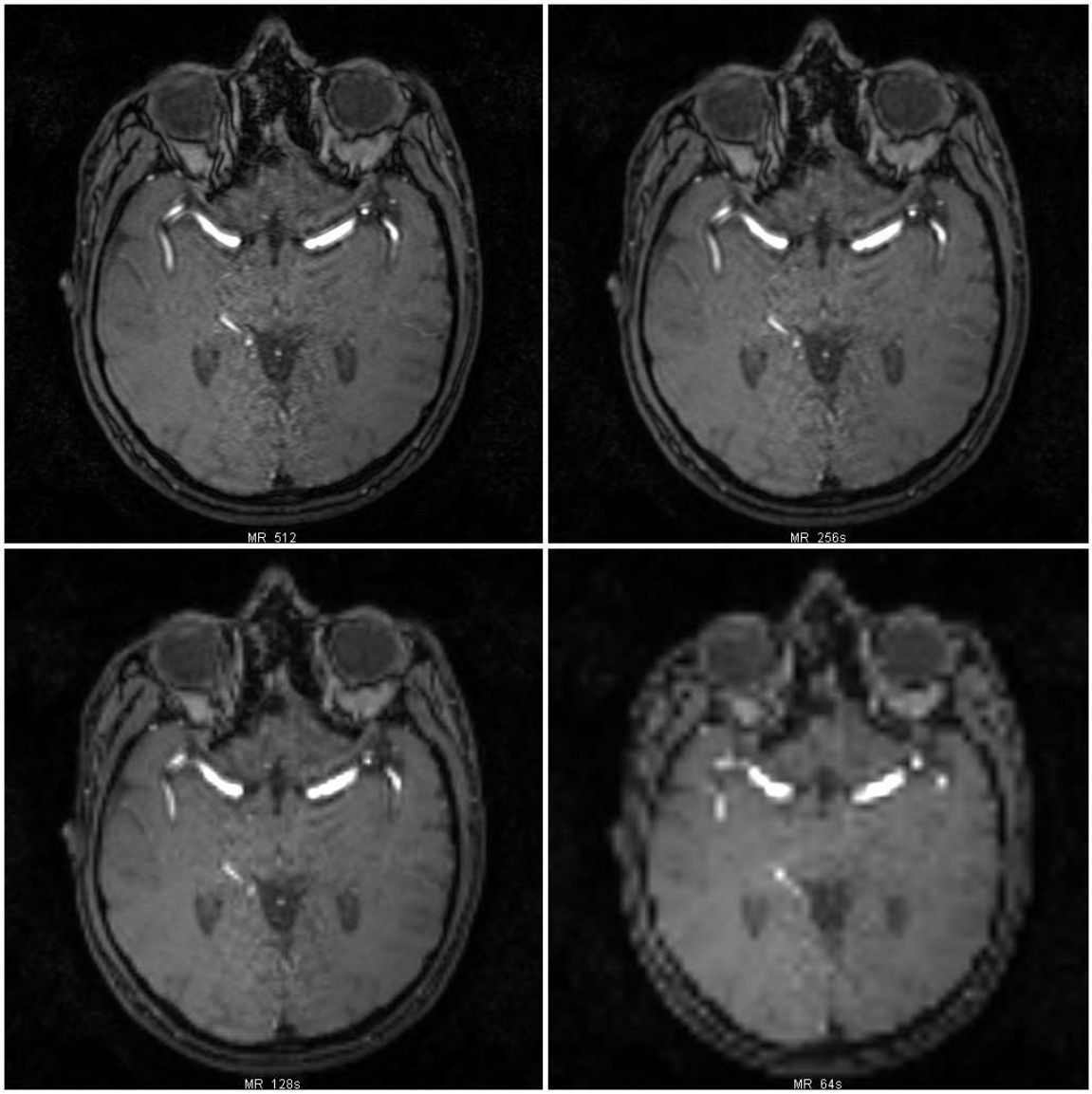

Figure 5: **Successively downsampled MRI images.** (Courtesy of SINTEF MedTech)

4 Promising Methods

This chapter summarizes the experience drawn from my in-depth-study, regarding ideas and algorithms and methods to solve the three registration procedures defined in chapter 1. I will also discuss the work done by Harg [9] during the last year, and propose possible enhancements to his methods. Different approaches will also be discussed, either based on previous reports, or as combinations of these. Arguments for choosing different methods are also presented, as well as possible problems and deficiencies. Optimizers will not be thoroughly discussed, as a choice among them, as mentioned in chapter 3.3, highly rely on experience in the field.

4.1 Preoperative 3D MRI Registration

For this problem, Harg explored a solution employing only translational transformations with Mutual Information, MI, as similarity metric. A gradient descent optimizer using trilinear interpolation, was employed to find the optimal solution. This registration method performed well and gave consistent results for subsequent executions [9]. No changes are needed for this procedure, but different approaches can be tested for comparison of stability, speed and computational expense.

Only translational transformations are believed to be sufficient for this task, as MRI volumes of different weightings are believed to have a rotational offset of zero [9]. Manual initialization is also believed to be unnecessary, as the different weightings of MRI are believed to be very close to be aligned automatically. MRI data is usually of high spatial resolution and contains little noise. Different MRI modes have slightly different characteristics, but they generally visualize the same anatomical structures. It is therefore possible to utilize most of the information available in the image, in a registration process. As Harg's results indicate, a procedure that uses intensity values only, should be feasible in registration of different modes of MRI. Both Correlation Ratio, CR, and Normalized Mutual Information, NMI, are untried in this project, and because of their proposed stability and performance, they should be optimal candidates for further investigation [28]. However, NMI, which is the overlap-invariant version of MI has more computational work than MI. On the other hand, NMI could possibly converge to a minimum more quickly because of its more sophisticated approach.

4.2 Preoperative 3D MRI to Intraoperative 3D US Registration

The most important, and difficult, step of the registration process, is the registration of a master MRI volume to subsequent US volumes. In order to do so, both rigid and non-rigid transformations must be considered. After obtaining a global, rigid transformation that takes the two volumes into alignment, a non-rigid procedure should be applied. This step will obtain the deformation field that is used to perturb the MRI master volume subsequently. This is not straight-forward, since several difficulties are related to multimodal MRI to US registration. While MRI volumes have a high resolution, and therefore a high level of detail, US volumes have a much more moderate level of detail. MRI pictures different tissues with different intensity values, and have an appealingly low level of noise. US on the other hand, visualize tissue boundaries only, and include a significant amount of noise. Also the field of view is different, i.e. MRI volumes are cubic, while US volumes have a conical shape. The mentioned rigid and non-rigid registration parts are related, but do not have to use the same algorithms. The last part

is definitely the most complicated, as no successful automatic non-rigid MRI-US registration procedure has yet been reported.

The *rigid* part has been performed by Letteboer et al. [15] with promising results, by maximizing the Normalized Mutual Information, NMI, of the gradient magnitude for the two volumes. This approach was adopted and tried by Harg [9] with an evolutionary optimizer (EVO) using trilinear interpolation. Because of incompatibilities with the similarity metric and the optimizer, with respect to a transform having six degrees of freedom (translation and rotation), only translations were incorporated into this procedure. This process might therefore have been under-constrained, since the coordinate systems of the two volumes could possibly be un-aligned at initialization. The results of this transformation also support this theory, as reliability of the registration process proved to be somewhat mixed; repeated execution returned inconsistent results. A remedy for this registration scheme could be to incorporate rotations for the transformation, possibly in combination with another optimizer. Harg also mentions a possibility for using an anisotropic diffusion filter on the images in order to preserve edges in a stricter way [9].

As an attempt to incorporate rotations into the transformations, Harg employed a specialized Mutual Information, MI, metric called Mattes MI, instead of NMI. Mattes' MI is also considered to be faster than the original MI metric. The original EVO optimizer was also replaced by a specialized gradient descent optimizer, which is designed to suit rotational transformations well. However, this approach proved to be even more erratic and unstable, as it returned different results in consecutive runs with the same parameters. This configuration may have to exchange the optimizer as it does not seem to work well in the given environment. Anisotropic diffusion filtering should also possibly be considered for this procedure [9].

For both of Harg's approaches, a few modifications of the procedure seemed to give better results. Angio volumes were easier to use in the registration process, and it is a fair assumption that a transformation found for this mode would also give similar results for the other modes. Using US volumes as a master, also seemed to improve the registration results. However, the best enhancement to this multimodal MRI to US registration, would be to manually initialize the registration procedure, by means of globally aligning the two images before the registration procedure starts. This way the parameters of the optimizer can be set more strictly, as no long steps will have to be considered, and the probability of finding the optimal transformation will increase. Both technicians at SINTEF Med Tech and clinicians at St Olavs Hospital in Trondheim, have indicated that this is tolerable, and even desirable [9].

Other approaches for the rigid multimodal step can be the bivariate version of the correlation ratio, that uses both the gradient and intensity information from MRI, which has been successfully used for this purpose by Roche et al. [30] [29]. Incorporating edge information from the MRI volume is done to try and get more similar information from the two modalities, and is therefore tailor made for registration of MRI and US. Also the approach taken by Lloret et al. [19] is promising, using multilocal creaseness feature for both images as a basis for a simple cross-correlation coefficient, CCC, as a similarity metric. However, no accuracy-measures exist for this similarity metric. Rotational transformations should in any case be accounted for.

Procedures for the *non-rigid* part, have also been reported by the above mentioned scientists, but none have been successfully implemented. Roche et al. [30] [29] make the assumption of disregarding spatial differences between the preoperative MRI volume and the intraoperative US volume acquired before start of surgery. They focus on tracking local deformations between the subsequent US volumes. By doing so, important information could be lost, and the procedure

must be used carefully. Lloret et al. [19] suggest to simply using their algorithm for rigid transformations on non-rigid transformations as well. What is known, is that these methods will have to expand the degrees of freedom of the transformation, by incorporating a non-rigid transformation.

4.3 Intraoperative 3D US Registration

A way of overcoming the problem related to multimodal MRI to US registration, is to perform unimodal US registration on successive US volumes. Registration of the preoperative MRI volume with the first intraoperative US volume will provide a global alignment, and possibly also a small local deformation. Each subsequent US volume should then be registered to the previous volume, in order to obtain transformation parameters that can be used to perturb the MRI volume as well. This will make the registration process more manageable, and possibly more accurate, because the registration will be on images from the same modality; i.e. unimodal registration.

Pennec et al. [23] use characteristics of US to form their approach for segmentation of subsequent US volumes. The sound pulse scattering caused by inhomogenities in the tissue (speckle), is considered to be quite consistent over time. Their approach concentrate on matching those high-valued voxel intensities in the volumes, and for this they propose using the simple Sum Squared Difference, SSD. Their approach also includes using a free form deformation field, smoothened by the use of a Gaussian weighting at each position, and a Levenberg-Marquardt optimizer.

Letteboer et al. [16] [15] proposes to find a B-spline-smoothened free form deformation field using Normalized Mutual Information, NMI. B-splines are used to avoid unnatural warpings, in order to achieve a smooth transition in the image. The use of B-splines can also be used in a hierarchical approach, by using a larger grid-density of control points for higher image resolution.

The success of the mentioned approaches is not guaranteed as they are not widely tested, but they may be the methods needed in order to successfully carry out the last step of the multimodal MRI to US registration.

5 Reader's Guide

Harg implemented phase I of the registration system satisfactory last year[9]. For that reason, I will not present algorithms for this step in this report. Because of the magnitude of the registration system and the time-constraints, methods for phase III were not finished in time to be presented in this report. Phase II on the other hand, has been thoroughly investigated, and a discussion of and prototype implementations for this step is the topic of parts II and III.

Each prototype should be evaluated for stability and reliability, speed and successfulness or accuracy. Speed and accuracy can be readily measured, while successfulness had to be somewhat more subjectively measured. Registration methods are often compared to a *gold standard*, which is based on manual selection of a number of homologous points in both data sets. Since SINTEF MedTech currently does not possess the equipment needed to perform manual registration, such as that needed here, other evaluation methods will be used. The prototypes were tested on three different data sets, and a presentation on those will be given in part IV. The results from the evaluation is the topic of part V, and the results are further discussed in part VI.

Part VII describes the future work to be done in order to realize the proposed registration procedures. This part also concludes the report.

The intended audience for the report is anyone with general knowledge in computer science and image processing, and an interest in medical image registration. However, it could be advantageous to read my in-depth-study before reading this report, as it discusses the building blocks of a registration system in more detail. Numerous references to other literature are included to enable the reader to seek out further information, while this report is nonetheless intended to be self-contained and comprehensible, using my in-depth-study as a supplement, without the use of secondary literature.

Part II

Discussion of Methods

In this part, methods that will be used to implement registration phase II, which has been my main focus, be discussed. Characteristics of the data for the different weightings of the imaging modalities will be accounted for, together with previous reports on successful registration application for the problem. Part III will subsequently present concrete registration algorithms, based on the information and assumptions made in this part.

6 Phase II - MRI-to-3DUS Registration

Phase II should, as stated in chapter 2.2, do registration of a selected preoperative master MRI volume to the initial US volume. This phase is assumed to be only a rigid transformation, since it is assumed that little or no deformation is taking place between the acquisition of the MRI volumes and the initial US volume. If there however are signs of any local deformation of the tissues, a non-rigid registration algorithm should be considered. A study of the acquisition of the image volumes shows that the preoperative MRI volumes are acquired at most 24 hours before the surgical operation. It is therefore a fair assumption to believe that little or no local deformation occurs between the acquisitions of the volumes. For that reason, my focus will be on rigid transformations only.

Letteboer et al. [15] reports promising results by maximization of the Normalized Mutual Information, NMI, of the gradient magnitude for the two volumes. This approach was adopted and tried by Harg [9] with an evolutionary optimizer (EVO) using trilinear interpolation, with average results.

Roche et al. [30] [29] proposes a bivariate version of the correlation ratio, BCR, that uses both the gradient and intensity information from MRI, which has been successfully implemented. Incorporating edge information from the MRI volume is done to try and get more similar information from the two modalities, and is therefore tailor made for registration of MRI and US.

Also the approach taken by Lloret et al. [19] is promising, using multilocal creaseness feature for both images as a basis for a simple cross-correlation coefficient, CCC, as a similarity metric. However, no accuracy-measures exist for this similarity metric.

6.1 Transform

As stated above, only rigid transformations will be considered. Studies of the image volumes show that little or no rotational offset is apparent between volumes from the two imaging modalities. For that reason, rotational components might be discarded in the registration applications. However, rotations are incorporated into one of the applications, to possess a solution if the mentioned assumption should turn out to be wrong.

6.2 Similarity measure

The three similarity measures mentioned above (NMI/MI, BCR and CCC) are good candidates to be used in the registration application, since they all have been reported to perform well in the given environment. However, no comparisons of the methods have been reported, and it is therefore difficult to say which is most promising. All three use a differential similarity basis, like gradient or ridge/valley operator, to extract image features prior to registration. However, the similarity measures that are already implemented by available toolkits will be explored first.

The reason for using features as the similarity basis, is to make the modalities more similar. As mentioned in chapter 2.2 US visualize mainly tissue boundaries, whereas MRI mainly contains information about tissue types. As an effect, the intensities in an MRI volume are more or less uniform in areas of uniform tissue, while the same areas in US volumes mainly has very low

values and speckle. By using a gradient magnitude filter on the MRI volume, this will emphasize tissue boundaries, while the areas of uniform intensity will be given low values, thus making it more similar to the US volume.

Angio-graphic images, however, are more similar in their representation for the two modalities, with the exception that the blood vessels appear "thicker" in the ultrasound volume than in case is for the MRI volume. A possible solution could be to blur the volumes by convolution of a Gaussian, or simply leave the volumes unchanged. The last alternative is the fastest, as no preprocessing of the images will have to be performed. Both gradient magnitude filtering, convolution with a Gaussian and no preprocessing should be examined to find the best solution.

6.3 Optimizer

The Insight Toolkit Software Guide [13] (see chapter 7.1) and the authors of the papers presenting the three successful methods described above, suggests an evolutionary and gradient descent optimizers for both NMI/MI and CC, while a Newtonian gradient descent optimizer should be used for BCR. However, Harg reports that gradient descent optimizers were more difficult to parameterize than the evolutionary optimizer. Both should however be examined for comparison.

The most common method used to interpolate voxel values at non-grid positions when calculating metric is linear interpolation. This technique is considered both accurate and fast enough in most registration procedures [13].

6.4 Other issues

Harg [9] reports that Angio volumes were easier to use in the registration process, and it is a fair assumption that a transformation found for this mode would also give similar results for the other modes. Using US volumes as a master, also seemed to improve the registration results. These two observations will be adopted in my registration procedures as well.

The best enhancement to the multimodal MRI to US registration, would be to manually initialize the registration procedure, by means of globally aligning the two images before the registration procedure starts. This way the parameters of the optimizer can be set more strictly, as no long steps will have to be considered, and the probability of finding the optimal transformation will increase. However, this will only make the registration procedures semi-automatic, and will therefore not be considered any further.

A multi-resolution, as described in chapter 3.4 setup should be considered, as this could be a possible speed-up for the applications. However, the choice of optimizer may affect the usefulness of the multi-resolution procedure. At least, this is the case for the evolutionary optimizer, which will be described in further detail in chapter 8.2.3. This optimizer smoothes the parameter space as the levels of the pyramide images, because of its multinormally distributed parameter change vector, and its Gaussian's covariance matrix based on previous success and failure. The multi-resolution approach is therefore not needed for this optimizer. The application may even become too slow for practical purposes with a multi-resolution approach.

Part III

Implementation

This part describes how the discussed methods from the previous part are implemented. This includes a presentation of the frameworks and software libraries that will be used. Parameters and other issues for the specific methods that are used in the prototype implementations are will described in detail in chapter 8. Finally, a summing-up on the computer platform and hardware, used for implementation and testing, as well as software availability, will be given in chapter 9.

7 Frameworks and Libraries

This chapter will focus on the frameworks and software libraries that are used to build the registration system. The only software library used in the registration system is the *Insight Toolkit* (ITK), a widely recognized software library in medical image processing and analysis. ITK will be described in chapter 7.1. To visualize image volumes prior to and after registration, SINTEF MedTechs *CustusX* were used. This visualization- and navigationsystem will be presented in chapter 7.2.

7.1 Insight Toolkit - ITK

The Insight Toolkit, ITK[3], is an open-source software toolkit for performing registration and segmentation. ITK is implemented in C++ and is a cross-platform, using the CMake[4] build environment to manage the compilation process. In addition, an automated wrapping process generates interfaces between C++ and interpreted programming languages such as Tcl, Java, and Python. This enables developers to create software using a variety of programming languages. ITK's C++ implementation style is referred to as generic programming (i.e., using templated code). Such C++ templating means that the code is highly efficient, and that many software problems are discovered at compile-time, rather than at run-time during program execution.

Because ITK is an open-source project, developers from around the world can use, debug, maintain, and extend the software, free of charge. ITK uses a model of software development referred to as extreme programming. The key features of extreme programming are communication and testing. Communication among the members of the ITK community is what helps manage the rapid evolution of the software. In ITK, an extensive testing process is in place that measures the quality on a daily basis, which in turn keeps the software stable.

The toolkit provides extensive support for the different data and file formats used in medical imaging, but is capable of processing other data types. The toolkit is organized around a data-flow architecture, which means that the data is represented using data objects which are in turn processed by process objects (filters). Data objects and process objects are connected together into pipelines, which are capable of processing the data in pieces according to a user-specified memory limit set on the pipeline. A command/observer design pattern is used for event processing, to extract important facts and figures from the iterative registration process. This way the parameters of the registration process can be changed during registration.

ITK is managed by the Insight Software Consortium, ISC, a non-profit organization set up to manage the development process of the participants. Sponsors and participants include the US National Library of Medicine of the National Institutes of Health, GE Corporate R&D, Kitware Inc, Insightful, University of North Carolina, University of Tennessee, and University of Pennsylvania.

[3]See: http://www.itk.org
[4]See: http://www.cmake.org

7.2 CustusX

We have developed a 3D navigation system for intraoperative use during minimally invasive surgical procedures. The system can also be used for planning the surgical procedure. This navigations system is called CustusX. CustusX's main features are to visualize 3D ultrasound data integrated with preoperative acquired CT (computed tomography or X-ray) or MR (magnetic resonance) images. With a positioning sensor attached to the surgical tools it is possible to track the position and orientation of the tools and let the tools control the visualizations. This means that e.g. corresponding CT and ultrasound slices are shown according to the position of the surgical tool. The 3D visualization is based on VTK. The registration and segmentation routines implemented are based on ITK.

CustusX is a visualization- and navigationsystem based on principles from navigation, 3D visualization and advanced processing of medical images. Surgical instruments may be controlled during operations by visualizing them in the image volumes. With a positioning sensor attached to the surgical tools it is possible to track the position and orientation of the tools and let the tools control the visualizations. In this way, the surgeons can see the instruments in relation to the anatomy of the patient. Several image volumes may also be visualized contemporary for manual inspection, as well as applying rotation and zooming operations on them.

The system is built on both ITK, as mentioned above, and the Visualization Toolkit, VTK[5]. VTK is an open source, freely available software system for 3D computer graphics, image processing, and visualization used by thousands of researchers and developers around the world, in the same manner as ITK.

The navigation system is developed at SINTEF MedTech in close collaboration with surgeons and radiologists at St. Olavs Hospital (Trondheim University Hospital).

[5]See: http://public.kitware.com/VTK/

8 Registration Methods

This chapter describes the specific implementation of the prototype registration applications, as discussed in chapter 6. All components that have been used are available from ITK libraries. This has been done, rather than developing new components, to ensure a full exploration of the already available components. This approach also eases the job of revisiting the constructed applications. Also worth mentioning, is that none of the applications make use of a hierarchical approach as described earlier in chapter 3.4. Because of the modularity of the ITK-components, this feature could easily be added later. Additionally, all applications will be designed to use angio-graphic input-volumes.

8.1 RegApp4

The first application presented for registering MRI to 3DUS will be implemented by combining the specific algorithms described below. To keep it as simple as possible only translations will be accounted for. This is also a good approach, as initial studies of typical data sets show little apparent rotational offset and deformation between the MRI volumes and the first US volume. If there, after rigid registration has been accomplished, is evidence that deformations are occurring, a non-rigid extension should be made to this program. A multi-resolution approach is not implemented, but because of the modulability of the program this feature can be added later on, possibly speeding up the application.

8.1.1 Translation Transform

The translation transform is probably one of the simplest, yet one of the most useful transform. It gives the registration 3 degrees-of-freedom, and is provided by:

`itk::TranslationTransform<TScalarType = double, NDimensions = 3>`,

templated over the data type for the transformation calculations and the number of dimensions. Translations also have the advantage of being fast to compute and having parameters that are easy to interpret in that the result is a translation in x-, y- and z-direction.

8.1.2 Mattes' Mutual Information Metric

The original Mutual Information Metric selects new spatial samples for every iteration of the registration process, in order to compute the mutual information value. Mattes' MI on the other hand, uses only one spatial sample set for the whole registration process instead of using new samples every iteration. Mattes MI' is therefore considered to be faster than the original MI metric. Additionally, the use of a single sample set results in a much smoother cost function, and hence allows the use of more intelligent optimizers. Another noticeable difference is that pre-normalization of the images is not necessary, as the metric rescales internally when building up the discrete density functions. Pre-normalization of the images is a time-consuming process, additionally making Mattes' MI more preferable. Using the mentioned set of intensity values, Mattes' MI computes the marginal and joint probability density functions (PDFs) and evaluates them at discrete positions, bins, which are uniformly spread within the dynamic range of the images. Entropy values are then computed by summing over the bins. Mattes' MI is provided from ITK by:

`itk::MattesMutualInformationImageToImageMetric<TFixedImage, TMovingImage>`,

templated over the image types of the input images. The metric only has two parameters that need to be set, the number of *spatial samples* and the number of *bins* to be used for the PDFs. The number of spatial samples to be used depends on the detail in the image, and should be at least 1 percent of the image voxels[13]. However, experience is the best way of finding suitable values for both parameters. Further, it is important to note that Mattes' MI computes the negative mutual information, and hence the cost function will have to be minimized by the optimizer.

8.1.3 Gradient Descent Optimizer

The optimizer used is a variant of gradient descent that attempts to prevent it from taking steps that are too large. At each iteration this optimizer will take a step along the direction of the Mattes' MI metric derivate. The initial length of the step is defined by the user. Each time the direction of the derivate abruptly changes, the optimizer assumes that a local extrema has been passed and reacts by reducing the step length by a half until a minimal step length or the maximum number of iterations is reached. The optimizer is provided by:

`itk::RegularStepGradientDescentOptimizer`.

Three values has to be set for the optimizer; *maximum (initial) step length*, emphminimum step length and the emphmaximum number of iterations. The upper step length boundary should be set so that the method accommodates reasonably large translations, but not much too large, to avoid the optimizer searching too wide an area in parameter space. The lower step length boundary should be set as small as the preferred accuracy. Setting it to low however, will likely make the procedure run much longer (until it runs out of iterations) without achieving more than hopping back an forth a very small distance. Additionally, when using the Mattes' MI metric, the optimizer should always be set to *minimize* the metric cost function.

8.1.4 Linear Interpolation

The method used to interpolate voxel values at non-grid positions when calculating metric is provided by:

`itk::LinearInterpolateImageFunction<TImageType, TCoordType=double>`,

templated over the image type and the pixel types. As mentioned in chapter 3.4, linear interpolation is considered both accurate and fast enough in most registration procedures.

8.1.5 Filters

In addition to no preprocessing of the input images, both gradient magnitude filtering and Gaussian blur filtering will be tested in order to find the best possible solution. The gradient magnitude filter can improve the matching of the MRI and US images, by making them look more similar. This filter is provided by:

`itk::GradientMagnitudeRecursiveGaussianImageFilter<TInputImageType, TOutputImageType>`,

templated over the input image type and the output image type of the filter. The filter computes the gradient magnitude by convolving the image with a recursive approximation of the Gaussian. The *standard deviation* for the Gaussian is a parameter that will have to be set, which results in a varying degree of edge smearing.

Because US-angio images seems ticker than the case is for MR-angio images, it should also be investigated a blurring of the images to make them more similar. This is provided by:

`itk::DiscreteGaussianImageFilter<TInputImageType, TOutputImageType>`,

also templated over the input image type and the output image type of the filter. This filter

performs Gaussian blurring by separable convolution of an image and a discrete Gaussian kernel. The *standard deviation* for the Gaussian is also a parameter that will have to be set for this filter, which results in a varying degree blurring.

As mentioned, it should also be investigated how well the registration is without any preprocessing of the input images, as this approach is believed to work best for angio-graphic input images.

8.2 RegApp5

The application that is presented in this chapter differ little from the one described above. Actually, the only difference is that the gradient descent optimizer is replaced by an evolutionary (1+1) optimizer. Because of the optimizer, the application will probably not benefit much from a multi-resolution approach as suggested for the previous application.

8.2.1 Translation Transform

The transform for this application will be the same translation transform, as described in chapter 8.1.1.

8.2.2 Mattes' Mutual Information Metric

The metric for this application will be Mattes' Mutual Information, as described in chapter 8.1.2.

8.2.3 Evolutionary Optimizer

Evolutionary optimizers try, as suggested by their name, to mimic the mechanisms of natural evolution, applying evolution-like rules to the iterative process of searching for the optimum. Evolutionary algorithms are therefore naturally well-suited for optimizing the Mutual Information metric, given its random and noisy behavior. The optimizer is provided by:

`itk::OnePlusOneEvolutionaryOptimizer`.

This optimizer is based on testing random variations of parameters, and ITK provide a random number generator to aid this by:

`itk::Statistics::NormalVariateGenerator`,

The generator generates values from a normal distribution. By successively changing the estimated transformation coefficient, the search proceeds towards the optimum value of the parameter space. At each iteration, one "child" of the current transformation coefficients is generated by mutating the "parent". Then, the next generation (next parent) is chosen as the transformation coefficients resulting in the best metric value of the current parent and child.

The optimizer takes three parameters; an *initial search radius*, the *maximum number of iterations*, and a *minimal value of* ϵ, the Frobenius norm of the covariance matrix. The last parameter decides how much the covariance matrix should be changed at each iteration, when a child that is more or less fit is found, ensuring that the next step will continue in the right direction. The initial search radius should be set high enough for the optimizer to find the path toward the wanted translational offset. ϵ should be set so high that it has a realistic chance of interrupting the registration process on the grounds of too little progress per iteration. Again, the Mattes' MI metric value should be *minimized*.

8.2.4 Linear Interpolation

The optimizer for this application will be linear interpolation, as described in chapter 8.1.4.

8.2.5 Filters

Also for this application, both gradient magnitude filtering, Gaussian blur filtering and no filtering should be tested for comparison. These filters are described in refchFilters.

8.3 RegApp6

The last application is designed to also incorporate rotations into the transformation, and will be tested in the same manner as the others. However, if there is any sign of rotational offset on the MRI volumes and the initial US volume, the application can be applied on the volume resulting from the applications that not incorporate rotations into the transformation.

8.3.1 Rigid Transform

ITK provides a rigid transformation with translation and rotation (6 degrees-of-freedom) by:

`itk::VersorRigid3DTransform<TScalarType = double>`,

templated over the data type for the transformation calculations. Because of the increased complexity of the transform, it also gives the registration application a greater parameter space to search for the optimal transformation.

8.3.2 Mattes' Mutual Information Metric

The metric for this application will be Mattes' Mutual Information, as described in chapter 8.1.2.

8.3.3 Specialized Gradient Descent Optimizer

The parameter space of the transform for this application is not a vector space as it is for only translational coefficients. The rotational coefficients introduce versor-components, which does not suit standard gradient descent algorithms well. A specialized optimizer designed for this situation is provided by:

`itk::VersorRigid3DTransformOptimizer`,

which uses versor composition for updating the rotational coefficient, and vector addition for updating the translational coefficients.

As for the regular step gradient optimizer, the *maximum (initial) step length*, *minimum step length* and the *maximum number of iterations* should be set. Further, the optimizer will have to scale the rotational and translational values, as they default have a widely different scaling - e.g. a change of 1.0 mm in translation will affect the result much less than a change of 1.0 in one of the versor components. The rule of thumb given by the ITK authors for setting the scales is to set the three rotational scales to 1.0, and the translational scales to $1/(10 * \sqrt{X^2 + Y^2 + Z^2})$, where X, Y and Z are the dimensions of the input images in physical units. Again, we are using Mattes' MI metric, which should be *minimized*.

8.3.4 Linear interpolation

The optimizer for this application will be linear interpolation, as described in chapter 8.1.4.

8.3.5 Filters

Also for this application, both gradient magnitude filtering, Gaussian blur filtering and no filtering should be tested for comparison. These filters are described in refchFilters.

9 Platforms and Availability

This chapter presents the platform used for developing, executing and testing the registration applications presented in chapter 8. As will be pointed out, even though the software was developed on a Microsoft Windows platform, it should work equally well on other platforms such as Mac OS X and GNU/Linux.

9.1 Microsoft Windows XP

The software was developed on a Microsoft Windows platform, which currently is at version XP. The environment used to construct and compile the source code, with ITK included, was Microsoft Visual Studio 2003 (cl-compiler). The computer had an AMD Athlon 64 3000+ (2.0GHZ) processor, and 512 MB DDR RAM. The execution-time of my applications could therefore be considerably reduced using a more powerful computer, as this only is an average computer in today's standards. At least, this would be a likely assumption with an increase in memory, as the image volumes make use of a significant amount.

9.2 Mac OS X

A computer running on Mac OS X, currently at version 10.4, was used to visualize the results of the registration procedures. Since the operating system vendor is also the supplier of the computer hardware, the Mac platform has earned a reputation for highly optimized performance. This is especially true in image processing, and was partly the reason for the choice of visualization-equipment.

9.3 Software Availability

Both Microsoft Windows, Mac OS X and GNU/Linux are supported by ITK, using CMake for configuration. No other libraries was used, and for that reason the application should compile on any of the mentioned platforms, without modifications. The registration algorithms currently available in ITK represent the most common and widely used ones. For that reason, my focus has been on the already existing algorithms, rather than developing others. This will also ensure that revisiting the applications later would be easier.

Part IV

Data Sets

The three data sets used to test and assess the prototype applications discussed in chapter 8 is presented in this part of the report. As we will se, both resolution, voxel sizes, number of volumes and type of surgical operation vary for the data sets. However, they all include angiographic volumes for both MRI and US (acquired before the opening of the dura mater; i.e. no/little local deformation), which has been decided to be the input type to the applications. Nevertheless, for visual presentation-purposes, tissue-volumes are also included.

10 Presentation of Data Sets

This section presents the data sets that is used to test and evaluate the registration algorithms presented in chapter 8. They are all from real surgical operations, and made available in MetaHeader/Raw format, exported from the SonoWand ultrasound navigation system. The pre-operative MRI volumes are imported into the system prior to the surgical operation, from the DI-COM series acquired by the MRI scanner. Subsequently, the SonoWand system has been used to reconstruct the acquired ultrasound scan into a 3D representation. The entire collection of volumes for a single surgical procedure has then been exported with a common representation, using the same file format, bit-depth, voxel-spacing and physical extent for all the volumes.

The file names are created using a time-stamp notation, representing when they were first imported/acquired in the navigation system, using a format like this: YYYYMMDDTHHMMSS.mha/raw, e.g.: texttt20060221T094807.mha. The volumes will in the following be referred to using a descriptive name. Appendix A includes a table showing names and descriptive names.

Harg used both Tumor 1 (see 10.1) and Aneurism 1 (see 10.3) to test his algorithms last year. He also used a data set called Tumor 2, but because that set does not include angio-graphic images, that data set has been replaced by another data set. As an attempt not to cause confusion, the new set will be known as Tumor 3. Additionally, since my focus has been on phase II of the registration system, no presentation of volumes acquired after the surgical procedure has started will be presented. Here follows, a presentation of the above-mentioned data sets.

10.1 Tumor 1

The data set known as Tumor 1 consists of seven (7) MRI volumes, and three (3) US volumes of a patient with a brain tumor. The first three volumes contain fMRI[6] data overlaid onto a T1-weighted MRI (included separately as the seventh volume), where the responding fMRI areas are given maximum intensity (255). The three fMRI volumes represent the following stimulations, respectively: Finger movement, language and tongue movement. The fourth volume is a T2 weighted MRI volume. A 3D rendering of the fMRI and the T2 MRI is included in figure 6. The fifth volume is a T1 weighted MRI volume. The sixth image is a MR-Angio (MRA)volume, which has the greatest interest, since my algorithm is based on angio-graphic input images. This volume is seen in 3D together with the MRI T2 volume in figure 7. The seventh volume is, as mentioned, the underlay for the fMRI, i.e. a T1 weighted MRI with contrast fluid.

The first US volume is a US tissue (UST#1) volume. The last two volumes are US-Angio (USA#1 and USA#2) volumes, acquired before opening the dura mater. The angio-graphic US volumes is as mentioned most interesting for this report. A 3D rendering of angio-graphic volumes from both modalities is included in figure 8.

This data set has a resolution of 290x290x196 (approx. 16.5 million) voxels and a voxel size of 0.4 mm, for both MRI and US volumes. Also worth mentioning, is that this data set is MRI-mastered, which means that the field-of-view is decided by the MRI images.

[6] functionalMRI - an MRI modality where a contrast fluid is used to determine the areas of the brain that are most active during specific stimulations

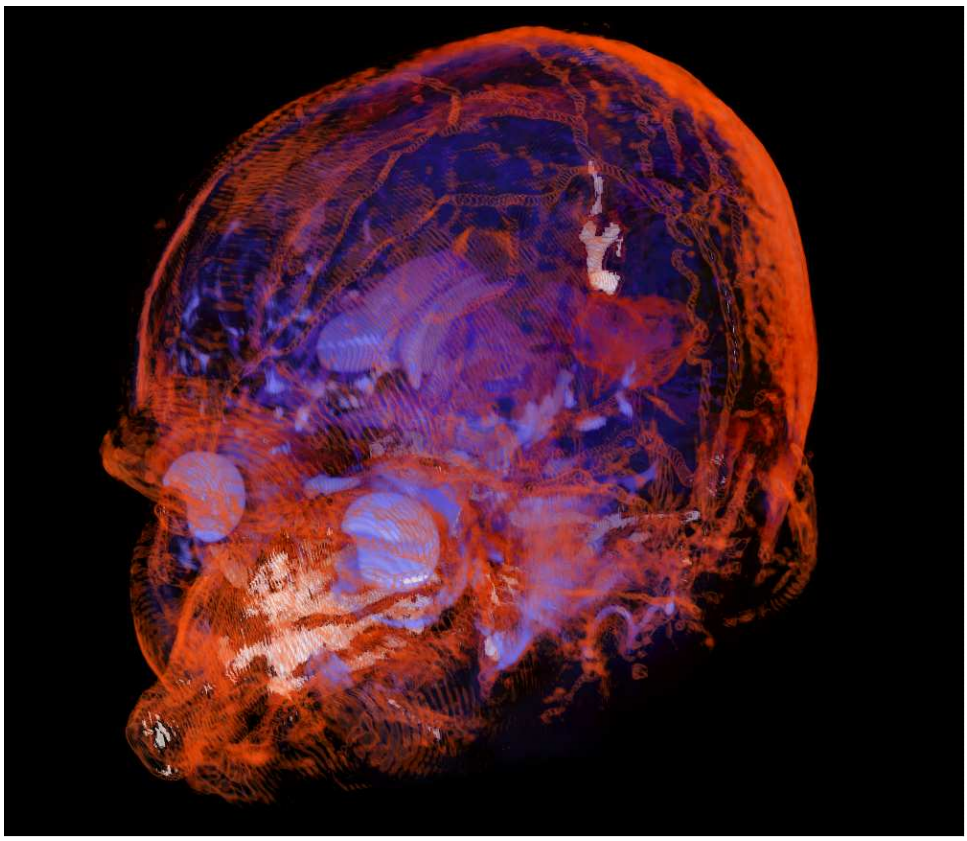

Figure 6: **Volume renderings of fMRI (*orange* MRI T1 with *white* fMRI tongue response overlay) and MRI T2 (*blue*)**

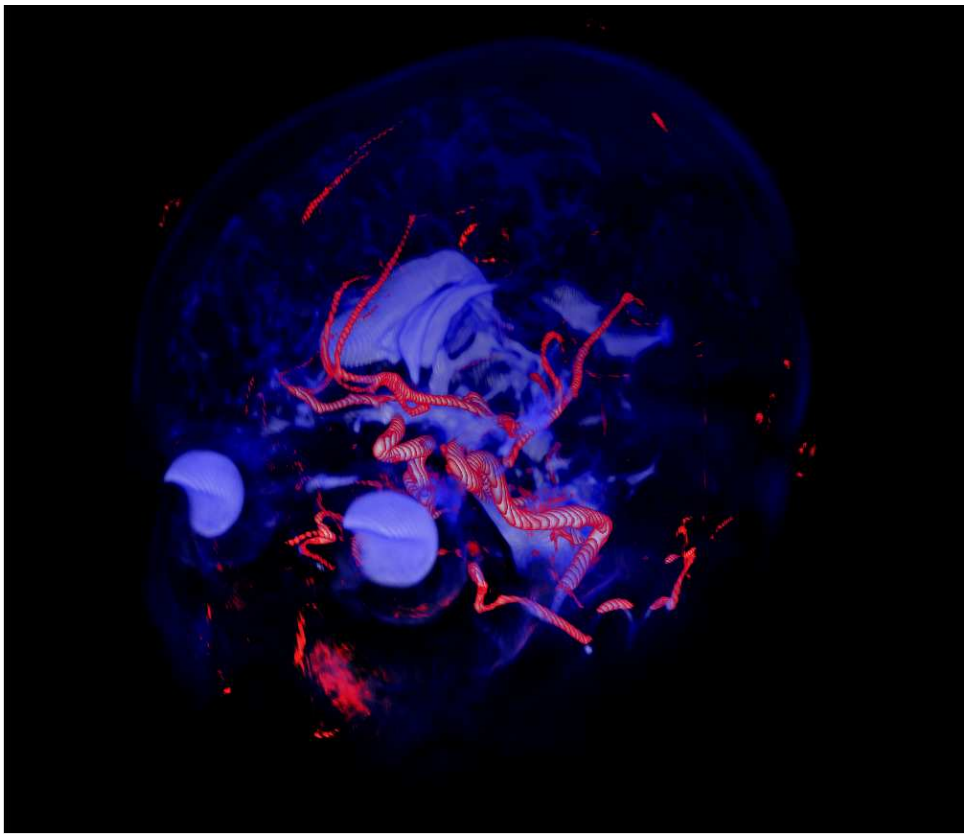

Figure 7: **Volume renderings of MRI T2 (*blue*) and MRA (*red*)**

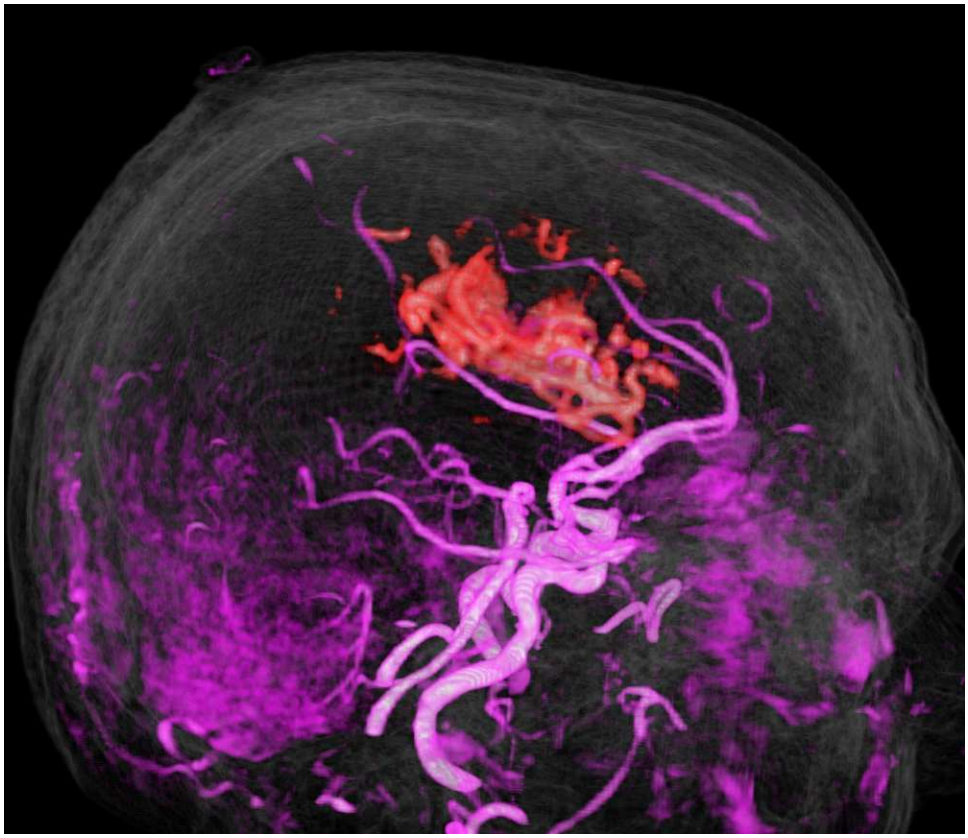

Figure 8: **Volume renderings of MRA (*pink*) and USA #1 (*red*)**

10.2 Tumor 3

This data set is also from a patient with a tumor. It consists of five (5) MRI-volumes, and one (1) US volume. The first two volumes are MRI-T1 and MRI-T2, respectively. The third volume is a MR-Angio volume, while volume four and five are fMRI volumes, representing language and tongue movement. Figure 9 shows a combined 3D rendering of the different MRI weightings. The last volume of the data set is an angio-graphic US volume, and the angio-graphic volumes from both modalities are rendered in figure 10.

The resolution of this data set is 355x355x271 (approx. 34.2 million) voxels, for both MRI and US volumes. This makes this data set the one with the greatest resolution of the three presented. The voxel size is the same as for tumor 1, 0.4 mm. However, this data set is US-mastered.

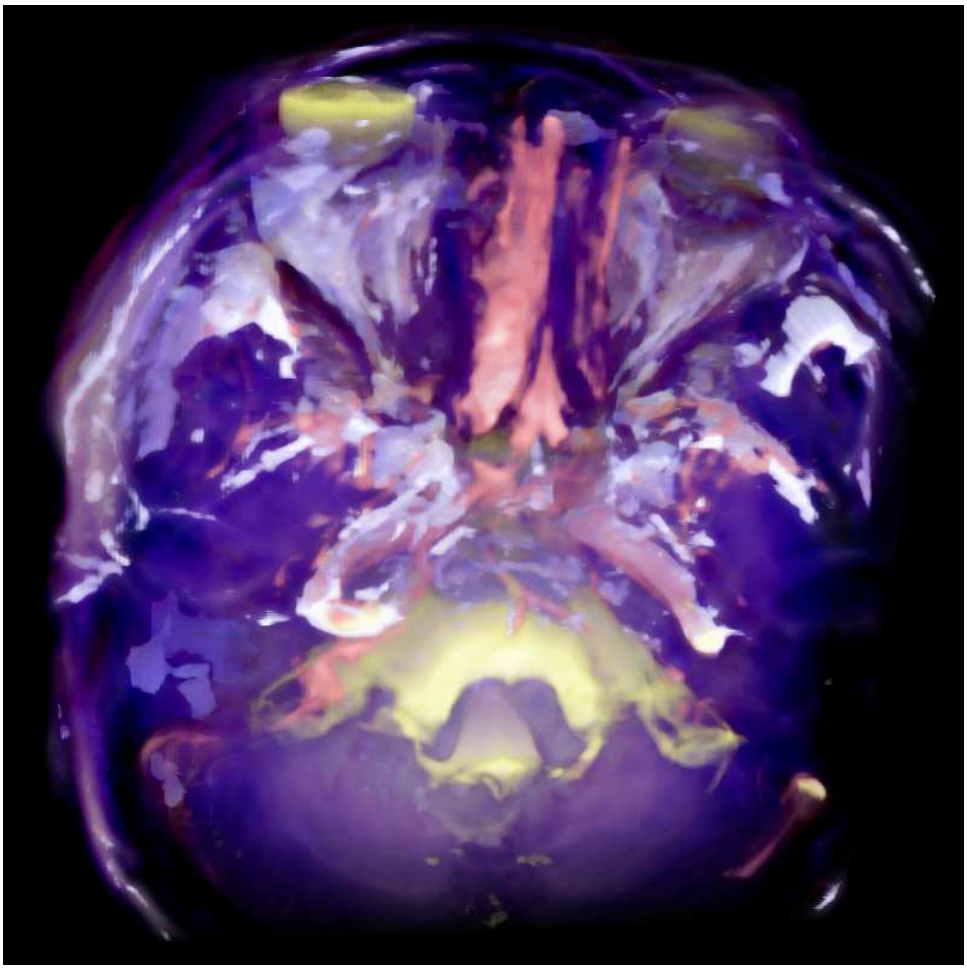

Figure 9: **Volume renderings of fMRI Language response (*blue*), MRI T1 (*red*) and MRI T2 (*yellow*)**

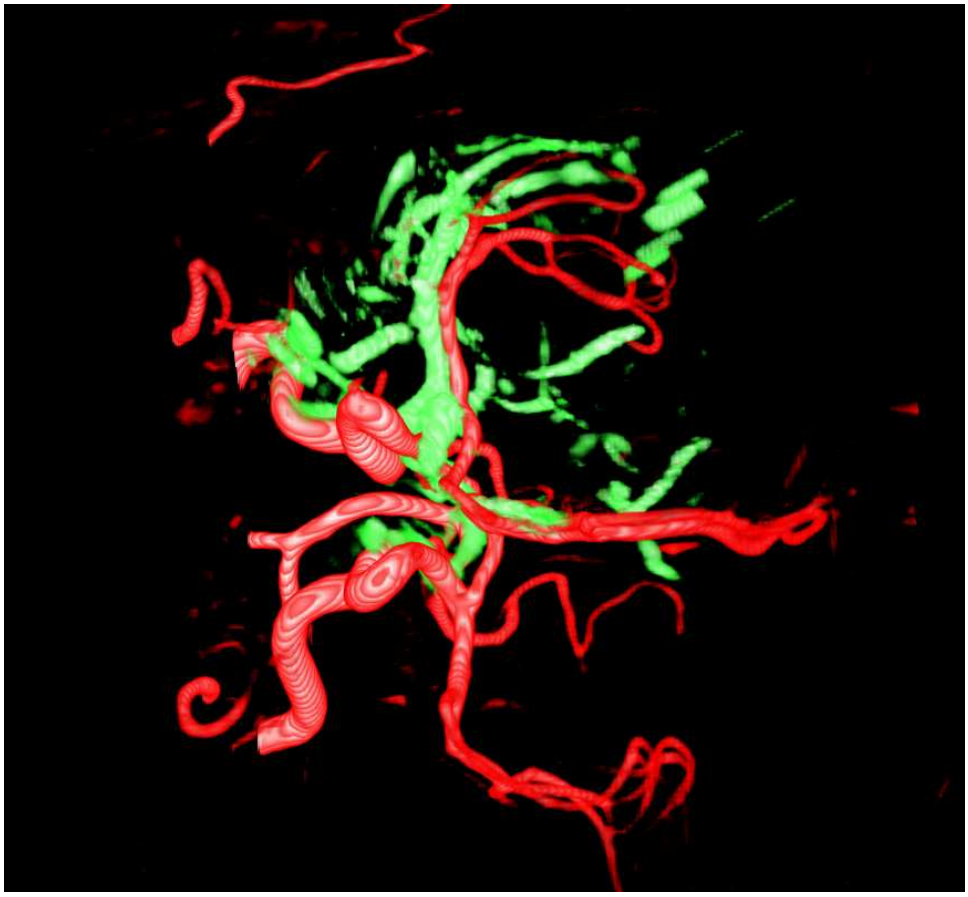

Figure 10: **Volume renderings of MRA (*red*) and USA (*green*)**

10.3 Aneurism 1

Aneurism 1 contains only two (2) MRI volumes, and one (1) US volume, and represent a patient with an aneurism in one of the principal cerebral arteries. The MRI volumes are a T1 weighted MRI volume and an MR-Angio (MRA) volume , respectively, and is presented as a 3D rendering in figure 11.

The only US volume is also an angio-graphic (USA) volume. A presentation of the angio-graphic volumes from both modalities is given in figure 12. This data set, however, is US-mastered.

This data set is the one with the smallest resolution of the three presented, more specifically, 203x203x103 (approx. 4.2 million) voxels, for both MRI and US volumes. A peculiarity of this data set, is that the voxel size varies in the different directions. That is, 0.39, 0.39 and 0.5 mm for x, y and z directions, respectively.

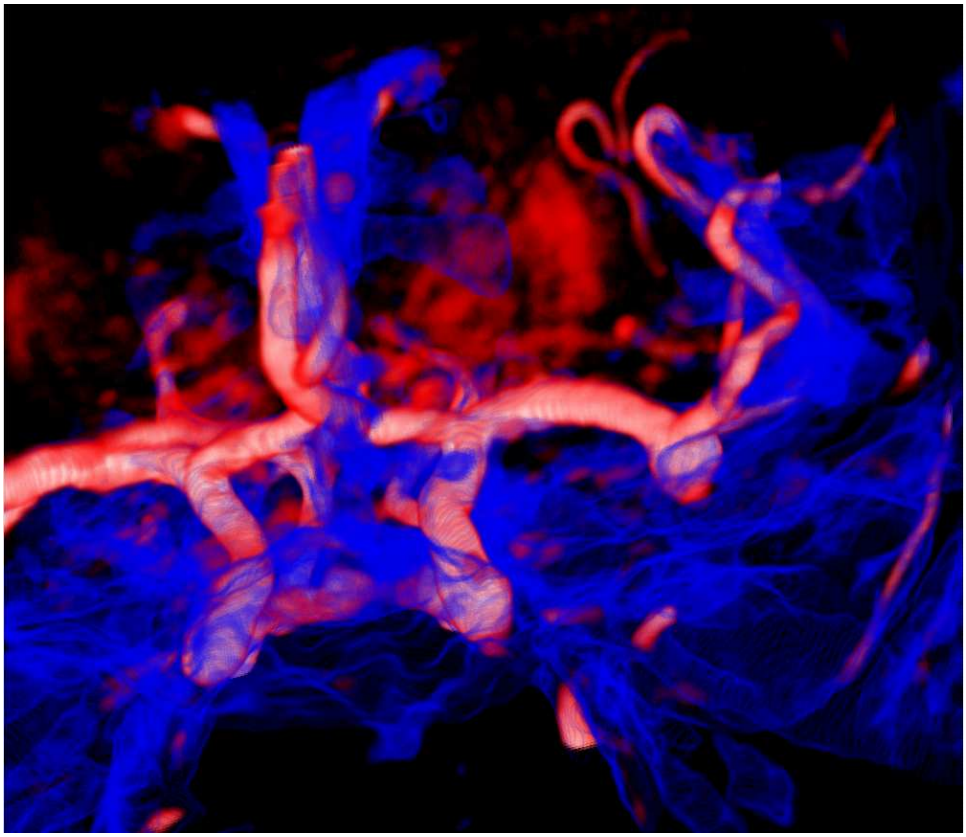

Figure 11: **Volume renderings of MRI T1 (*blue*) and MRA (*red*)**

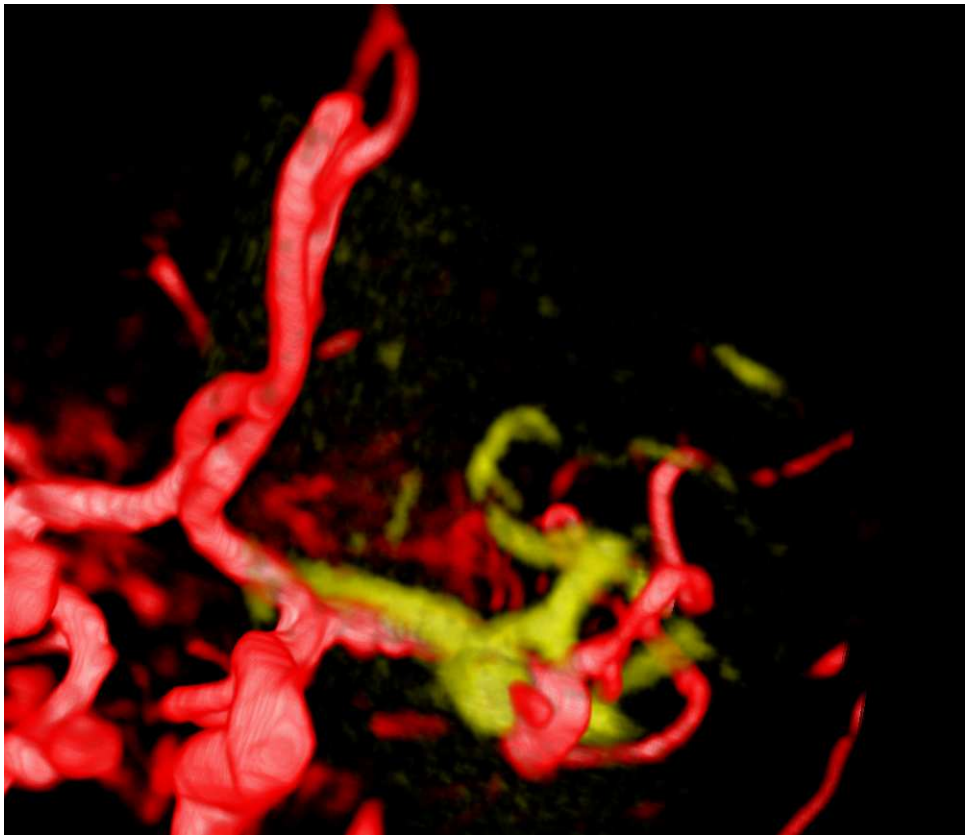

Figure 12: **Volume renderings of MRA (*red*) and USA (*yellow*)**

Part V

Results

In this part the results of the registration applications discussed in chapter 8, applied on the data sets presented in the previous part, is presented as 3D renderings. A set of parameter settings for each registration is also presented, along with the 3D renderings. The 3D renderings will display both situation before registration, after transformation of the moving volume, and a combined view of both. Additionally, a second view for all registrations, enabling an opportunity to discover any potential displacement in other directions, can be found in appendix B. Note, that no manual initialization has been performed for the registrations.

To simplify the visual inspection of the results, the different volumes have been given color coding. First of all, the fixed volume is rendered green. The moving image, before registration, is rendered as red, while other colors are given for the moved image after registration. RegApp4 is rendered blue, RegApp5 is rendered grey, and RegApp6 is given the color yellow.

The 3D renderings presented in this part will be the principal source for interpretation and discussion of the results, in the subsequent part VI. Thus, in this part, the presented registration results will represent typical results, which will give an indication of how well the applications may perform. How reliable the different registration application is, is therefore postponed until the subsequent evaluation part.

11 Tests and Methods

To test the registration applications, several tests on the data sets presented in the previous part has been conducted. These tests are listed in table 1. As Harg [9] suggests, the US volumes are always kept as the fixed volume. Additionally, no preprocessing of none of the input volumes has been performed. The next chapters will present the results from these registration executions.

Reg.no.	**Reg.app**	**Fixed volume**	**Moving volume**
1	4	Tumor 1 USA#1	Tumor1 MRA
2	5	Tumor 1 USA#1	Tumor1 MRA
3	4	Tumor 3 USA	Tumor3 MRA
4	5	Tumor 3 USA	Tumor3 MRA
5	4	Aneurism 1 USA	Aneurism 1 MRA
6	5	Aneurism 1 USA	Aneurism 1 MRA
7	6	Aneurism 1 USA	Aneurism 1 MRA

Table 1: **Registrations that should be performed**

12 Tumor 1 Registration Results

Data set Tumor 1 has been used to test RegApp4 and RegApp5, which allow for translational transformation only; i.e. 3 degrees-of-freedom. The results for RegApp4 and RegApp5 are presented in chapters 12.1 and 12.2, respectively.

12.1 Registration #1

The first registration that has been performed, is between the volumes USA #1 (fixed) and MRA (moving), using RegApp4. The parameters for this registration is presented in table 2. The resulting translation-parameters, along with the metric value and number of iterations used, is presented in table 3. As we can se, the greatest translation takes place in the z-direction.

Figures 13 through 15 show 3D renderings of the image volumes, both before and after registration as well as a combined view.

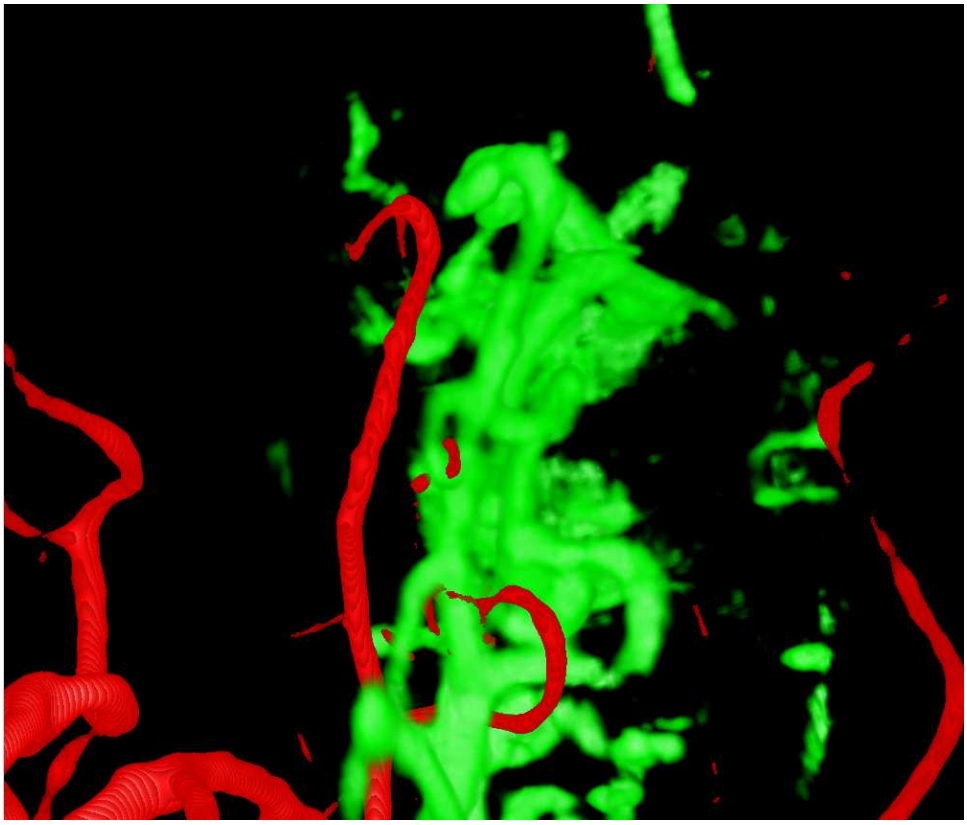

Figure 13: **Registration #1 - View 1 before registration - MRA (*red*) and USA #1 (*green*)**

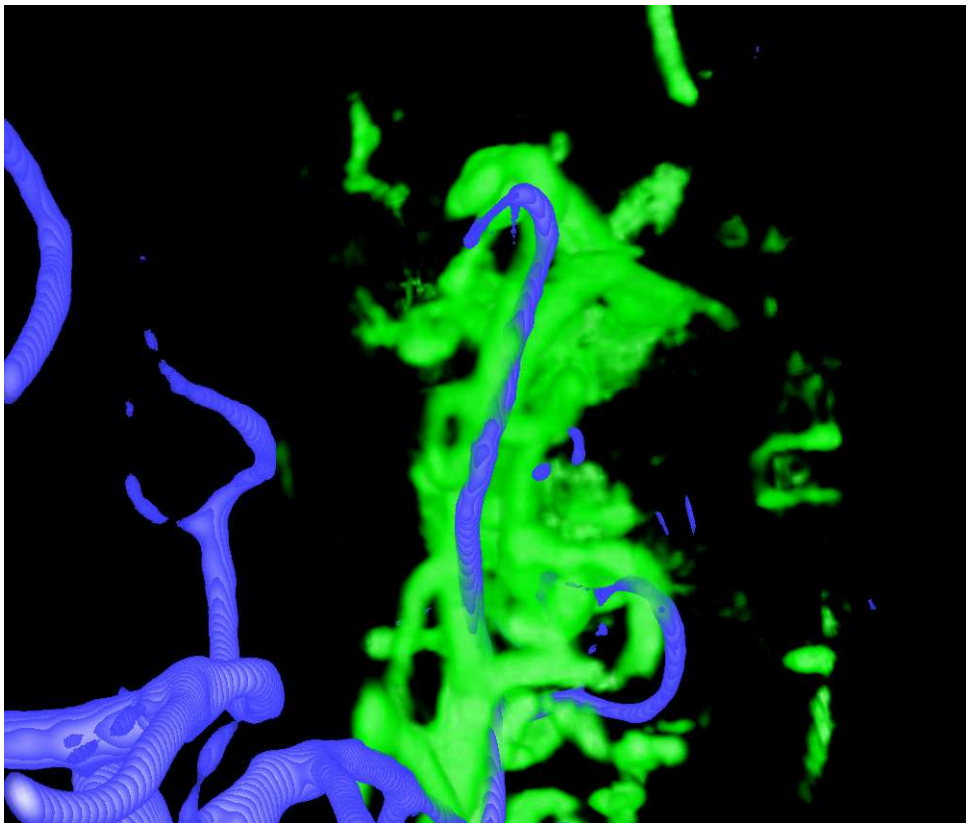

Figure 14: **Registration #1 - View 1 after registration - MRA (*blue*) and USA #1 (*green*)**

Parameter	**Value**
Test number	01_43
Max iterations	50
Min step length	0.1
Max step length	5
Spatial samples	50000
Histogram bins	128

Table 2: **Parameters used for registration #1 - Tumor 1**

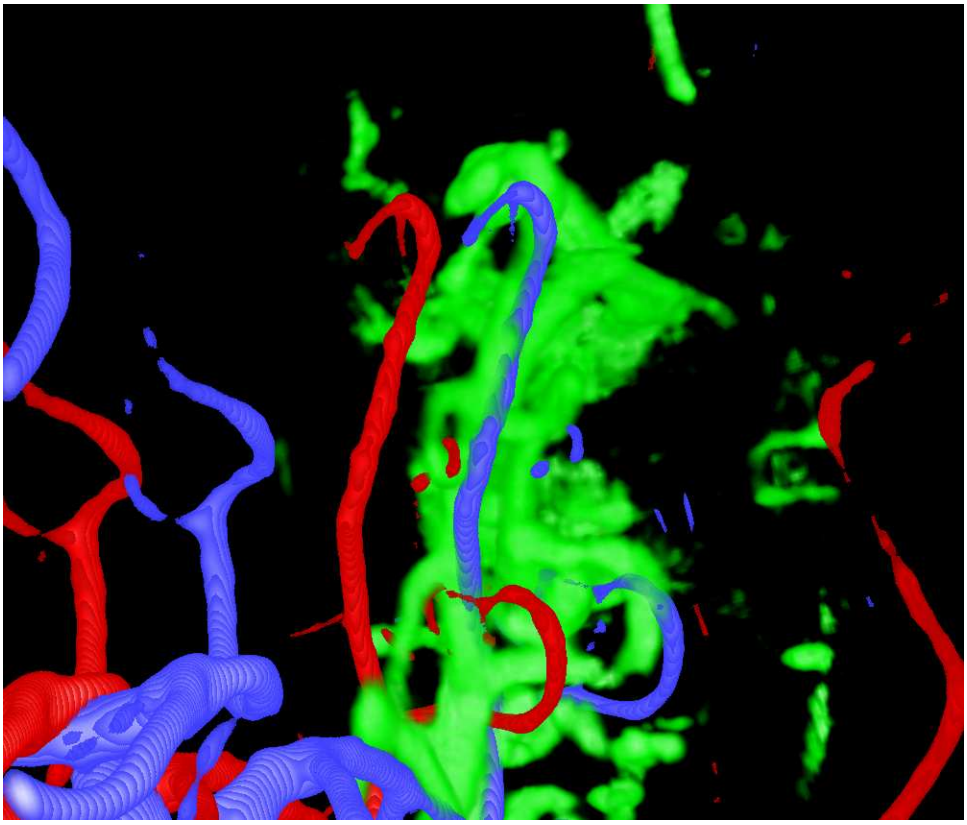

Figure 15: **Registration #1 - View 1 combined - MRA before (*red*), MRA after (*blue*) and USA #1 (*green*)**

Parameter	**Value**
Test number	01_43
X translation	-2.58385
Y translation	1.75104
Z translation	-9.32404
Metric value	-0.0299424
Iterations used	10

Table 3: **Resulting transform and values for registration #1 - Tumor 1**

12.2 Registration #2

This registration has been performed between the volumes USA #1 (fixed) and MRA (moving), using RegApp5. The parameters for this registration is presented in table 4. The resulting translation-parameters, along with the metric value and number of iterations used, is presented in table 5. As we can see, the resulting translation is very similar to the one presented for RegApp4 in the previous chapter.

Figures 16 through 18 show 3D renderings of the registration process.

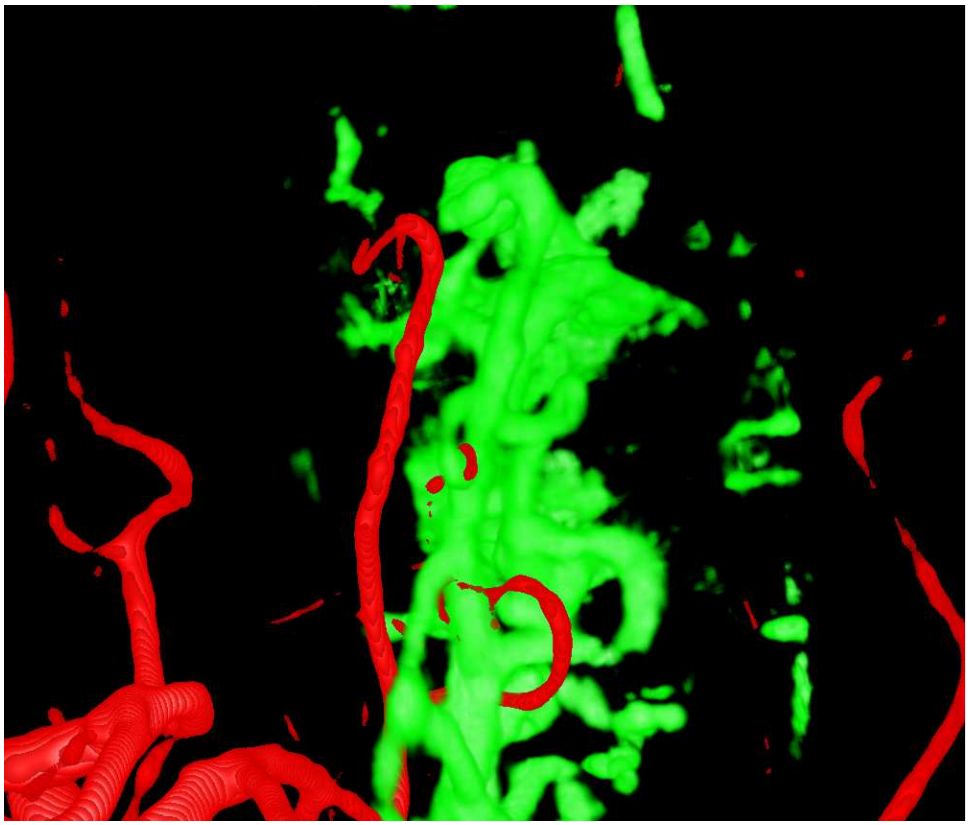

Figure 16: **Registration #2 - View 1 before registration - MRA (*red*) and USA #1 (*green*)**

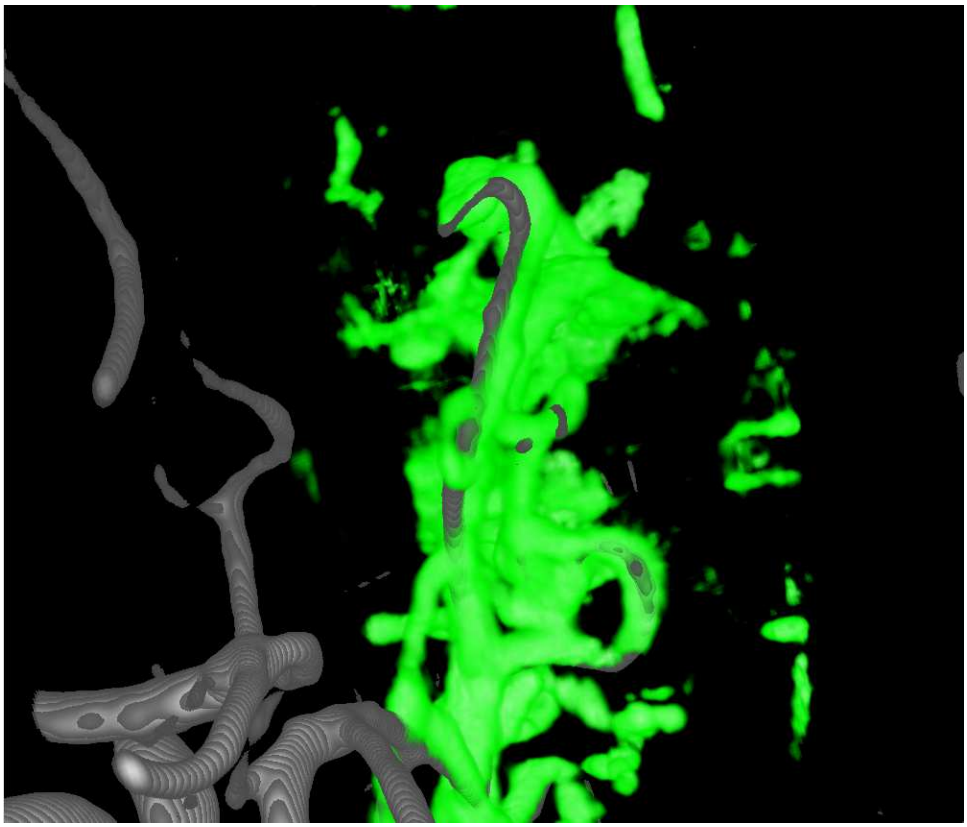

Figure 17: **Registration #2 - View 1 after registration - MRA (*grey*) and USA #1 (*green*)**

Parameter	**Value**
Test number	02_47
Max iterations	50
Initial radius	1.0
Minimum epsilon	0.015
Spatial samples	50000
Histogram bins	128

Table 4: **Parameters used for registration #2 - Tumor 1**

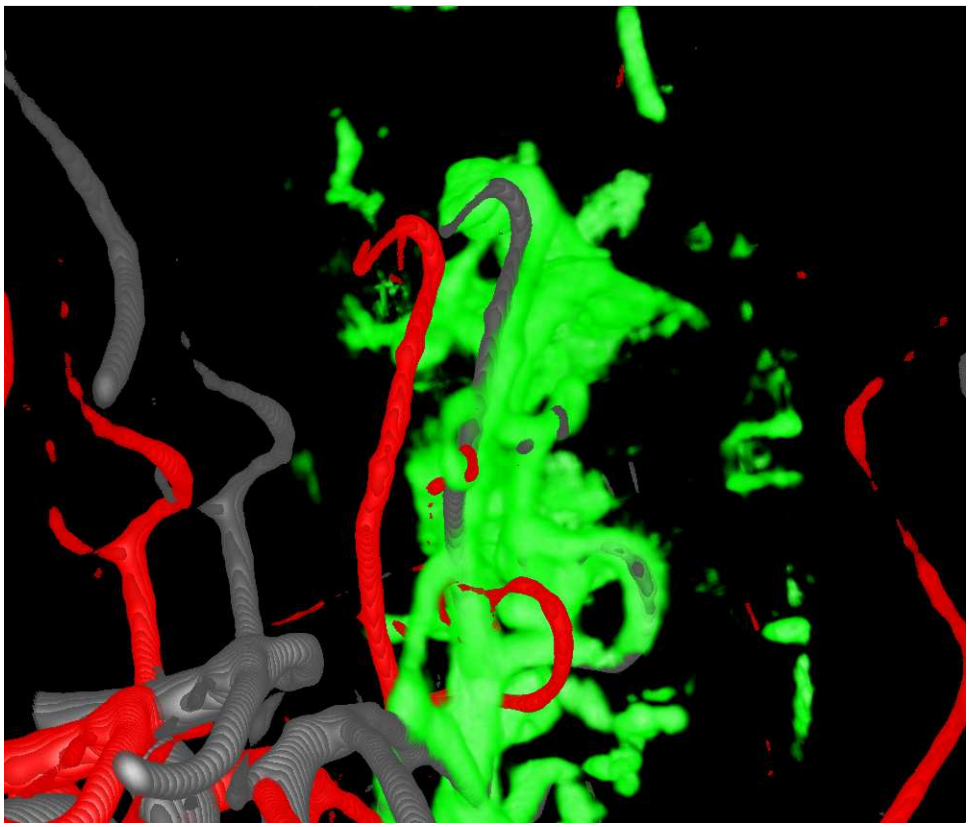

Figure 18: **Registration #2 - View 1 combined - MRA before (*red*), MRA after (*grey*) and USA #1 (*green*)**

Parameter	**Value**
Test number	02_47
X translation	-2.00232
Y translation	-0.821251
Z translation	-8.29955
Metric value	-0.030154
Iterations used	50

Table 5: **Resulting transform and values for registration #2 - Tumor 1**

13 Tumor 3 Registration Results

Data set Tumor 3 has also been used to test RegApp4 and RegApp5. Renderings of the resulting volumes are presented in the following chapters.

13.1 Registration #3

The first registration that has been performed for Tumor 3, is between the volumes USA (fixed) and MRA (moving), using RegApp4. The parameters for this registration is presented in table 6. The resulting translation-parameters, along with the metric value and number of iterations used, is presented in table 7. For this registration, the greatest translation is along the x-axis.

Figures 19 through 21 show 3D renderings of the image volumes, both before and after registration as well as a combined view.

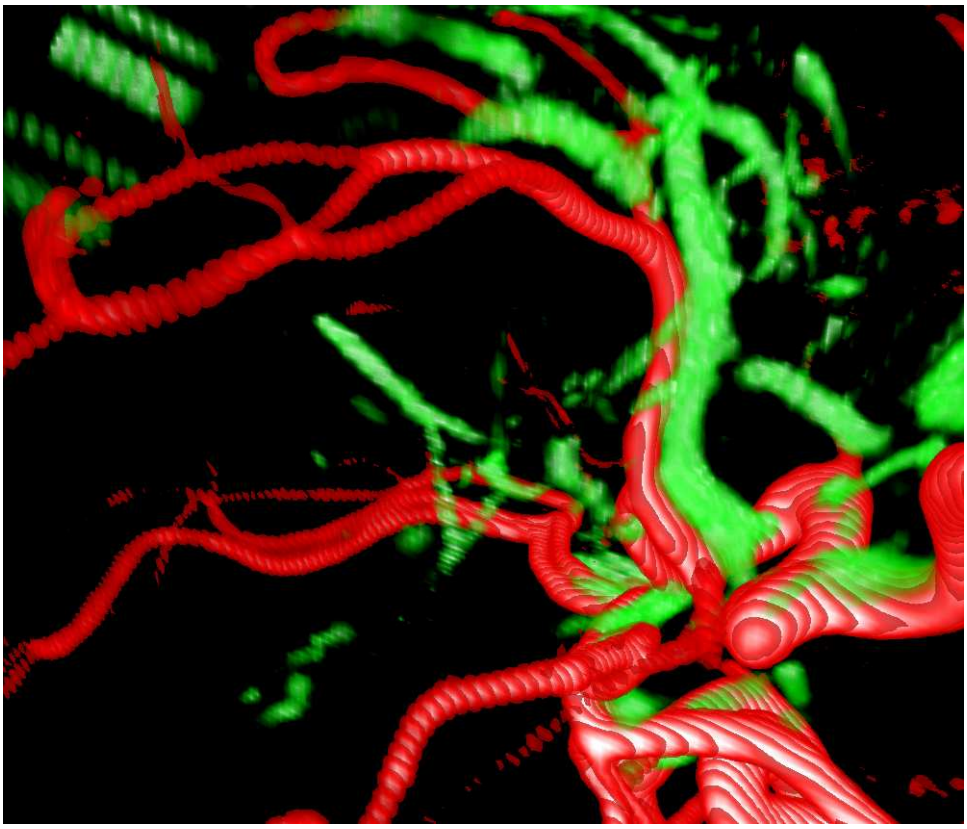

Figure 19: **Registration #3 - View 1 before registration - MRA (*red*) and USA (*green*)**

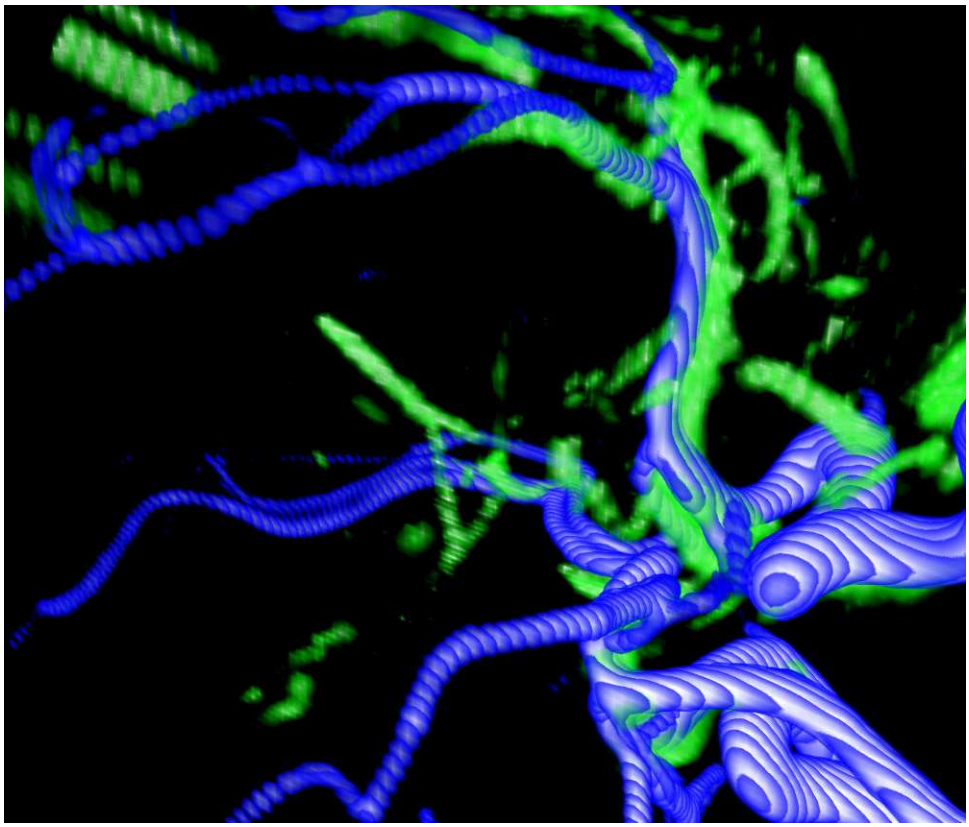

Figure 20: **Registration #3 - View 1 after registration - MRA (*blue*) and USA (*green*)**

Parameter	**Value**
Test number	03_02
Max iterations	50
Min step length	0.1
Max step length	5
Spatial samples	50000
Histogram bins	128

Table 6: **Parameters used for registration #3 - Tumor 3**

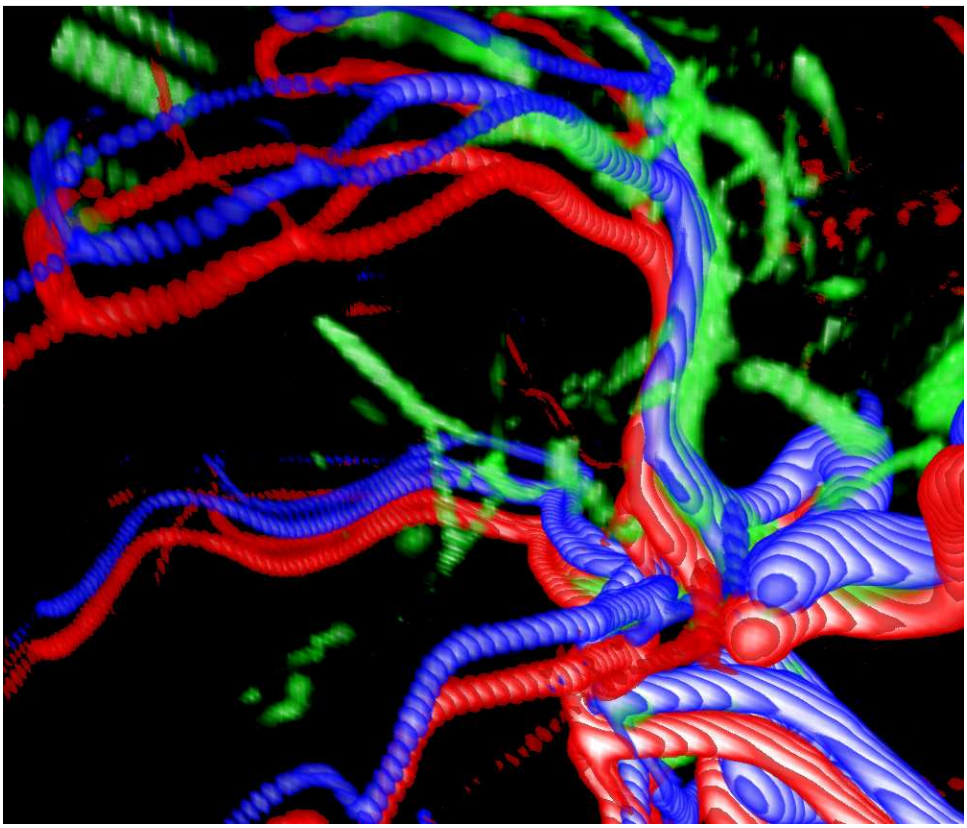

Figure 21: **Registration #3 - View 1 combined - MRA before (*red*), MRA after (*blue*) and USA (*green*)**

Parameter	**Value**
Test number	03_02
X translation	-5.09559
Y translation	-0.15675
Z translation	1.3554
Metric value	-0.0255
Iterations used	15

Table 7: **Resulting transform and values for registration #3 - Tumor 3**

13.2 Registration #4

Registration 4 has also been performed between the volumes USA (fixed) and MRA (moving) for Tumor 3, using RegApp5. The parameters for this registration is presented in table 8. The resulting translation-parameters, along with the metric value and number of iterations used, is presented in table 9. If we compare to the translation that was found for registration #3, the resulting translation in the x-direction differs with about 2 mm. This is also notable, by a manual comparison of the renderings.

Figures 22 through 24 show 3D renderings of the registration process.

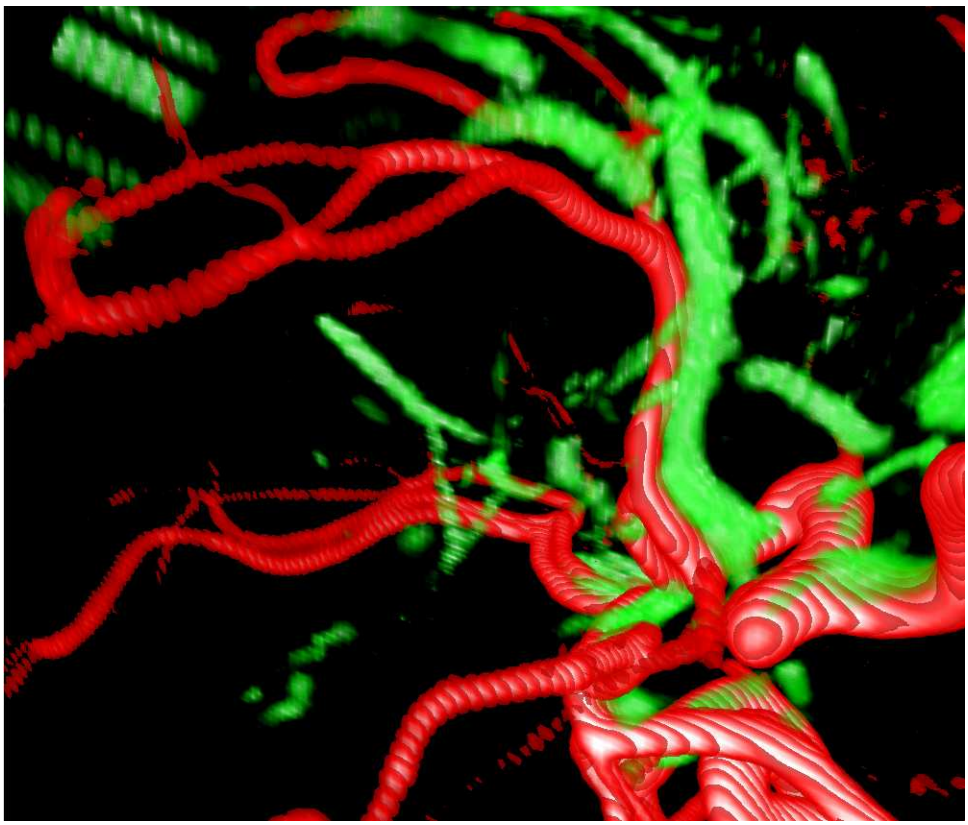

Figure 22: **Registration #4 - View 1 before registration - MRA (*red*) and USA (*green*)**

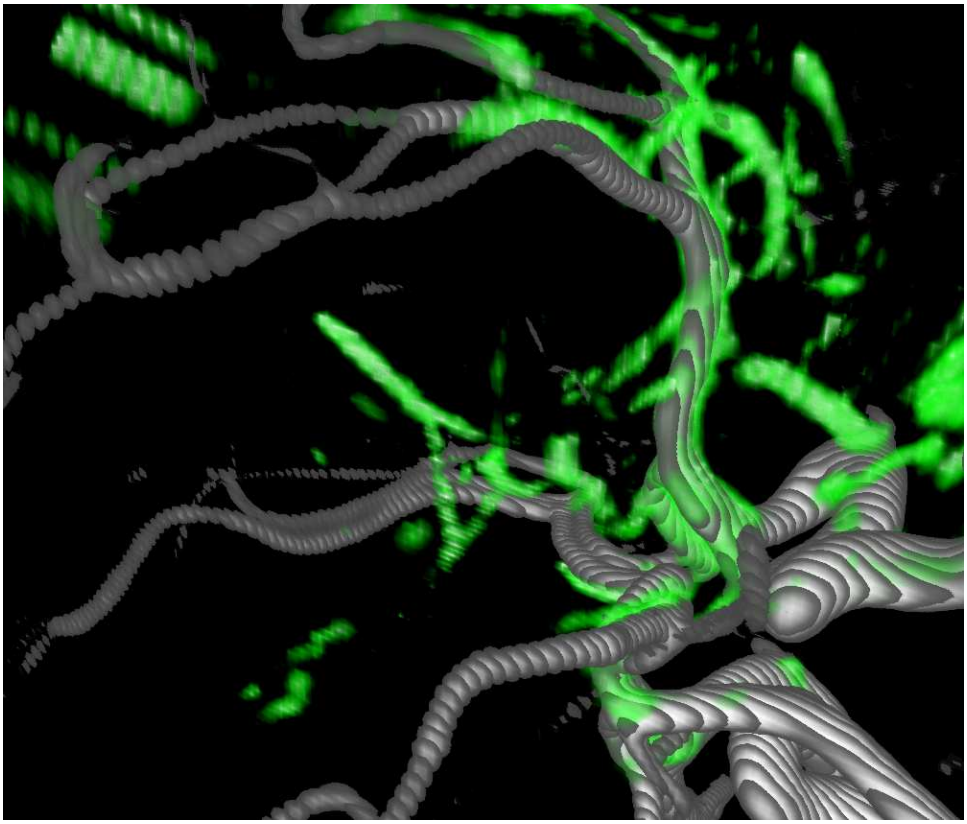

Figure 23: **Registration #4 - View 1 after registration - MRA (*grey*) and USA (*green*)**

Parameter	**Value**
Test number	04_02
Max iterations	50
Initial radius	1.0
Minimum epsilon	0.015
Spatial samples	50000
Histogram bins	128

Table 8: **Parameters used for registration #4 - Tumor 3**

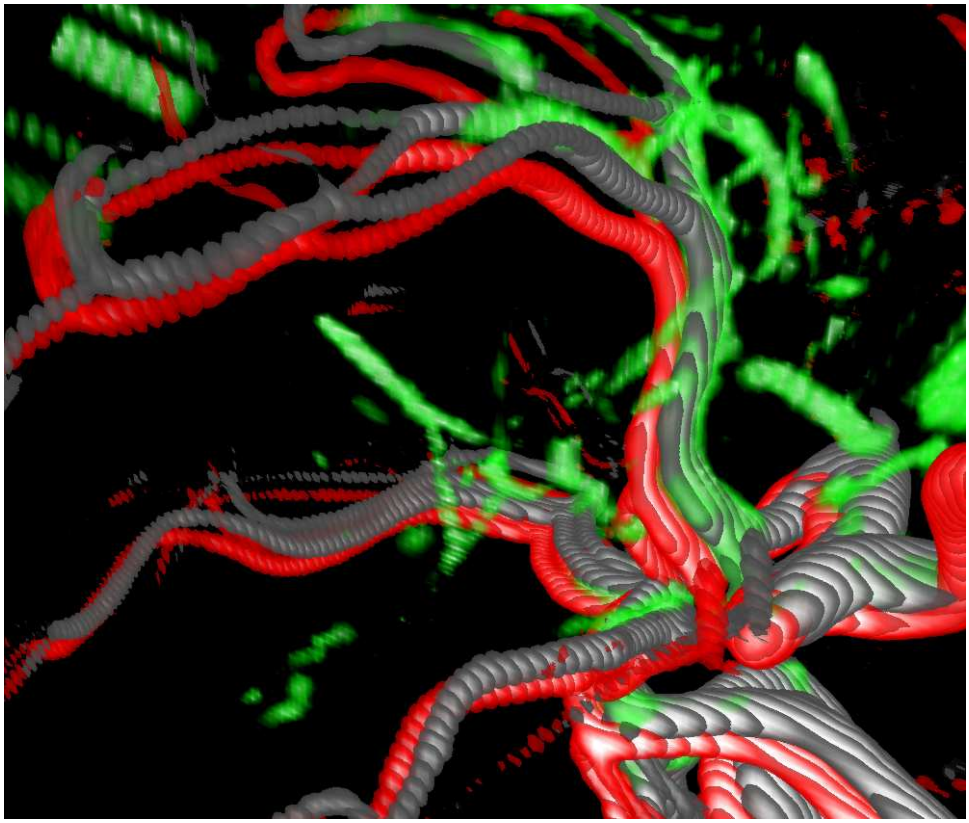

Figure 24: **Registration #4 - View 1 combined - MRA before (*red*), MRA after (*grey*) and USA (*green*)**

Parameter	**Value**
Test number	04_02
X translation	-2.95599
Y translation	-0.6468
Z translation	2.44463
Metric value	-0.031617
Iterations used	50

Table 9: **Resulting transform and values for registration #4 - Tumor 3**

14 Aneurism 1 Registration Results

Data set Aneurism 1 has been used to test all three applications. RegApp6 has 6 degrees-of-freedom, as it incorporates rotations as well as translations. The results for RegApp4, RegApp5 and RegApp6 are presented in chapters 14.1, 14.2 and 14.3, respectively.

14.1 Registration #5

The results of the registration between the volumes USA (fixed) and MRA (moving) on Aneurism 1, using RegApp4, is presented in this chapter. The parameters for this registration is presented in table 10. The resulting translation-parameters, along with the metric value and number of iterations used, is presented in table 11. For this registration, the greatest translation is along the x-axis.

Figures 25 through 27 show 3D renderings of the image volumes, both before and after registration as well as a combined view.

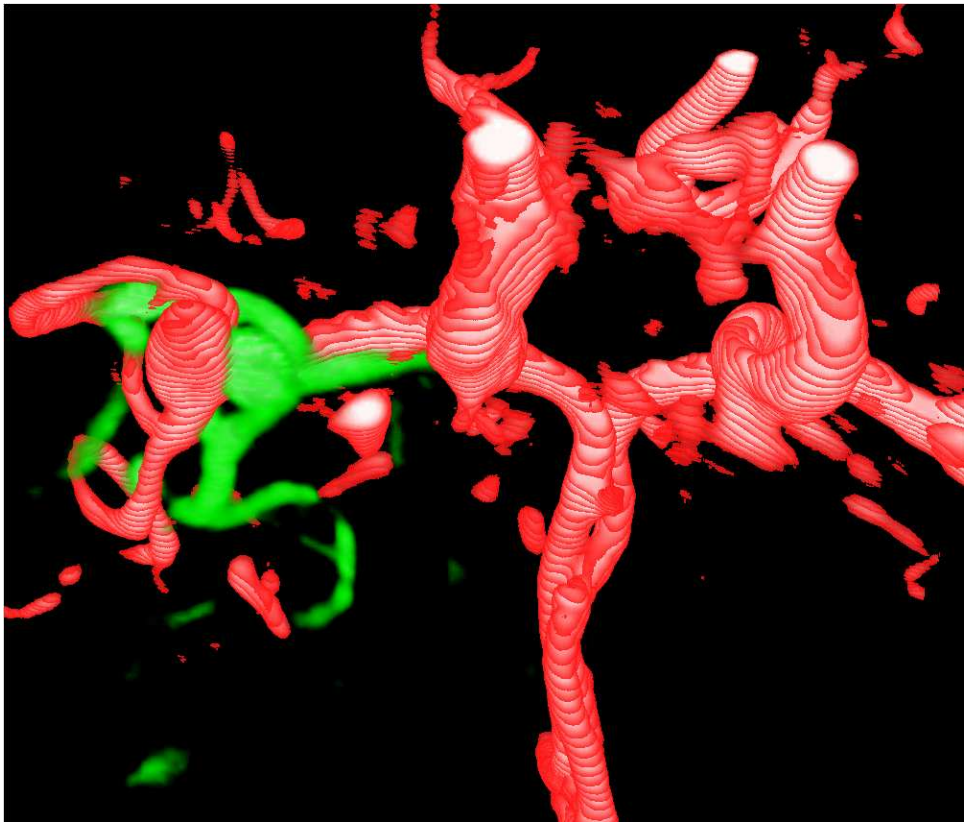

Figure 25: **Registration #5 - View 1 before registration - MRA (*red*) and USA (*green*)**

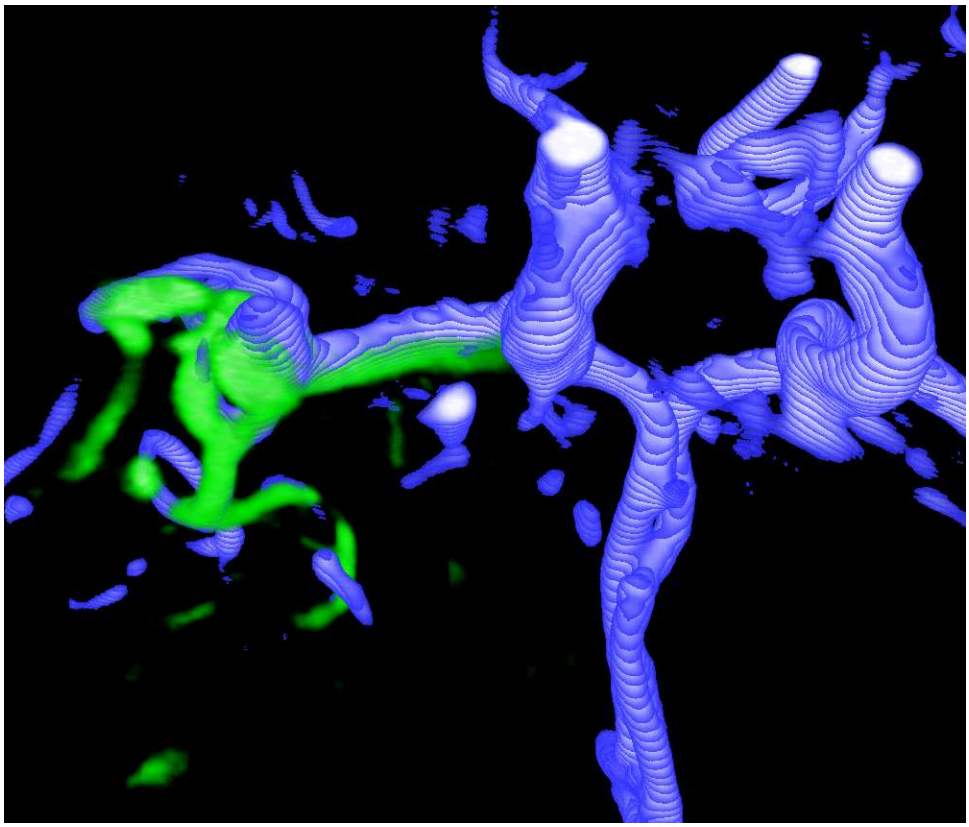

Figure 26: **Registration #5 - View 1 after registration - MRA (*blue*) and USA (*green*)**

Parameter	**Value**
Test number	05_02
Max iterations	50
Min step length	0.1
Max step length	5
Spatial samples	50000
Histogram bins	128

Table 10: **Parameters used for registration #5 - Aneurism 1**

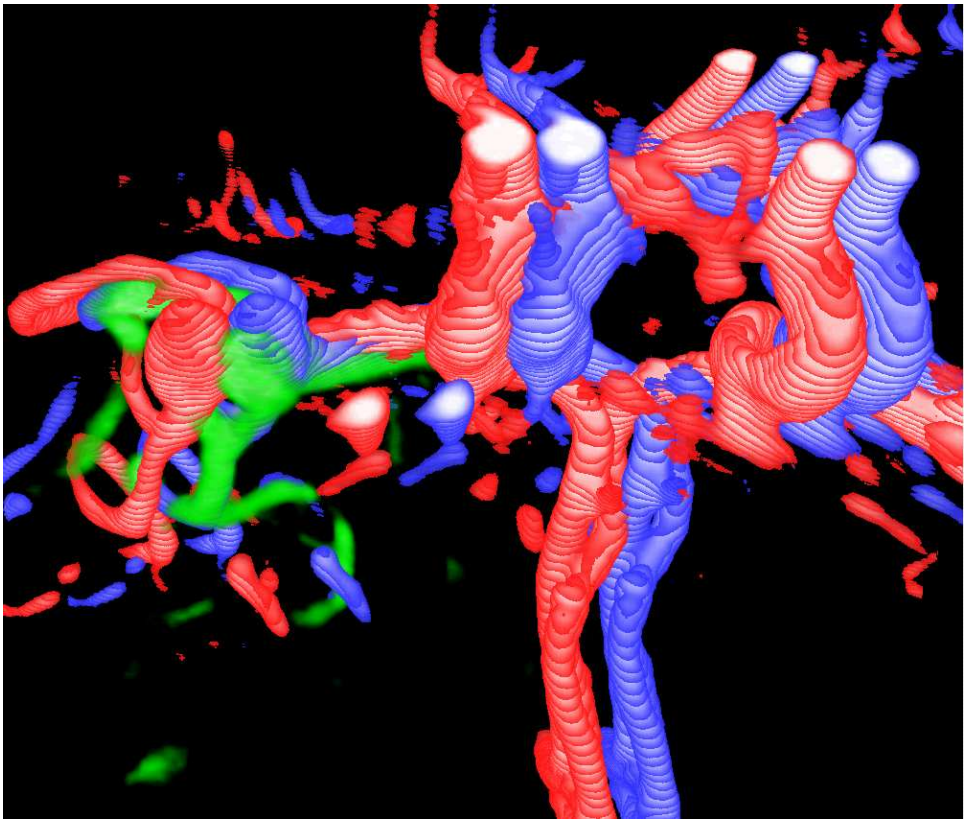

Figure 27: **Registration #5 - View 1 combined - MRA before (*red*), MRA after (*blue*) and USA (*green*)**

Parameter	**Value**
Test number	05_02
X translation	4.76304
Y translation	-2.40139
Z translation	-1.18243
Metric value	-0.02567
Iterations used	13

Table 11: **Resulting transform and values for registration #5 - Aneurism 1**

14.2 Registration #6

Registration 6 has also been performed between the volumes USA (fixed) and MRA (moving) for Aneurism 1, but now with RegApp5. The parameters for this registration is presented in table 12. The resulting translation-parameters, along with the metric value and number of iterations used, is presented in table 13. The difference in translation values, compared to registration #5 is less than, or about, 1 mm in all directions.

Figures 28 through 30 show 3D renderings of the registration process.

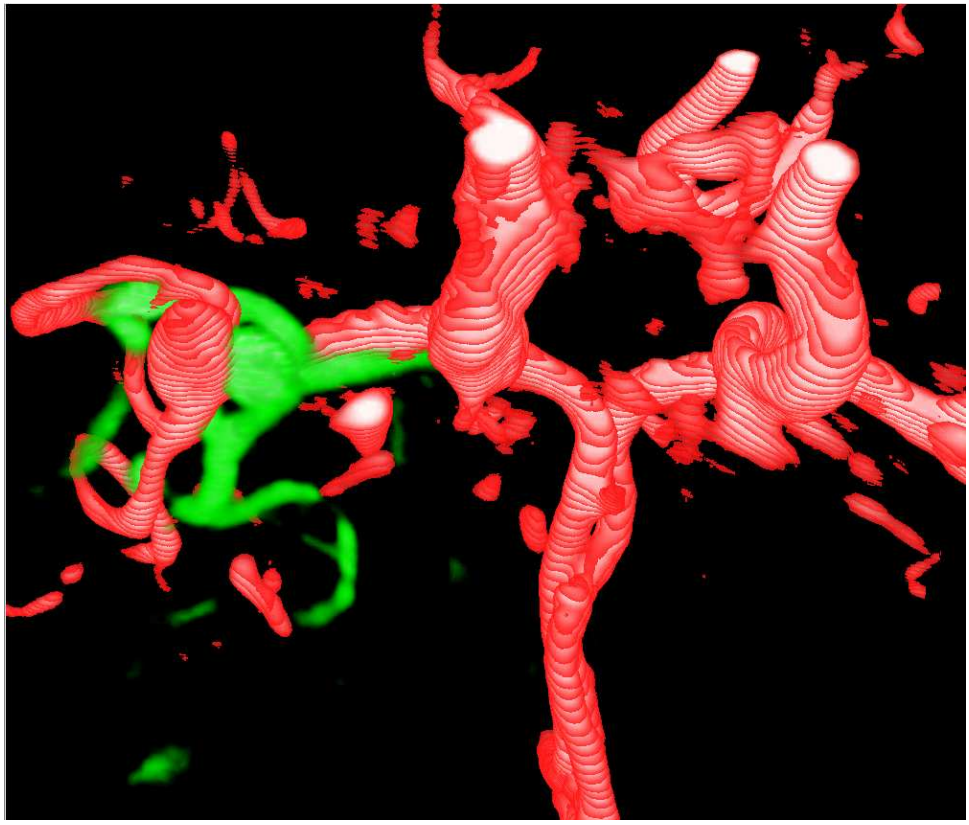

Figure 28: **Registration #6 - View 1 before registration - MRA (*red*) and USA (*green*)**

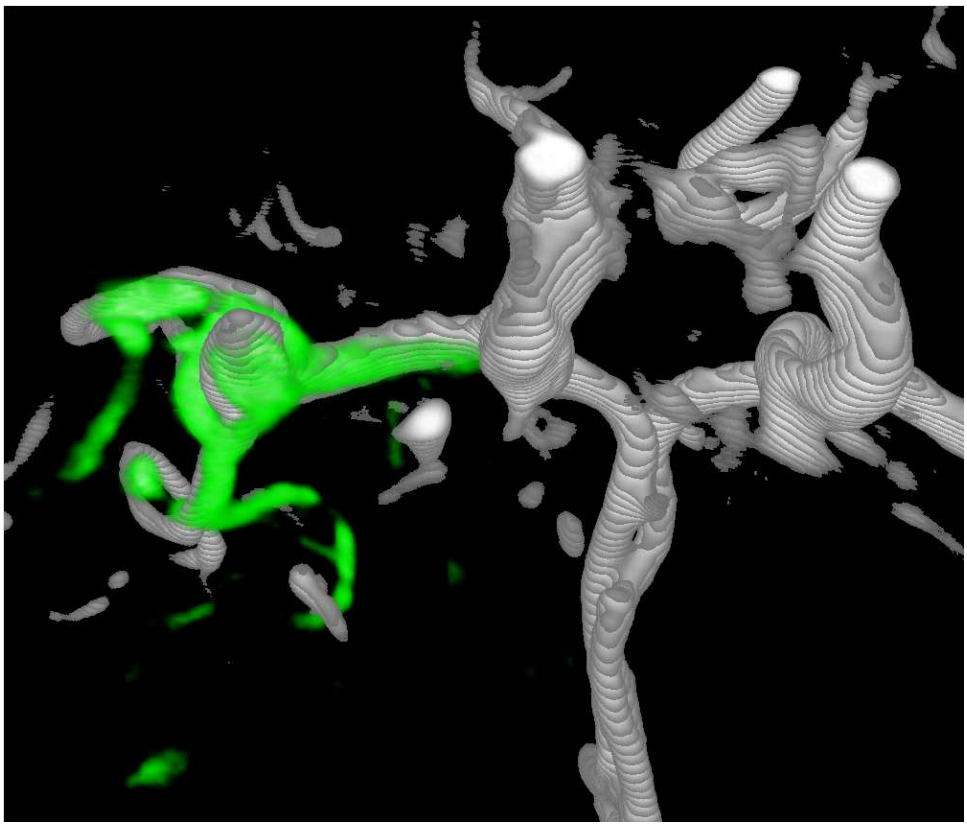

Figure 29: **Registration #6 - View 1 after registration - MRA (*grey*) and USA (*green*)**

Parameter	**Value**
Test number	06_02
Max iterations	50
Initial radius	1.0
Minimum epsilon	0.015
Spatial samples	50000
Histogram bins	128

Table 12: **Parameters used for registration #6 - Aneurism 1**

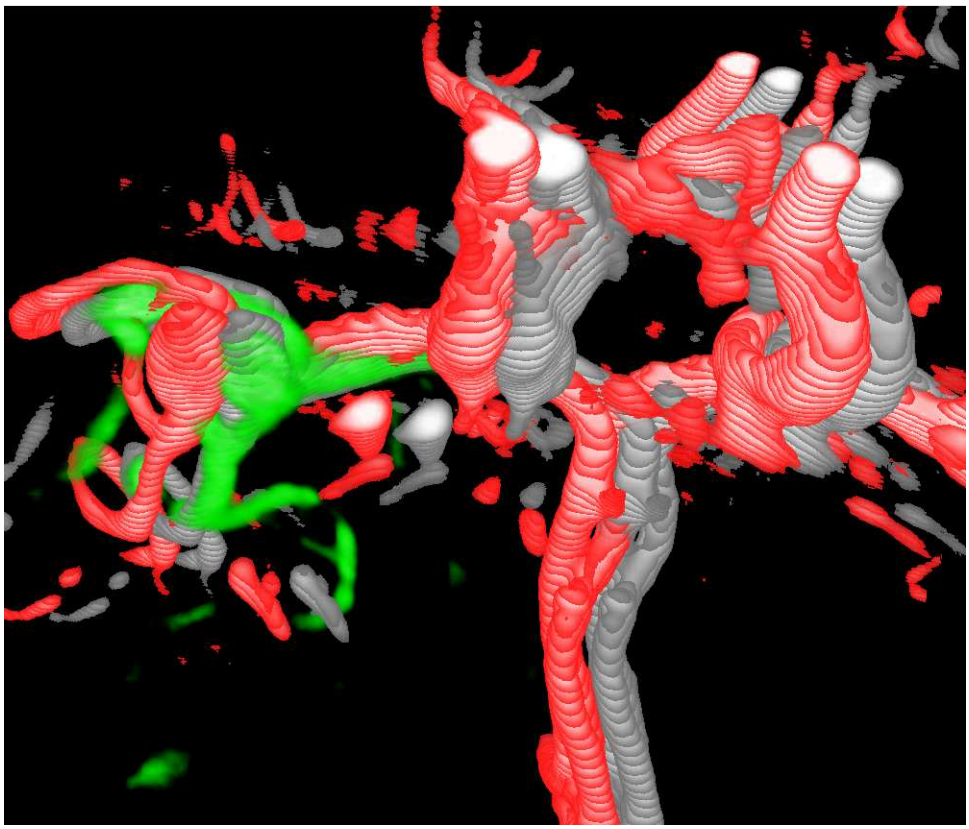

Figure 30: **Registration #6 - View 1 combined - MRA before (*red*), MRA after (*grey*) and USA (*green*)**

Parameter	**Value**
Test number	06_02
X translation	3.44712
Y translation	-1.34058
Z translation	-1.69735
Metric value	-0.0226275
Iterations used	50

Table 13: **Resulting transform and values for registration #6 - Aneurism 1**

14.3 Registration #7

The only registration that has been performed for RegApp6, is between the volumes USA (fixed) and MRA (moving) for Aneurism 1. The parameters for this registration is presented in table 14. The resulting translation-parameters, along with the metric value and number of iterations used, is presented in table 15. As we can se, the rotational values for this registration are almost neglectable.

Figures 31 through 33 show 3D renderings of the image volumes, both before and after registration as well as a combined view.

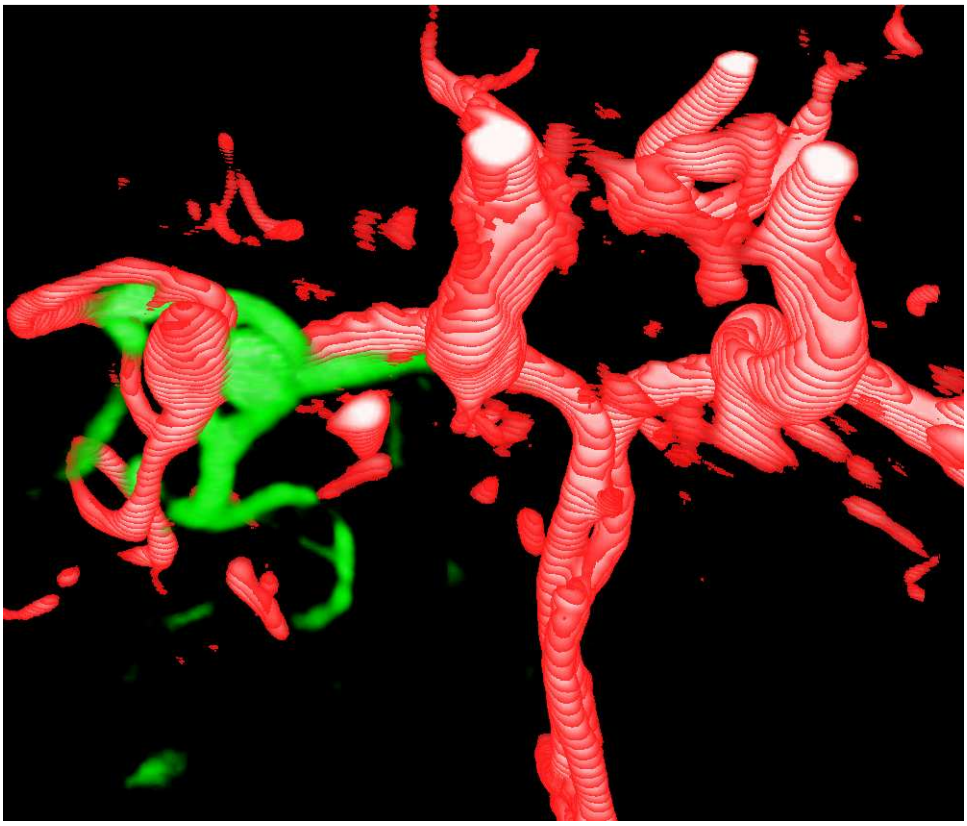

Figure 31: **Registration #7 - View 1 before registration - MRA (*red*) and USA (*green*)**

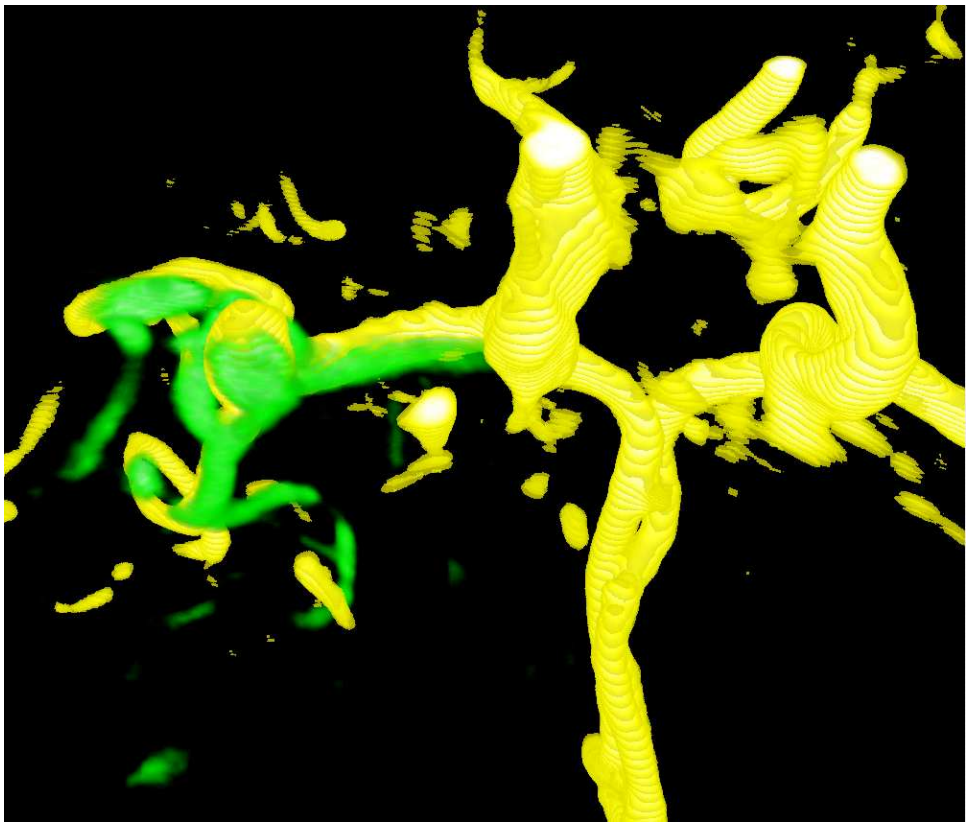

Figure 32: **Registration #7 - View 1 after registration - MRA (*yellow*) and USA (*green*)**

Parameter	**Value**
Test number	07_46
Max iterations	50
Min step length	0.1
Max step length	5
Spatial samples	50000
Histogram bins	128

Table 14: **Parameters used for registration #7 - Aneurism 1**

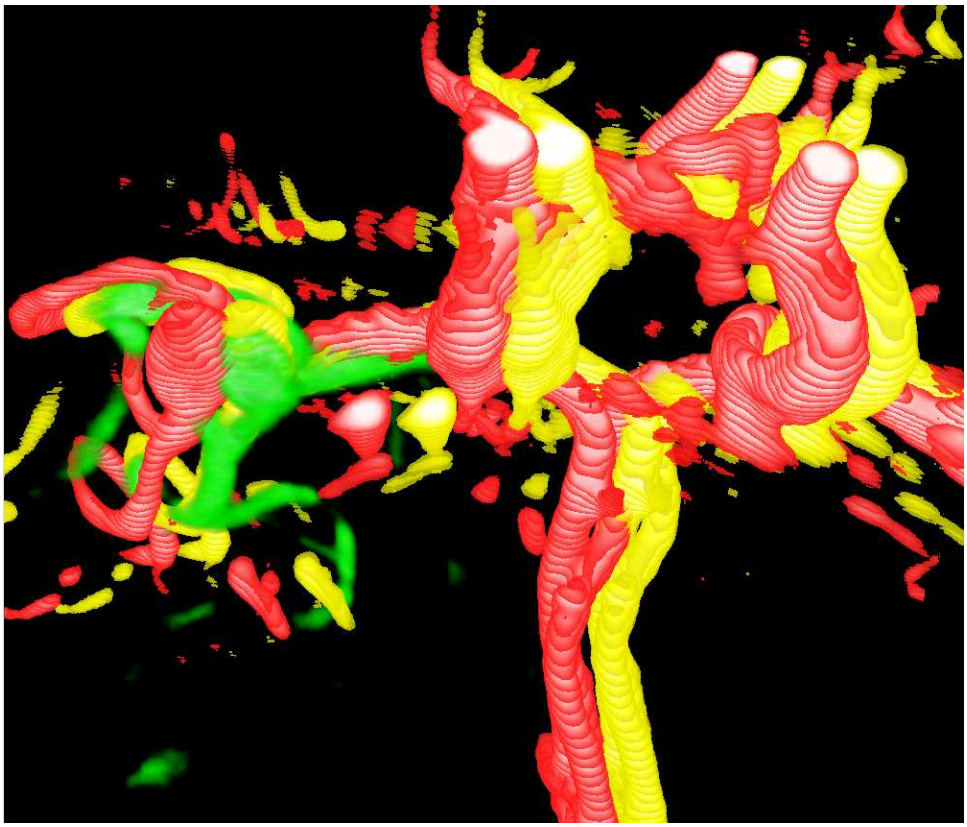

Figure 33: **Registration #7 - View 1 combined - MRA before (*red*), MRA after (*yellow*) and USA (*green*)**

Parameter	**Value**
Test number	07_46
X translation	3.66902
Y translation	-1.96558
Z translation	-1.37951
versor rotation	(0.0628226, -0.05273, -0.0083284)
Metric value	-0.1257314
Iterations used	36

Table 15: **Resulting transform and values for registration #7 - Aneurism 1**

Part VI

Discussion of Results

The results presented in the previous chapter are examples of successful registrations, at least from a subjective point of view. However, the applications differed in their performance, in both accuracy, performance, stability and reliability. These issues will be discussed in the following chapters. As we will se, some of the measures will be have to interpreted manually and subjectively, hence not making all of the them equally easily measured. Chapter 15 will discuss the stability, reliability and repeatability of the prototype applications. Performance, in terms of speed or execution times, is the topic of chapter 16, while a discussion on different measures of success is postponed to chapter 17. This chapter will also account for the goodness of the measures, used to evaluate the registration results acquired from the different registration methods.

This part will lead up to thoughts on improvements on the implementations and necessary future work, and a final conclusion, in part VII.

15 Stability and Reliability

The results presented in chapters 12 to 14 represented how well the applications *can* be. However, not all applications performed equally well. Each registration application will therefore be discussed and handled separately, with a presentation on their behavior regarding stability and reliability. The reasons for some of the algorithms' problems will be addressed as well. Executions with RegApp5 showed that registration with no preprocessing at all on the input images, gave the most stable results. This knowledge was therefore incorporated into the other registration applications as well, with a slight improvement in stability. The use of un-preprocessed input images also lowers the execution times, but this will not be discussed until chapter 16.

15.1 RegApp4

Even though RegApp4 was not the hardest to control, the reliability and stability of the results was somewhat mixed. The application returned many good results, but equally many poor results. A visual inspection of the results showed that the algorithm had a tendency of finding local minima in the wrong direction, even for consecutive runs with the same parameters. The application also converged fast towards an optimal value; i.e. got stuck. Nothing seemed to help on guiding the registration application in the right direction, and the best remedy seemed to be to use a minimal step length of 0.1, instead of skipping back and forth below the voxel size. The maximum step length had to be set as high as 5.0, especially for the data set Tumor 1 which had an apparent z-translation of about 10 mm, in order to be able to find the right translational coefficient.

By setting the spatial samples as high as 50 000, the application seemed to be a little more stable, but not sufficient to be considered a candidate for real-life applications. Un-preprocessed images seemed to be the best choice for all the applications, but neither that, nor an increase of the number of histogram bins (128), made the application fully reliable. In any case, the number of histogram bins is considered to have little impact on the calculations, as long as it is kept above a reasonable value of about 30. The best conceivable enhancement seems to be to transform it into RegApp5. That is, the only difference between RegApp4 and RegApp5 is that the gradient descent optimizer has been replaced by an evolutionary (1+1) optimizer for the latter.

15.2 RegApp5

Evidently the gradient descent optimizer has been difficult to parameterize. By exchanging the optimizer by an evolutionary (1+1) optimizer, the stability and reliability problems of the RegApp4 seems to be solved. This application rarely misses on finding a seemingly good transformation for any of the data sets. After a fine-tune on the parameters, there has been no need to adjust them at all, for any of the data sets. Taking into consideration that the *distance*, calculated as the length of the resulting transformation vector, varies from about 4 mm for tumor 3 to about 11 mm for tumor 1, this application seems to be a very flexible one.

The standard deviation of each of the translation components varies from 0.6 to 1.2 for translation components with a mean of 0 to 10, respectively. These measures has been calculated on the basis of 20 consecutive runs with the same parameters for a given data set. Figure 34 shows

such a diagram calculated from 20 consecutive runs on tumor 1. In appendix D similar tables for the other two data sets, utilizing RegApp5, is given. The parameters for the testing were the same as they were for registration #2, registration #4 and registration #6, presented in part V, which can be seen for instance in table 12. Technicians at SINTEF MedTech indicated that these results were good and sufficient.

The spatial samples had to be set as high as 50 000 for this application as well, in order to achieve stable results. An initial radius of 1.0 seemed to provide stable results, given an ϵ value of about 0.015. However, further investigation on parameter tuning could be performed, in order to get an even more stable application. Especially the ϵ value should be more tested, as the algorithm, roughly speaking, ran out of iterations every time.

15.3 RegApp6

The RegApp6 registration has been the most difficult application to parameterize. It has been even more erratic than RegApp4. Some descent results has been achieved, but mainly, the resulting translation parameters has been in different directions. The number of spatial samples has been as high as 200 000, to ensure a statistically sound estimation of the metric, but still the resulting transformation has been very mixed. Results for this application was therefore only presented for the smallest data set, Aneurism1. The number of histogram bins has been set to 128, which should be sufficient. The maximum step length has to be about 5.0, to prevent the optimizer to search too small an area.

A possible solution to the problematic behavior of this application would be a manual initialization. This way the bounds of the optimizer could be set much stricter, hence reducing the search area. Additionally, the application could be used on the results from RegApp5 as a good initial transformation, if there is evidence of a rotational offset. However, an initial inspection of the volumes show little signs of misalignment of the coordinate axes of the volumes. At the moment, an application that incorporates rotations does not seem necessary for this step.

	x-translation	y-translation	z-translation	Mattes' MI	distance
1	-2,69891	-1,56608	-9,86831	-0,030539	10,34989198
2	-2,43769	-0,964135	-9,99387	-0,0299011	10,33195656
3	-3,55081	-3,23935	-11,2958	-0,0308325	12,27585996
4	-3,05451	-2,51663	-10,4643	-0,0315082	11,18771793
5	-2,59401	-2,58896	-12,0202	-0,0304366	12,56649553
6	-2,04248	-2,40154	-8,36472	-0,030802	8,939108434
7	-2,62684	-2,8747	-10,165	-0,0304862	10,88537613
8	-2,30852	-1,13124	-8,01689	-0,032008	8,418996009
9	-2,03924	-2,99836	-8,90176	-0,0323709	9,611971367
10	-2,8302	-3,0297	-10,5818	-0,0314363	11,36501673
11	-1,47995	-2,22475	-10,7918	-0,0320158	11,11767565
12	-1,7298	-4,15945	-9,5235	-0,0300573	10,53519267
13	-3,26324	-3,06032	-10,0946	-0,0299747	11,04152358
14	-4,2361	-3,31453	-12,3186	-0,030036	13,44167245
15	-0,951828	-2,34701	-9,09129	-0,0306351	9,437477753
16	-2,33448	-2,80407	-8,32607	-0,0317886	9,090437123
17	-2,82285	-2,19652	-11,291	-0,033851	11,84398004
18	-2,36303	-2,45498	-11,2431	-0,0307003	11,74811198
19	-3,64798	-3,76036	-10,4089	-0,0317739	11,65303671
20	-2,80769	-2,86689	-10,4143	-0,0302866	11,16063734
mean	-2,5910079	-2,62497875	-10,1587905	-0,031072005	10,8501068
st.dev	0,763364274	0,786937022	1,193957534	0,001007632	1,288081114

Figure 34: **Standard deviations for Registration #2**

16 Performance

Registration of 3D images is a computationally expensive task, including repeated calculations of the similarity metric and transformation coefficients, and interpolations of off-grid positions. However, the use of angio-graphic images without any preprocessing steps is time-saving. Additionally, no normalization of the volumes is needed when Mattes' Mutual Information is used, as this metric rescales internally. This metric also picks its sample points once, and not every iteration, which is an economic approach. A possible incorporation of rotations also slows down the registration, as the parameter space grows dramatically from 3 to 6 degrees-of-freedom. If there is not any signs of a rotational offset, such methods should be avoided.

None of my methods incorporate a hierarchical approach, which may slow down the registration procedure. This is due to the construction of the image-pyramide prior to registration. However, this could be gained with a faster convergence to the optimum.

As mentioned in part IV, the test data sets range from a total number of voxels of 4.2 to 34.2 million. This is also noticeable on the applications, as larger data sets increase the running times. Volumes should therefore be kept as small as possible, without loosing important information. All execution times for this chapter includes the reading in of the fixed and moving image, and the writing of the transformed moving image. The characteristics of the computer used for the registration procedures was given in chapter 9.

16.1 RegApp4

This application, along with RegApp5 did not have the performance-drawback of incorporating rotations. Actually, no additional and time-consuming operations were performed. The execution times for this operation varied from 15 to 20 minutes depending on the size of the input-volumes. However, it is believed that this figure could drop a bit, if the testing was to be performed on a high-end computer. Especially, the amount of memory has a bigger potential.

16.2 RegApp5

As mentioned in the previous chapter, this application was the most reliable and stabile one of the three applications that was tested. Not only that, it was also the fastest application. Execution times varied from 3 to 9 minutes, depending on the volume-sizes of the input volumes. The reading and writing of the images was the most time-consuming part, as the registration itself was done in seconds. If the input volumes are kept small and the computer is replaced, the execution times of this application has real potential of approaching very appealing figures. Because of the fact that RegApp4 and RegApp5 are equal, except from the optimizer, this shows that the evolutionary (1+1) optimizer is preferable.

16.3 RegApp6

As mentioned earlier, RegApp6 incorporate rotations into the transformation, which yields a significantly increased parameter space for the optimizer. It has also been proved that types of gradient descent optimizer are relatively slow, at least compared to the evolutionary (1+1)

optimizer. This is also reflected by the execution times for this application. A typical registration procedure lasted for about 25-30 minutes, and that was for the smallest data set. This demonstrates that rotational components should not be used, unless a study of the data sets indicate a rotational misalignment. It is worth mentioning that all the applications' execution times possibly could be somewhat reduced, if parallelism was built into both the registration hardware and software. Especially, this could be utilized in the point sampler function, as no sampled point in the moving image depends on any other voxel in the moving image.

17 Measures of Success

Volume-to-volume registration is not an easily manageable problem. It is actually ill-posed, meaning that no obvious result exists. This considerably complicates the task of measuring the successfulness of registration results. The question is, how does one decide whether a particular registration was successful, or how close it came to the true registration? And likewise, how can a set of registration results be compared, and one decided to be the best? This is a problem in registration evaluation, as an *objective* measure of success would be preferable in this setting.

A similarity measure is an objective measure, but the use of this to measure success would just give the same result as the registration itself. A different similarity measure than the one used in the registration process, would possibly measure the degree of successfulness differently, but the question then is; why was not this similarity measure used in the registration process itself? Another aspect of this, is that the optimal similarity measure value does not necessarily correspond to an optimal registration. This indicates that a measure that is *independent* of the registration process should preferably be used for measuring success.

This chapter presents the way that success was measured for this report. Additionally, other ways of measuring success is given.

17.1 Use of "Gold Standard"

The common way of measuring success is to compare a resulting registration to a known correct transformation, a gold standard, and was introduced by West et al. [33]. This correct transformation can be obtained by a careful manual selection of homogenous points in the volumes. The resulting transformation of the volumes with respect to the selected points, defines an optimal transformation. Any transformation obtained by automatic algorithms, without the use of such points, can therefore be compared to the golden standard. This will give both an objective and independent measure of success for the automatic registration [33].

The number of points used to obtain the golden standard must exceed the degree of freedom (DOF) of the transformation used in the registration process. Only translations would require 3 points, the use of rotations as well would require 6 points, and so on [33]. Additionally, the points would have to be collinear in order to restrict the transformation in the intended way. The use of a gold standard has one requirement though, a navigation system with support for choosing points in the two volumes must exist.

17.2 Manual Inspection by Experts

If there is no available system for calculating a gold standard, other ways of measuring success must be employed. Because the registration process' goal is to facilitate the use of multiple imaging modalities in neurosurgical guidance, a way to measure success would be to ask trained clinicians of their opinion of obtained results. This is a highly subjective approach, but they could verify if the images are well enough aligned to be used during surgery. This approach was employed by Harg in his master assignment [9], and will be adopted in this one as well . A navigation system with the ability to rotate, zoom and cut out cross planes in the images, is however preferable in order to obtain reasonable opinions from the experts, but this was not accessible for Harg [9]. Angio-graphic volumes, however, have high visual quality and are more

easily evaluated than the case is for tissue volumes.

To get an evaluation of the 3D renderings presented in V, they was presented to 4 neurosurgeons, as well as 6 researchers at SINTEF MedTech. They were asked to rate the registrations with either *not sufficient*, *possibly sufficient* or *sufficient*, for clinical purposes. The questionnaire-form is presented in appendix C. Note also that the view presented in appendix B was not presented at that time. The results of the questionnaire are included in table 16.

Reg.no.	**Overall**			**Clinicians**			**Researchers**		
	N	**P**	**S**	**N**	**P**	**S**	**N**	**P**	**S**
1	6	4	0	2	2	0	4	2	0
2	0	3	7	0	1	3	0	2	4
3	1	6	3	0	2	2	1	4	1
4	0	2	8	0	1	3	0	1	5
5	1	7	2	0	3	1	1	4	1
6	0	4	6	0	0	4	0	4	2
7	1	7	2	0	3	1	1	4	1

Table 16: **Result of the evaluation by clinicians and researchers. Number of responses per registration no. and option (N = Not sufficient, P = Possible sufficient, S = Sufficient).**

What we can conclude from the results, is that all the tests for RegApp5, registrations number 2, 4 and 6, was successfully registered. Actually, none of the participants felt that any of the tests for RegApp5 was not sufficient to be used for clinical purposes. Registration #4 was the registration that was considered the overall best, but registration #6 was regarded especially well by the clinicians. However, a cross-sectional cutting plane would ease the evaluation process additionally, in the way that a cut through the blood vessel renderings could be performed.

Part VII

Conclusion

Throughout this report, various approaches for future improvement has been mentioned. These will be commented in this final part of the report. Finally, a conclusion of the work done in this report is given, summarizing the results and experiences that has been achieved.

18 Future Work

Even though the results of RegApp5 is promising, much work remains, in order to possess the registration system that was described in chapter 2.2. The most difficult part of the registration system has yet not been solved. Additionally, in order to be able to test promising applications, proper equipment must become available. Nevertheless, the methods that has been developed should be further investigated, in order to achieve a possible increase in usability. These topics will be commented upon below.

18.1 Phase III of the Registration System

Last year, Harg developed an adequate registration application for phase I [9]. With my contribution to phase II, only phase III remains unaddressed. A non-rigid extension to the US-to-MRI registration is, perhaps, the most difficult one as well. Little literature exists, and for that reason it will be a tremendous challenge. Nevertheless, with phase III incorporated, medical imaging modalities will be better utilized, in order to help neurosurgeons perform clinical operations.

18.2 Tools for Software Evaluation

To ensure stability and reliability of the applications, they will have to be thoroughly tested. Currently, there exists no system available at SINTEF MedTech to perform evaluation with the use of gold standards. The existence of such a system is highly desirable, and should optimally be implemented as soon as possible. This way, the value of the registration algorithms could more easily be determined. The approach using experts' opinions, is not optimally adjusted for either, as no method currently exists to obtain a cross-section view of the volumes. Preferably, this should also be part of the navigation system as soon as possible, to aid inspection of the results.

18.3 Further Testing of RegApp5

RegApp5 should be further investigated, in order to verify, and enhance, both the stability and quickness of the application. Fully elaborated, RegApp5 should be incorporated into CustusX (see chapter 7.2), to be used intraoperatively.

19 Conclusion

The goal of this thesis was to propose, and implement methods for solving registration of a preoperative MRI volume, with an intraoperative US volume, acquired before the start of an operation. Solutions based on Mattes' Mutual Information have been implemented, along with a variety of optimization techniques and transformations. Further, all of the applications used angio-graphic volumes that was not preprocessed with any filter as input-volumes.

These applications have been tested on clinical data from relevant surgical operations. One of the solutions, using an evolutionary (1+1) optimizer while discarding rotational movement, has proven to be both stable, reliable, fast and accurate. A very similar application using a regular step gradient descent optimizer proved to be more unreliable and slow. However, the most unreliable application considered rotational transformations as well. This application employed a type of gradient descent optimizer as well. The applications that were based on such optimizers, also proved to be significantly slower than the one based on the evolutionary optimizer. The gradient descent-based optimizers were very hard to parameterize, and produced inconsistent results for subsequent executions with the same parameters.

The application based on the evolutionary optimizer, achieved very good evaluation results, through a visual inspection, by clinicians and researchers, of 3D renderings of the registrations. The results was said to be sufficiently accurate to be used in clinical applications, for all test sets of MRI-to-US registration.

References

[1] Richard D. Bucholz, David D. Yeh, Jason Trobaugh, Leslie L. McDurmont, Christopher D. Sturm, Carol Baumann, Jaimie M. Henderson, Ari Levy, and Paul Kessman. The correction of stereotactic inaccuracy caused by brain shift using an intraoperative ultrasound device. In *Proceedings of the First Joint Conference on Computer Vision, Virtual Reality and Robotics in Medicine and Medial Robotics and Computer-Assisted Surgery*, pages 459–466. Springer-Verlag, 1997.

[2] P.J. Edwards, D.J. Hawkes, G.P. Penney, and M.J. Clarkson. *Medical Image Registration*, volume 5 of *Biomedical Engineering*, chapter 12. Guiding Therapautic Procedures, pages 253–280. CRC Press, 2001. Ed. Hajnal, J.V. and Hill, D.L.G. and Hawkes, D.J.

[3] J.M. Fitzpatrick, D.L.G. Hill, and C.R. Maurer Jr. *Handbook of Medical Imaging*, volume 2. Medical Image Processing and Analysis, chapter 8. Image Registration. SPIE Press, 2004. Ed. M. Sonka and J.M. Fitzpatrick.

[4] David G. Gobbi, Roch M. Comeau, Belinda K.H. Lee, and Terry M. Peters. Integration of intra-operative 3d ultrasound with pre-operative mri for neurosurgical guidance. In *Engineering in Medicine and Biology Society, 2000. Proceedings of the 22nd Annual International Conference of the IEEE*, volume 3, pages 1738–1740. IEEE EMBS Society, 2000.

[5] David G. Gobbi, Belinda K. H. Lee, and Terence M. Peters. Correlation of preoperative mri and intraoperative 3d ultrasound to measure brain tissue shift. In Seong K. Mun, editor, *Medical Imaging 2001: Visualization, Display, and Image-Guided Procedures*, volume 4319, pages 264–271. SPIE, 2001.

[6] David G. Gobbi and Terry M. Peters. Interactive intra-operative 3d ultrasound reconstruction and visualization. In Takeyoshi Dohi and Ron Kikinis, editors, *Medical Image Computing and Computer-Assisted Intervention - MICCAI 2002, 5th International Conference, Tokyo, Japan, September 25-28, 2002, Proceedings, Part II*, volume 2489 of *Lecture Notes in Computer Science*, pages 156–163. Springer, 2002.

[7] Aa. Gronningsaeter, A. Kleven, S. Ommedal, T.E. Aarseth, T. Lie, F. Lindseth, T. Langø, and G. Unsgård. Sonowand, an ultrasound-based neuronavigation system. *Neurosurgery*, 47(6):1373–1380, December 2000.

[8] E. Harg. Multimodal volume-to-volume registration. Depth Study, 2004.

[9] E. Harg. Volume-to-volume registration. Master's thesis, Norwegian University of Science and Technology, NTNU, 2005.

[10] D.J. Hawkes. *Medical Image Registration*, volume 5 of *Biomedical Engineering*, chapter 2. Registration Methodology - Introduction, pages 11–38. CRC Press, 2001. Ed. Hajnal, J.V. and Hill, D.L.G. and Hawkes, D.J.

[11] D.L.G. Hill and P. Batchelor. *Medical Image Registration*, volume 5 of *Biomedical Engineering*, chapter 3. Registration Methodology: Concepts and Algorithms, pages 39–70. CRC Press, 2001. Ed. Hajnal, J.V. and Hill, D.L.G. and Hawkes, D.J.

[12] D.L.G. Hill and J. Jarosz. *Medical Image Registration*, volume 5 of *Biomedical Engineering*, chapter 10. Registration of MR and CR images for clinical applications, pages 217–232. CRC Press, 2001. Ed. Hajnal, J.V. and Hill, D.L.G. and Hawkes, D.J.

[13] Luis Ibañes, William Schroeder, Lydia Ng, and Josh Cates. *ITK Software Guide*, chapter 8. Registration, pages 215–312. Kitware Inc., 2003.

[14] Thomas Lange, Sebastian Eulenstein, Michael Hünerbein, and Peter-Michael Schlag. Vessel-based non-rigid registration of mr/ct and 3d ultrasound for navigation in liver surgery. *Computer Aided Surgery*, 8:228–240, 2003.

[15] M. Letteboer. *Intraoperative 3D ultrasonography for image-guided neurosurgery.* PhD thesis, University of Utrecht, 2004.

[16] M.M.J. Letteboer, P.W.A. Willems, M.A. Viergever, and W.J. Niessen. Non-rigid registration of 3d ultrasound images of brain tumors acquired during neurosurgery. In R.E. Ellis and T.M. Peters, editors, *Medical Image Computing and Computer-Assisted Intervention - MICCAI 2003 6th International Conference, Montréal, Canada, November 15-18, 2003, Proceedings, Part II*, volume 2879 of *Lecture Notes in Computer Science*, pages 408–415. Springer, 2003.

[17] F. Lindseth, J.H. Kaspersen, S. Ommedal, T. Langø, G. Unsgaard, and T.A.N. Hernes. Multimodal image fusion in ultrasound-based neuronavigation: improving overview and interpretation by integrating preoperative mri with intraoperative 3d ultrasound. *Computer Aided Surgery*, 8:49–69, 2003.

[18] F. Lindseth, S. Ommedal, J. Bang, G. Unsgård, and T.A.N. Hernes. Image fusion of ultrasound and mri as an aid for assessing anatomical shifts and improving overview and interpretation in ultrasound-guided neurosurgery. In *Proceedings of Computer Assisted Radiology and Surgery (CARS)*, pages 247–252, Berlin, Germany, 2001. Elesvier Science B.V.

[19] D. Lloret, J. Serrat, A.M. López, and J.J Villanueva. Ultrasound to magnetic resonance volume registration for brain sinking measurement. In F.J. et al. Perales, editor, *IbPria 2003*, number 2652 in Lecture Notes in Computer Science, pages 420–428. Springer-Verlag, Berlin, 2003.

[20] Frederik Maes, Dirk Vandermeulen, and Paul Suetens. Comparative evaluation of multiresolution optimization strategies for multimodality image registration by maximization of mutual information. *Medical Image Analysis*, 3(4):373–386, 1999.

[21] C. Matula. Intra-operative ct and image-guided surgery: an introduction. *MedicaMundi*, 42(1):2–5, 1998.

[22] C. Nimsky, O. Ganslandt, P. Hastreiter, and R. Fahlbusch. Intraoperative compensation for brain shift. *Surgical Neurology*, 56(6):357–364, December 2001.

[23] X. Pennec, P. Cachier, and N. Ayache. Tracking brain deformations in time sequences of 3d us images. *Pattern Recogn. Lett.*, 24(4-5):801–813, 2003.

[24] X. Pennec, A. Roche, P. Cathier, and N. Ayache. Non-rigid mr/us registration for tracking brain deformations. In R.S. Blum and Zh. Liu, editors, *Multi-Sensor Image Fusion and Its Application.* Marcel Dekker Inc, 2005.

[25] Terry Peters, Bruce Davey, Patrice Munger, Roch Comeau, Alan Evans, and André Olivier. Three-dimensional multimodal image-guidance for neurosurgery. *Medical Imaging, IEEE Transactions on*, 15(2):121–128, 1996.

[26] William H. Press. *Numerical Recipes in C - The Art of Scientific Computing.* Cambridge University Press, Cambridge, second edition, 1992.

[27] D.W. Roberts, A. Hartov, F.E. Kennedy, M.I. Miga, and K.D. Paulsen. Intraoperative brain shift and deformation: A quantitative analysis of cortical displacement in 28 cases. *Neurosurgery*, 43:749–760, 1998.

[28] A. Roche, G. Malandain, X. Pennec, and N. Ayache. Multimodal image registration by maximization of the correlation ratio. Rapport de recherche 3378, INRIA, Sophia Antipolis, France, 1998.

[29] A. Roche, X. Pennec, G. Malandain, and N. Ayache. Rigid registration of 3-d ultrasound with mr images: A new approach combining intensity and gradient information. *Medical Imaging, IEEE Transactions on*, 20(10):1038–1049, 2001.

[30] A. Roche, X. Pennec, G. Malandain, N. Ayache, and S. Ourselin. Generalized correlation ratio for rigid registration of 3d ultrasound with mr images. Rapport de recherche 3980, INRIA, Sophia Antipolis, France, 2000.

[31] O.M. Skrinjar and J.S. Dunca. Real time 3d brain shift compensation. In A. Kuba, M. Samal, and A. Todd-Pokropek, editors, *Information Processing in Medical Imaging: 16th International Conference, IPMI'99, Visegrad, Hungary, June/July 1999. Proceedings*, volume 1613 of *Lecture Notes in Computer Science*, pages 42–55. Springer, 1999.

[32] C. Studholme, D.L.G. Hill, and D.J. Hawkes. Automated 3-d registration of mr and ct images of the head. *Medical Image Analysis*, 1(2):163–175, 1996.

[33] J. West, J.M. Fitzpatrick, M.Y. Wang, B.M. Dawant, C.R. Jr Maurer, R.M. Kessler, R.J. Maciunas, C. Barillot, D. Lemoine, A. Collignon, F. Maes, Suetens. P., D. Vandermeulen, P. van den Elsen, S. Napel, T.S. Sumanaweera, B. Harkness, P.F. Hemler, D.L.G. Hill, D.J. Hawkes, C. Studholme, J.B.A. Maintz, M.A. Viergever, G. Malandain, X. Pennec, M.E. Noz, G.Q. Jr Maguire, M. Pollack, C.A. Pelizzari, R.A. Robb, D. Hanson, and R.P. Woods. Comparison and evaluation of retrospective intermodality brain image registration techniques. *Journal of Computer Assisted Tomography*, 21(4):554–568, 1997.

[34] C.R. Wirtz, F.K. Albert, M. Schwaderer, C. Heuer, A. Staubert, V.M. Tronnier, M. Knauth, and S. Kunze. The benefit of neuronavigation for neurosurgery analyzed by its impact on glioblastoma surgery. *Neurological Research*, 22:354–360, 2000.

Part VIII

Appendix

A File names and descriptive names

This appendix describes the relationship between file names and descriptive names, for the image volumes used for testing the applications described in this report.

Descriptive name	File name
fMRI-Finger w/contrast	20041006T160127.mha
fMRI-Sentence w/contrast	20041006T160309.mha
fMRI-Tongue w/contrast	20041006T160445.mha
MRI-T2	20041006T160749.mha
MRI-T1	20041006T161007.mha
MRA (Angio)	20041006T161259.mha
MRI-T1 w/contrast	20041006T161642.mha
UST (Tissue)	20041007T110127.mha
USA (Angio) #1	20041007T110555.mha
USA #2	20041007T110944.mha

Table 17: **Tumor 1 - Corresponding descriptions and file names**

Descriptive name	File name
MRI-T1	20060220T082000.mha
MRI-T2	20060220T082119.mha
MRA	20060220T082249.mha
fMRI-Sentence w/contrast	20060220T083027.mha
fMRI-Tongue w/contrast	20060220T083255.mha
USA (Angio)	20060220T104218.mha

Table 18: **Tumor 3 - Corresponding descriptions and file names**

Descriptive name	File name
MRI-T1	20050126T091032.mha
MRA (Angio)	20050126T091242.mha
USA (Angio)	20050126T105634.mha

Table 19: **Aneurism 1 - Corresponding descriptions and file names**

B Additional Views of Results

As stated earlier in the report, renderings of additional views has been acquired. Here follows a presentation of them, from registration #1 to registration #7. Tables of parameters and resulting translation is found in part V.

B.1 Registration #1 - View 2

Figures 35 through 37 show 3D renderings of view 2 for registration #1. The parameters for this registration is presented in table 2. The resulting translation-parameters, along with the metric value and number of iterations used, is presented in table 3. Both tables are found in chapter 12.1.

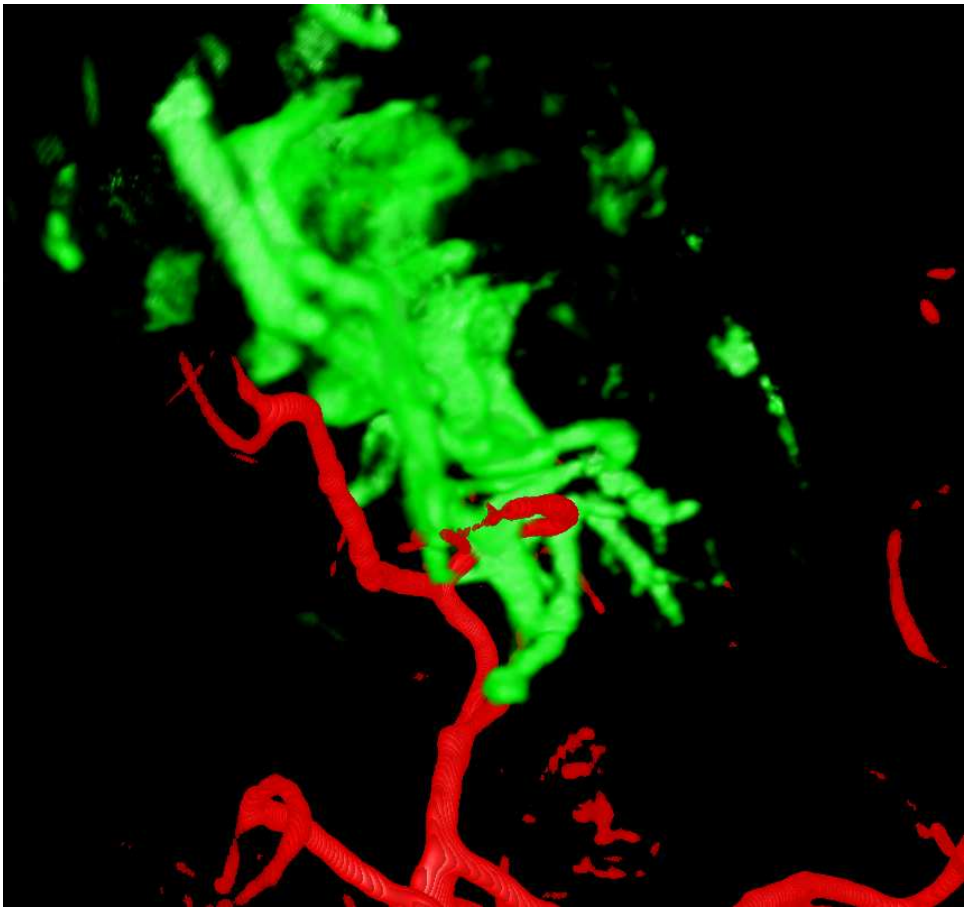

Figure 35: **Registration #1 - View 2 before registration - MRA (*red*) and USA #1 (*green*)**

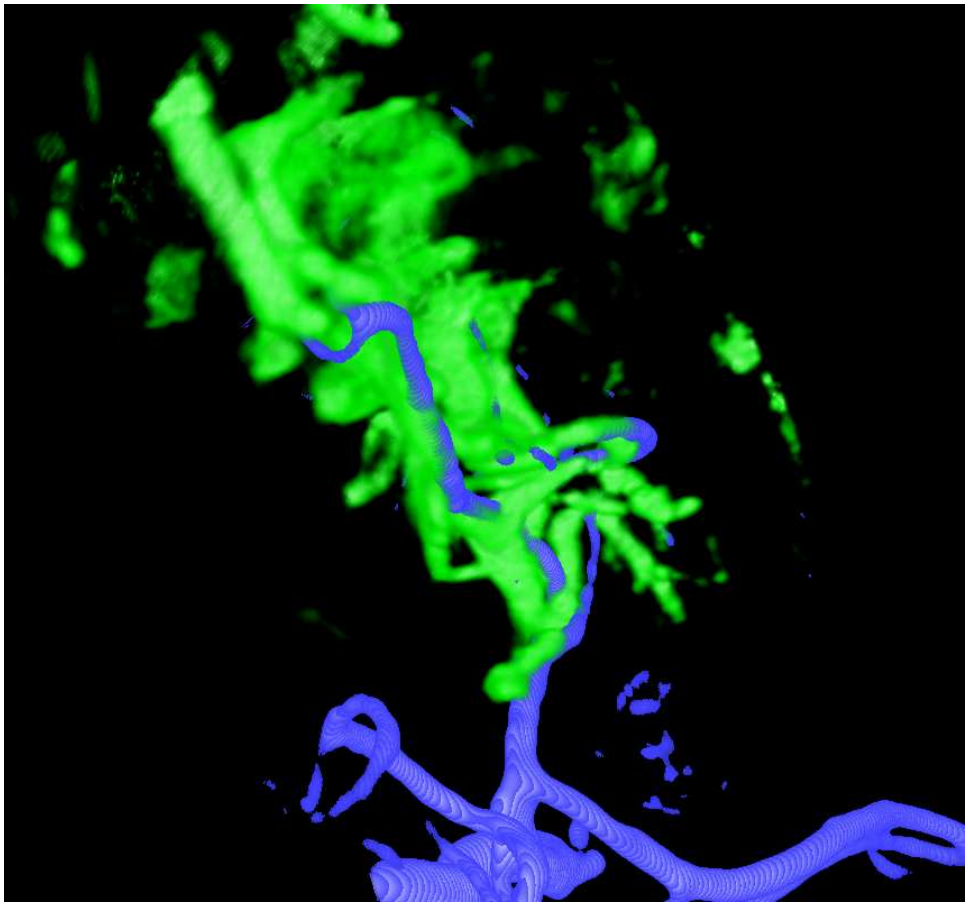

Figure 36: **Registration #1 - View 2 after registration - MRA (*blue*) and USA #1 (*green*)**

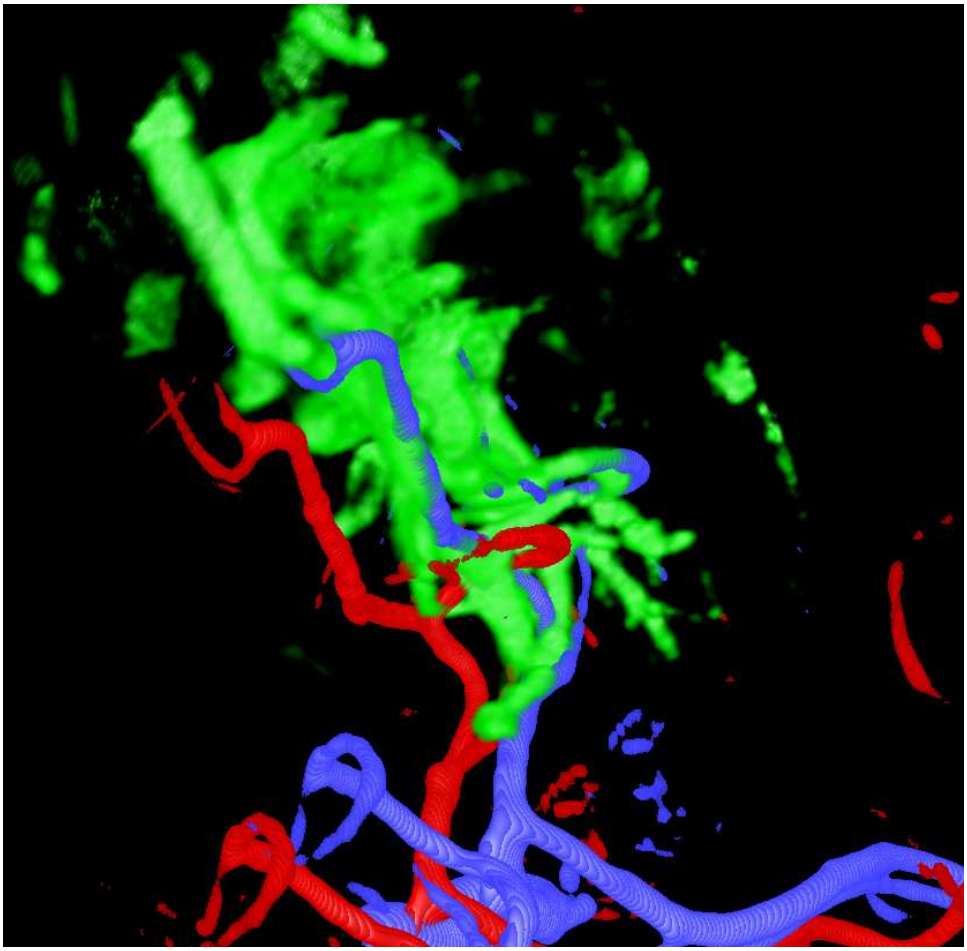

Figure 37: **Registration #1 - View 2 combined - MRA before (*red*), MRA after (*blue*) and USA #1 (*green*)**

B.2 Registration #2 - View 2

Figures 38 through 40 show 3D renderings of view 2 for registration #2. The parameters for this registration is presented in table 4. The resulting translation-parameters, along with the metric value and number of iterations used, is presented in table 5. Both tables are found in chapter 12.2.

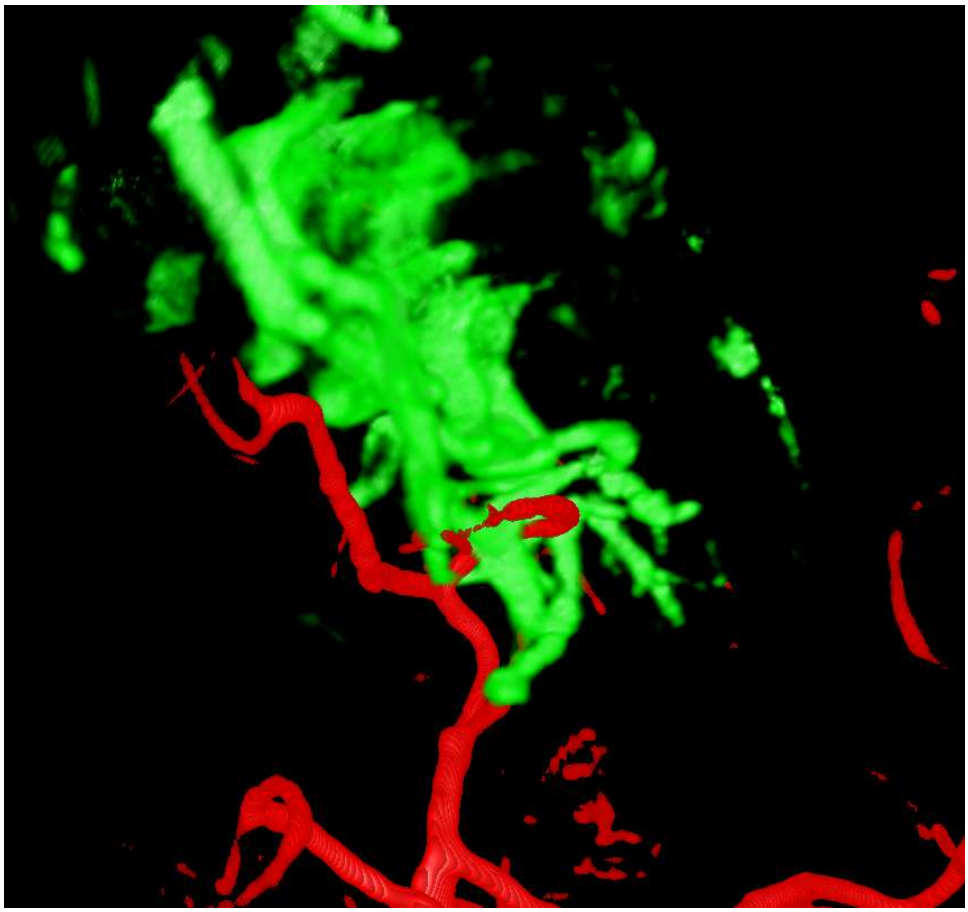

Figure 38: **Registration #2 - View 2 before registration - MRA (*red*) and USA #1 (*green*)**

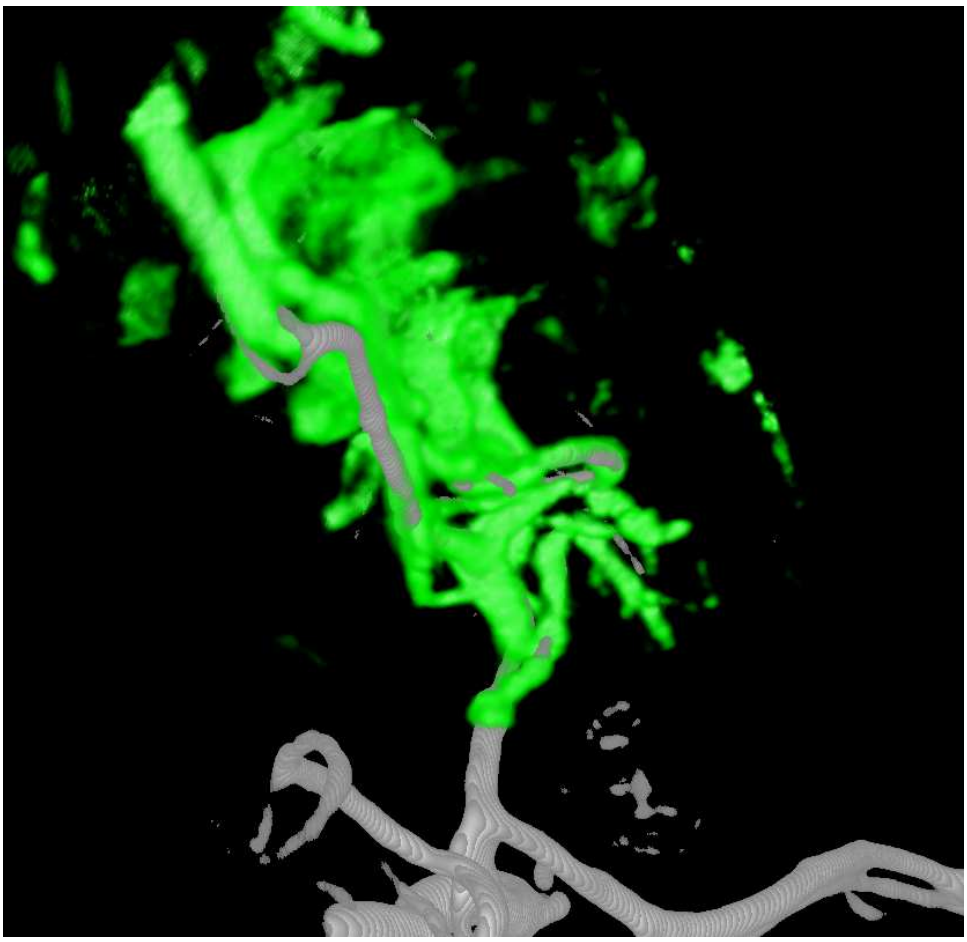

Figure 39: **Registration #2 - View 2 after registration - MRA (*grey*) and USA #1 (*green*)**

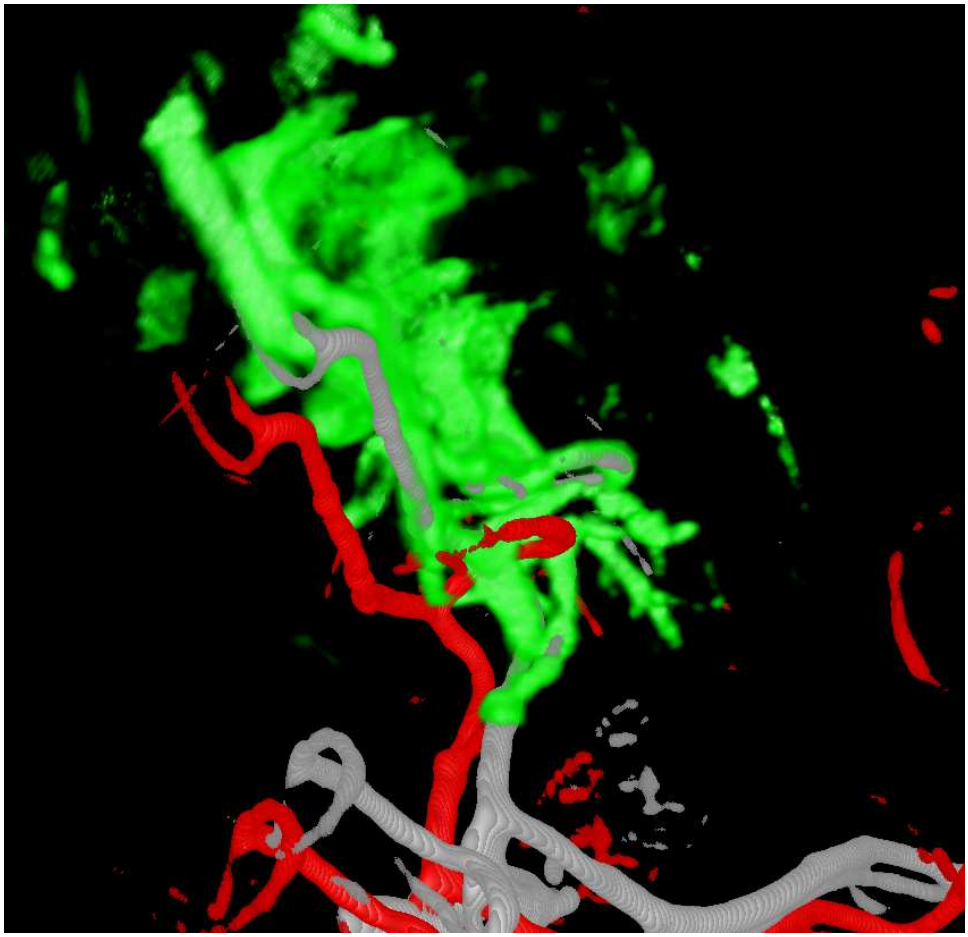

Figure 40: **Registration #2 - View 2 combined - MRA before (*red*), MRA after (*grey*) and USA #1 (*green*)**

B.3 Registration #3 - View 2

Figures 41 through 43 show 3D renderings of view 2 for registration #3. The parameters for this registration is presented in table 6. The resulting translation-parameters, along with the metric value and number of iterations used, is presented in table 7. Both tables are found in chapter 13.1.

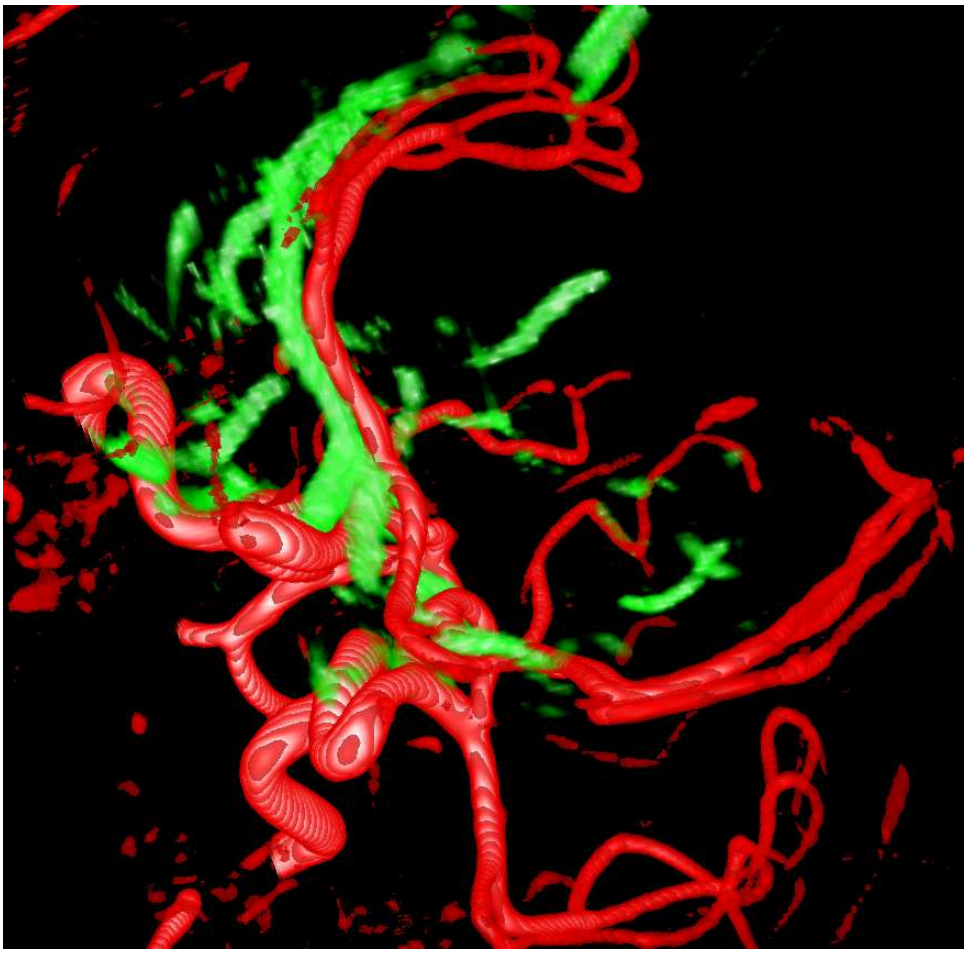

Figure 41: **Registration #3 - View 2 before registration - MRA (*red*) and USA (*green*)**

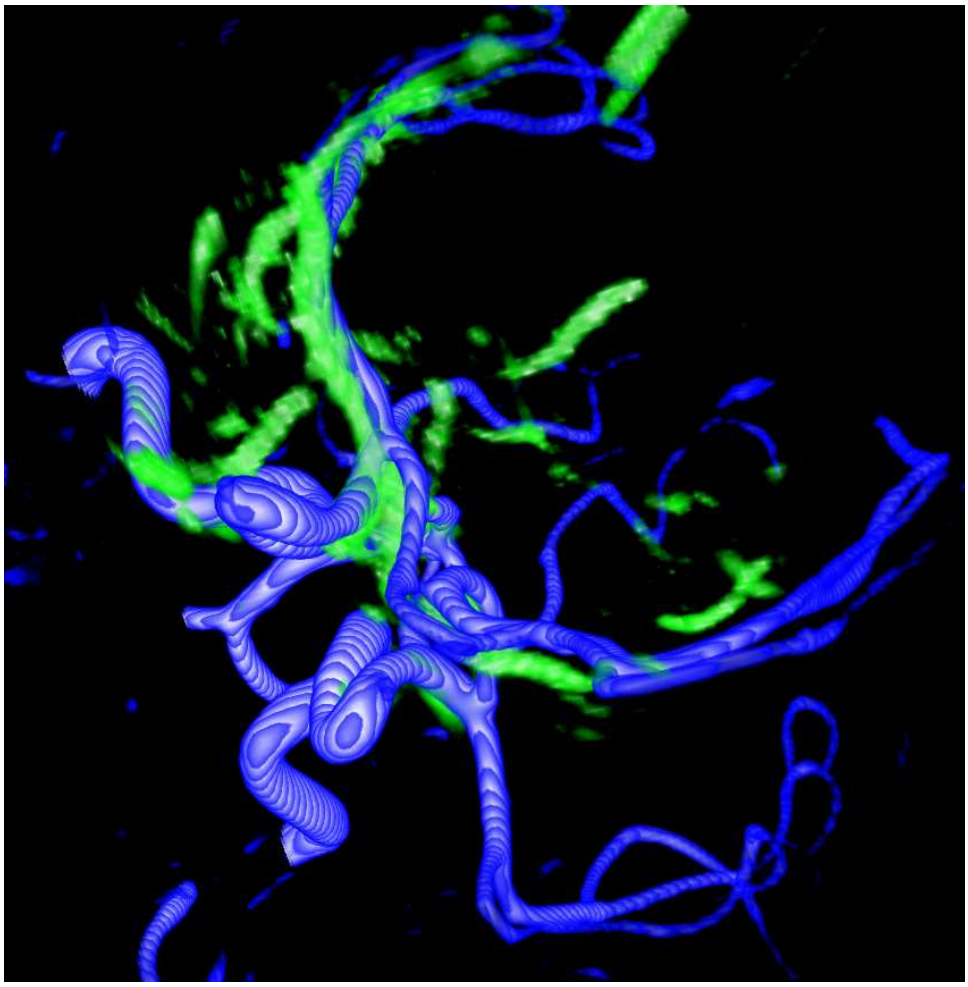

Figure 42: **Registration #3 - View 2 after registration - MRA (*blue*) and USA (*green*)**

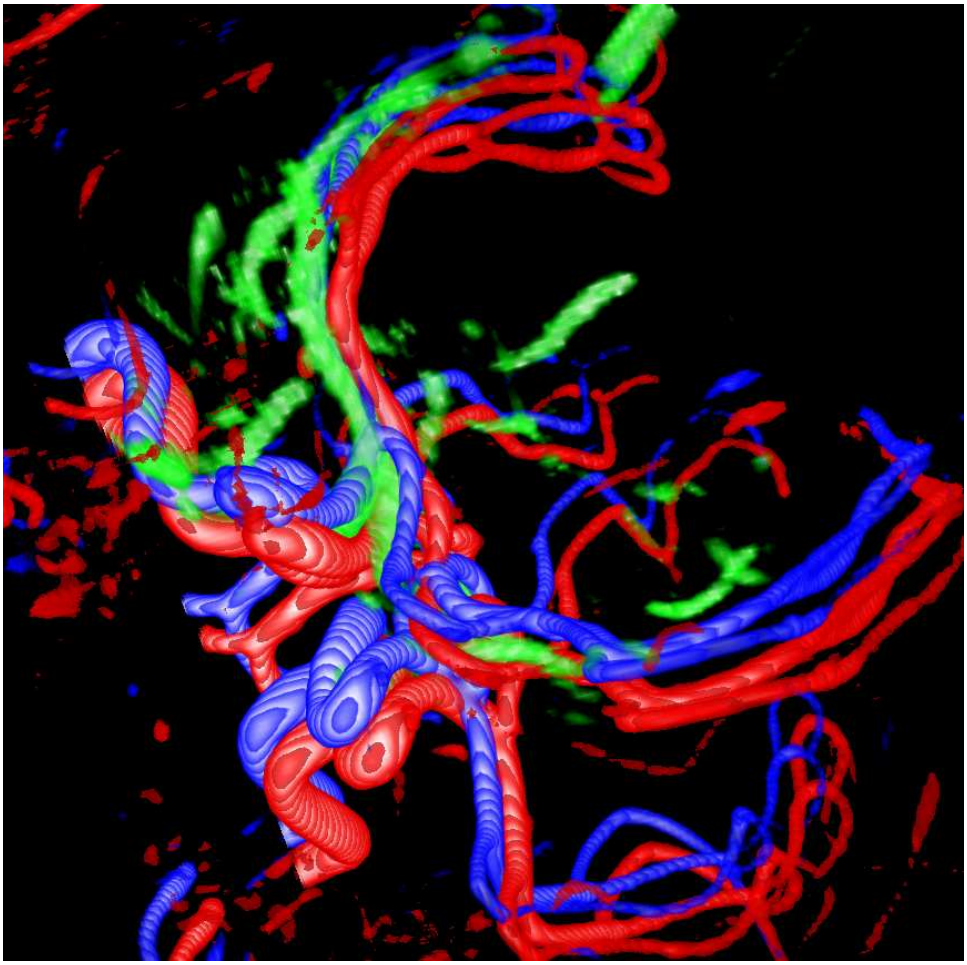

Figure 43: **Registration #3 - View 2 combined - MRA before (*red*), MRA after (*blue*) and USA (*green*)**

B.4 Registration #4 - View 2

Figures 44 through 46 show 3D renderings of view 2 for registration #4. The parameters for this registration is presented in table 8. The resulting translation-parameters, along with the metric value and number of iterations used, is presented in table 9. Both tables are found in chapter 13.2.

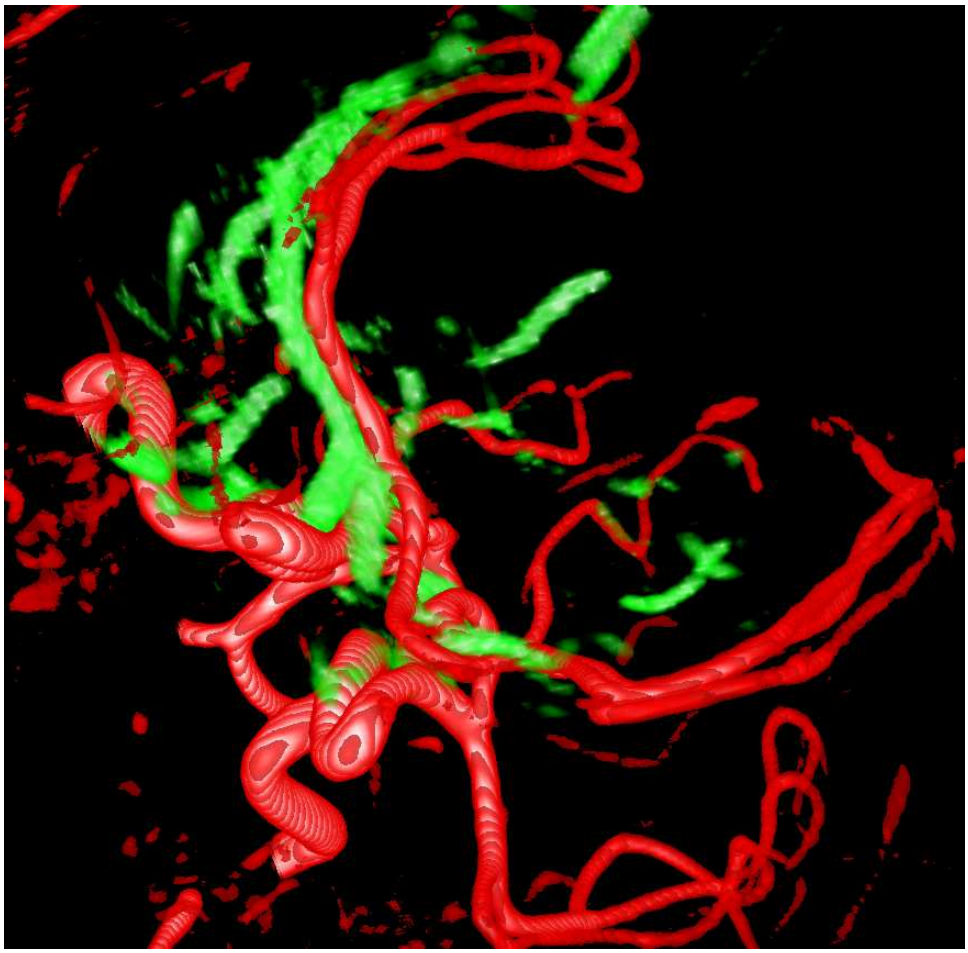

Figure 44: **Registration #4 - View 2 before registration - MRA (*red*) and USA (*green*)**

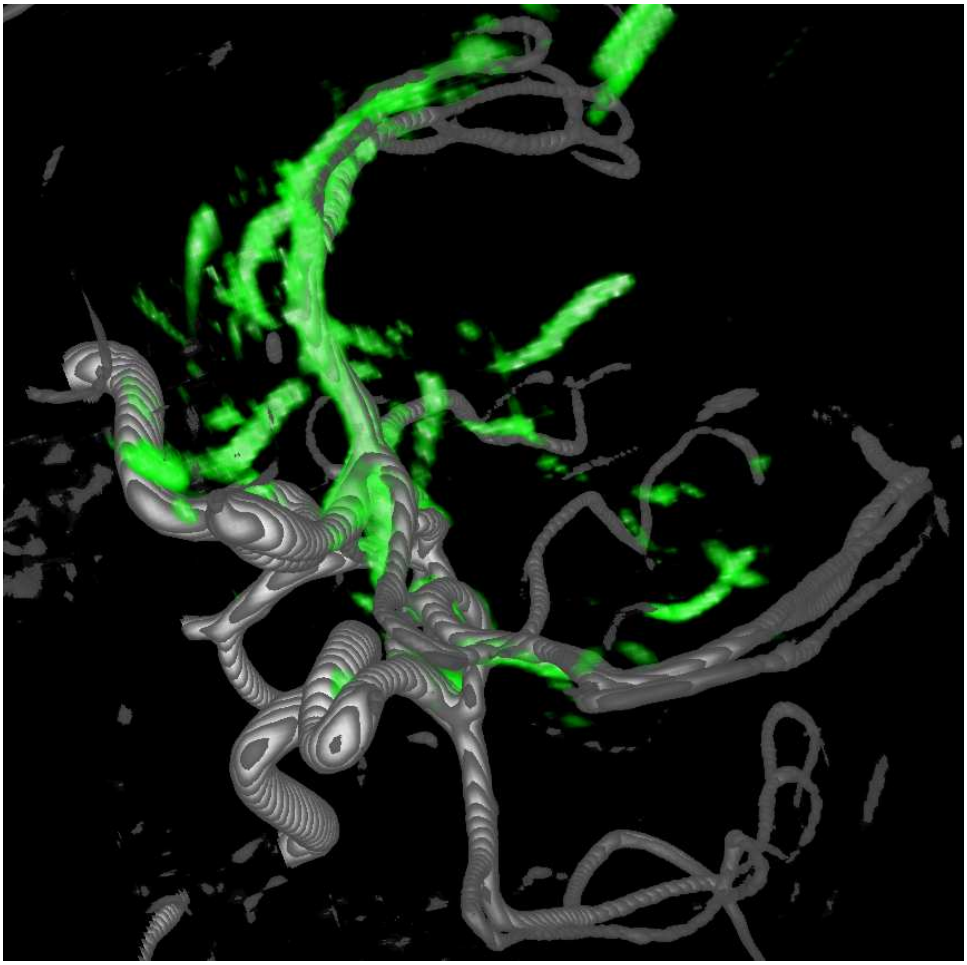

Figure 45: **Registration #4 - View 2 after registration - MRA (*grey*) and USA (*green*)**

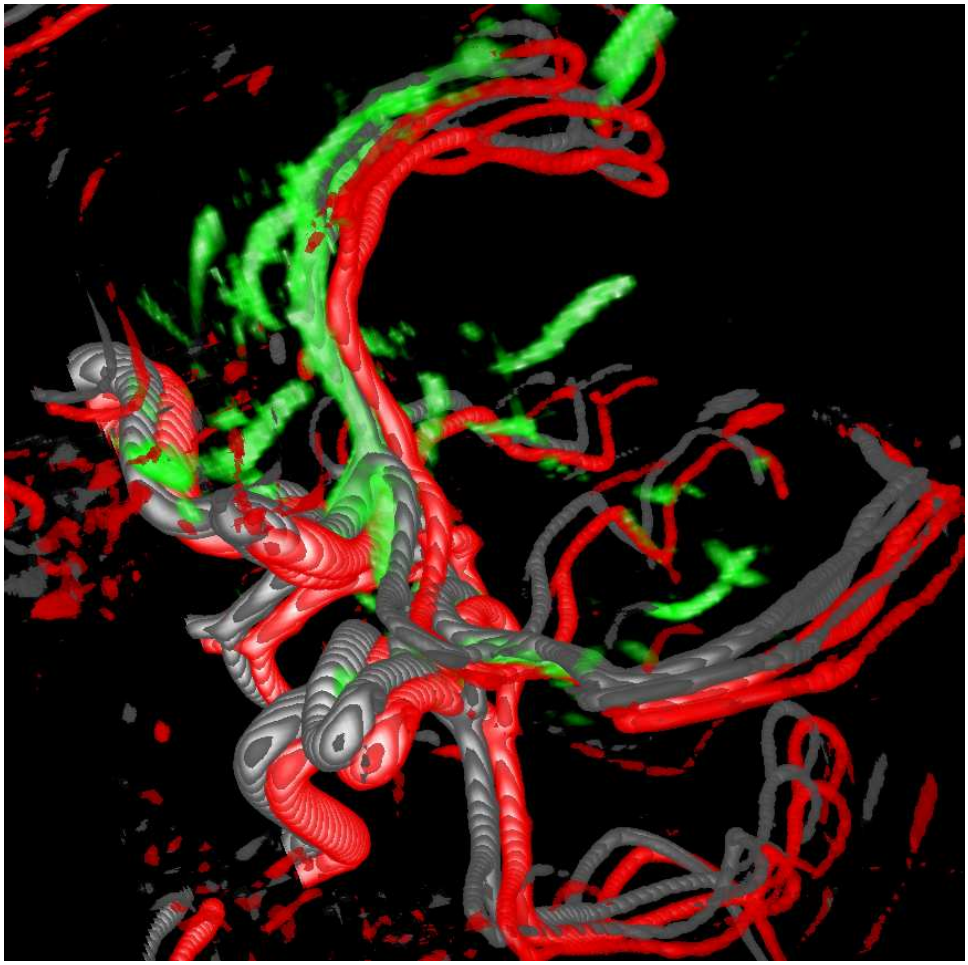

Figure 46: **Registration #4 - View 2 combined - MRA before (*red*), MRA after (*grey*) and USA (*green*)**

B.5 Registration #5 - View 2

Figures 47 through 49 show 3D renderings of view 2 for registration #5. The parameters for this registration is presented in table 10. The resulting translation-parameters, along with the metric value and number of iterations used, is presented in table 11. Both tables are found in chapter 14.1.

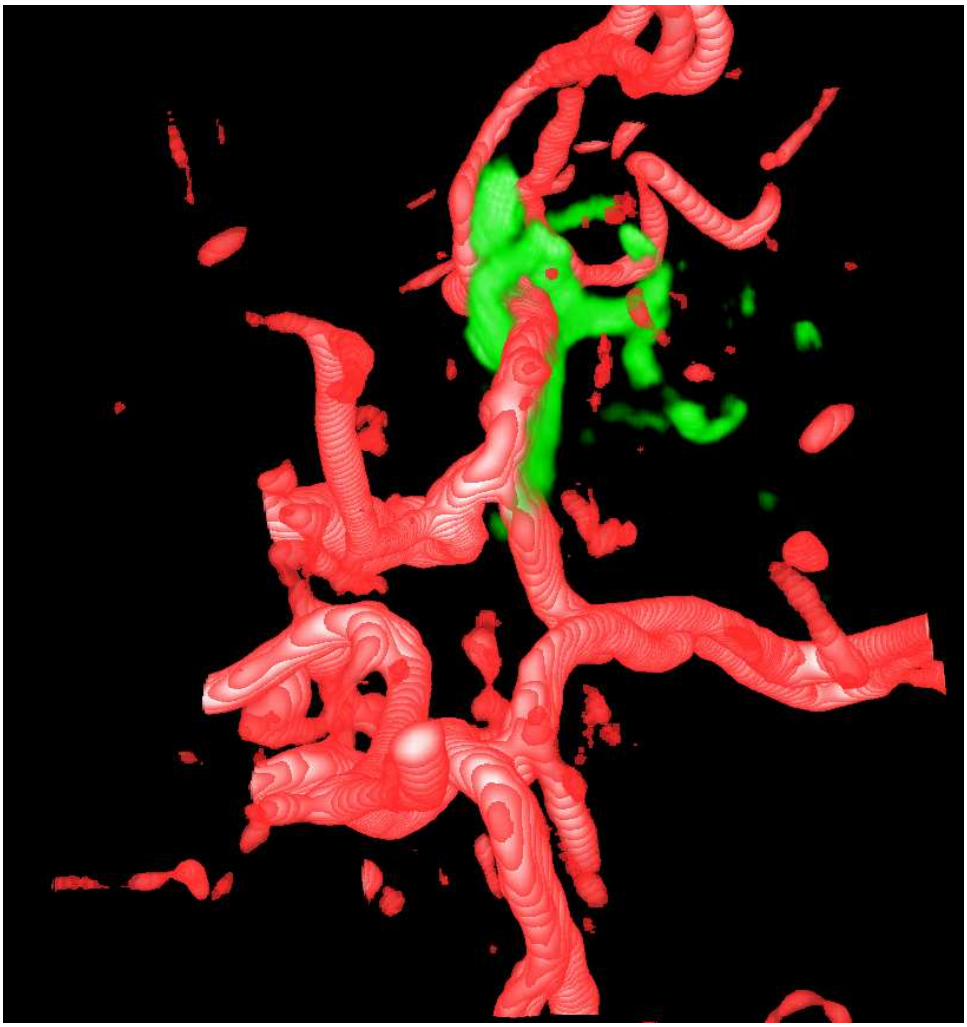

Figure 47: **Registration #5 - View 2 before registration - MRA (*red*) and USA (*green*)**

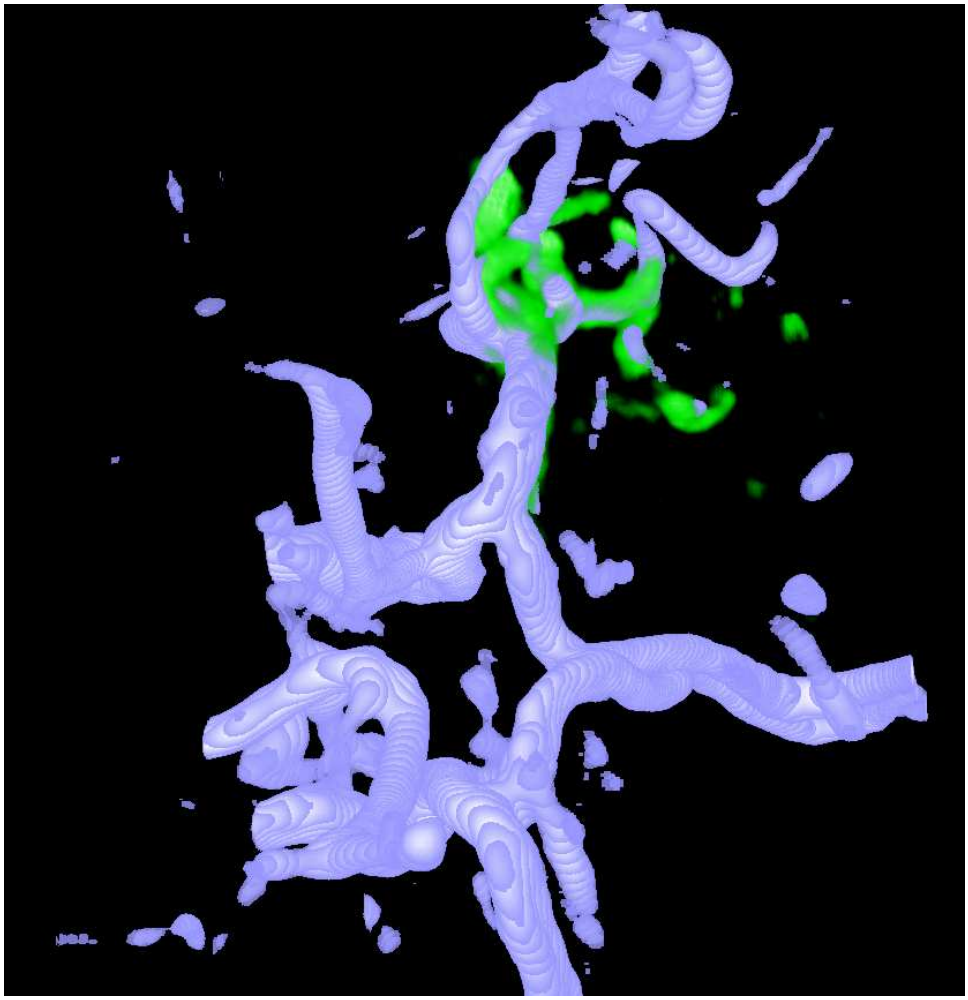

Figure 48: **Registration #5 - View 2 after registration - MRA (*blue*) and USA (*green*)**

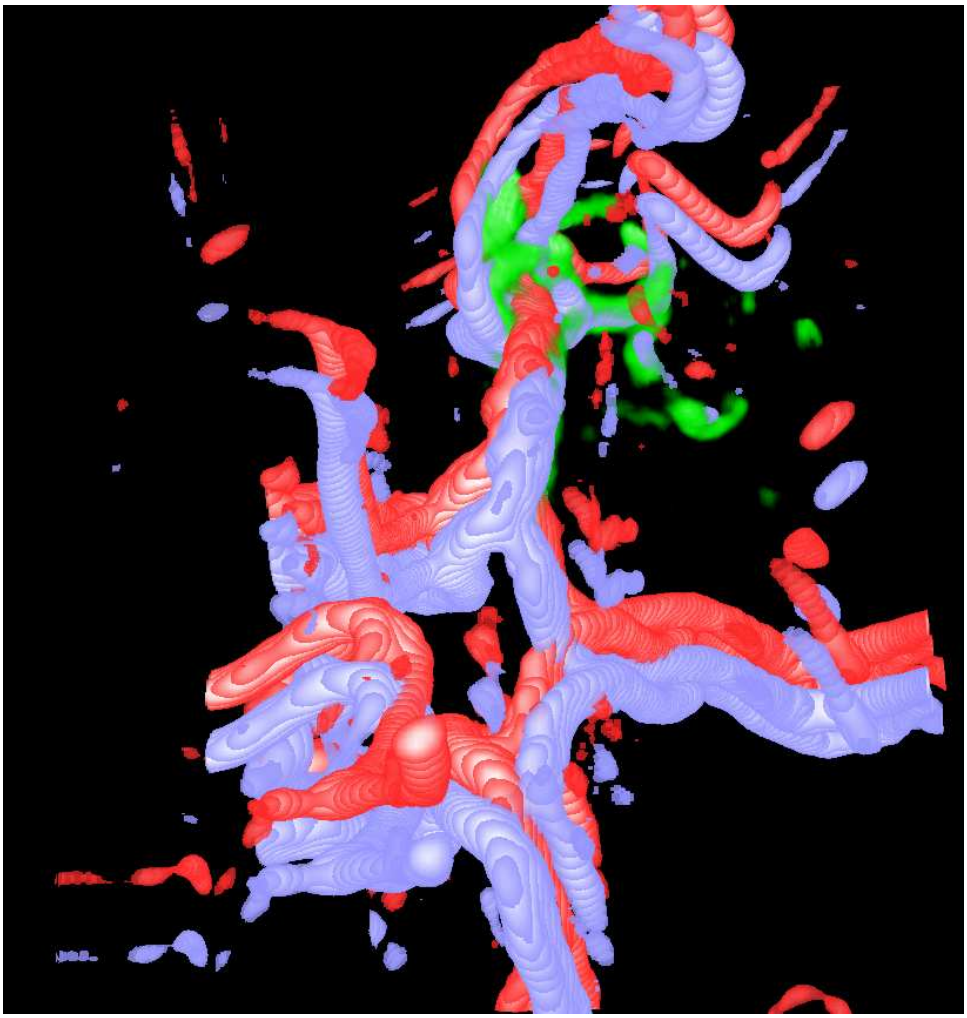

Figure 49: **Registration #5 - View 2 combined - MRA before (*red*), MRA after (*blue*) and USA (*green*)**

B.6 Registration #6 - View 2

Figures 50 through 52 show 3D renderings of view 2 for registration #6. The parameters for this registration is presented in table 12. The resulting translation-parameters, along with the metric value and number of iterations used, is presented in table 13. Both tables are found in chapter 14.2.

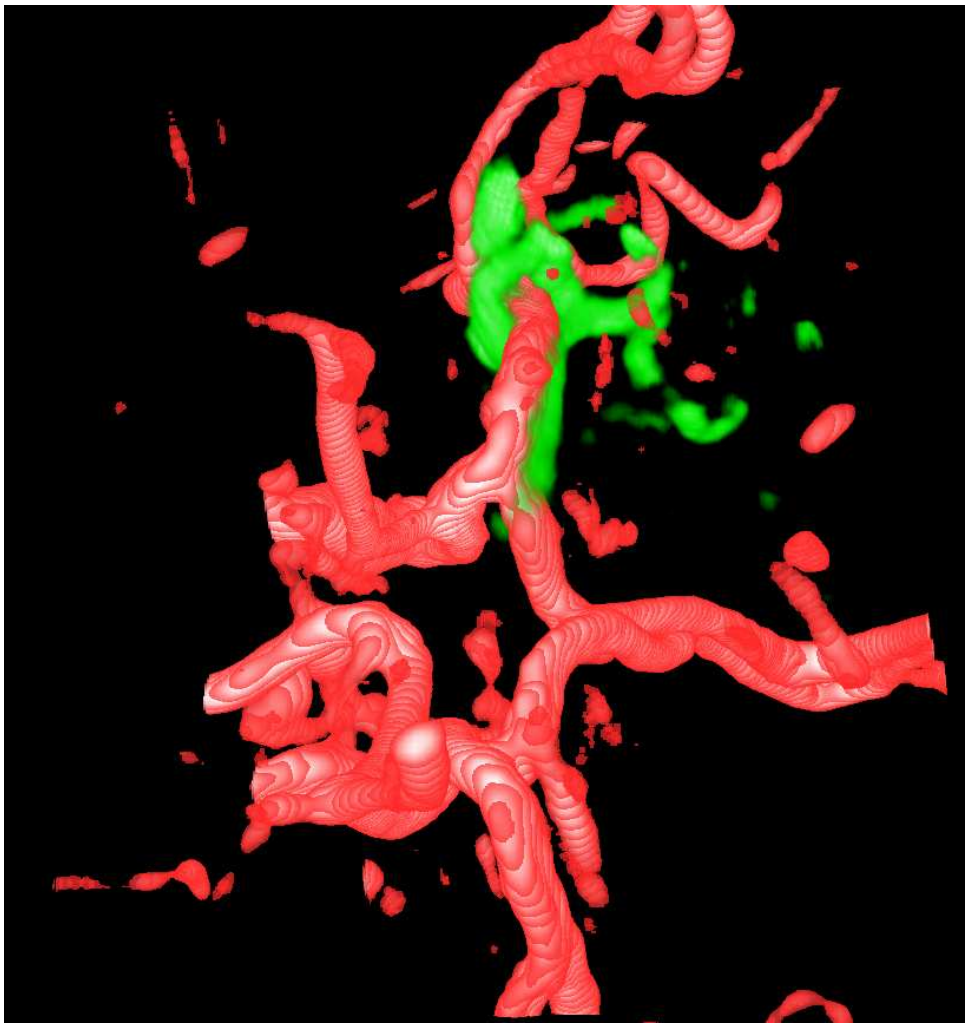

Figure 50: **Registration #6 - View 2 before registration - MRA (*red*) and USA (*green*)**

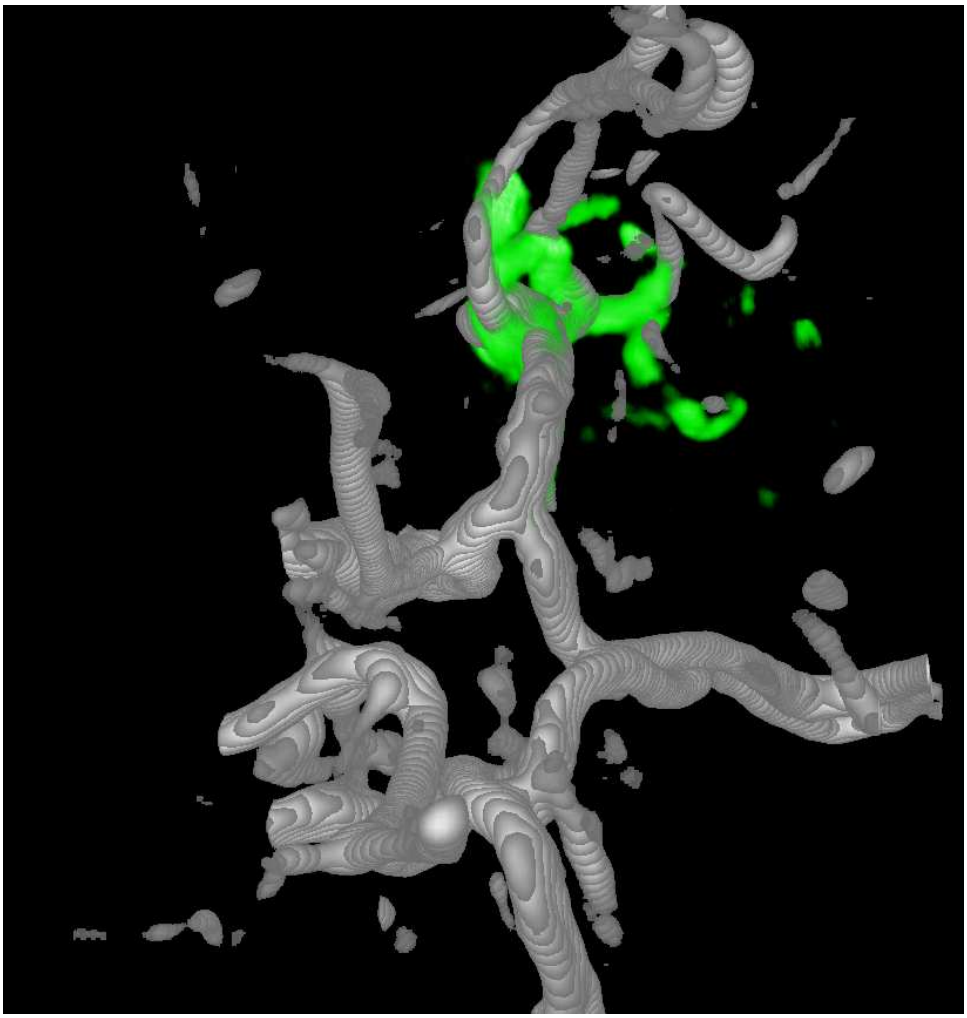

Figure 51: **Registration #6 - View 2 after registration - MRA (*grey*) and USA (*green*)**

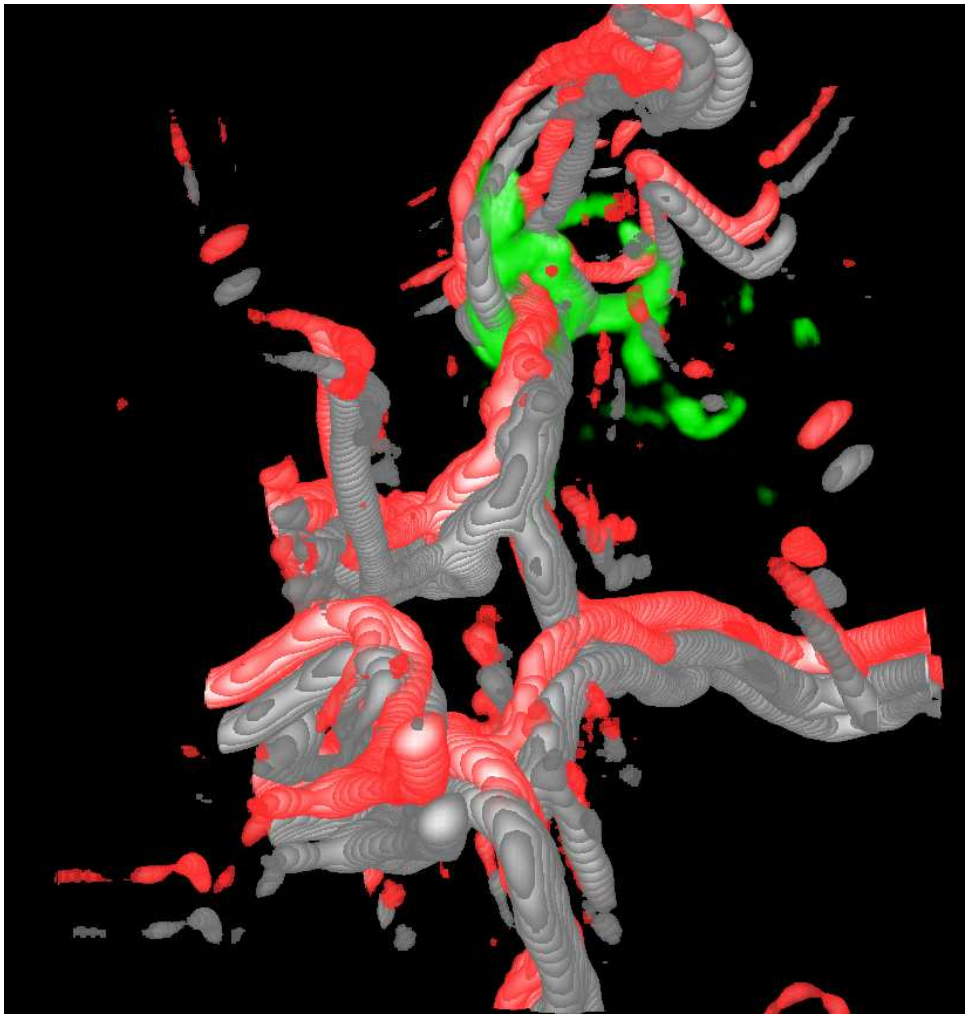

Figure 52: **Registration #6 - View 2 combined - MRA before (*red*), MRA after (*grey*) and USA (*green*)**

B.7 Registration #7 - View 2

Figures 53 through 55 show 3D renderings of view 2 for registration #7. The parameters for this registration is presented in table 14. The resulting translation-parameters, along with the metric value and number of iterations used, is presented in table 15. Both tables are found in chapter 14.3.

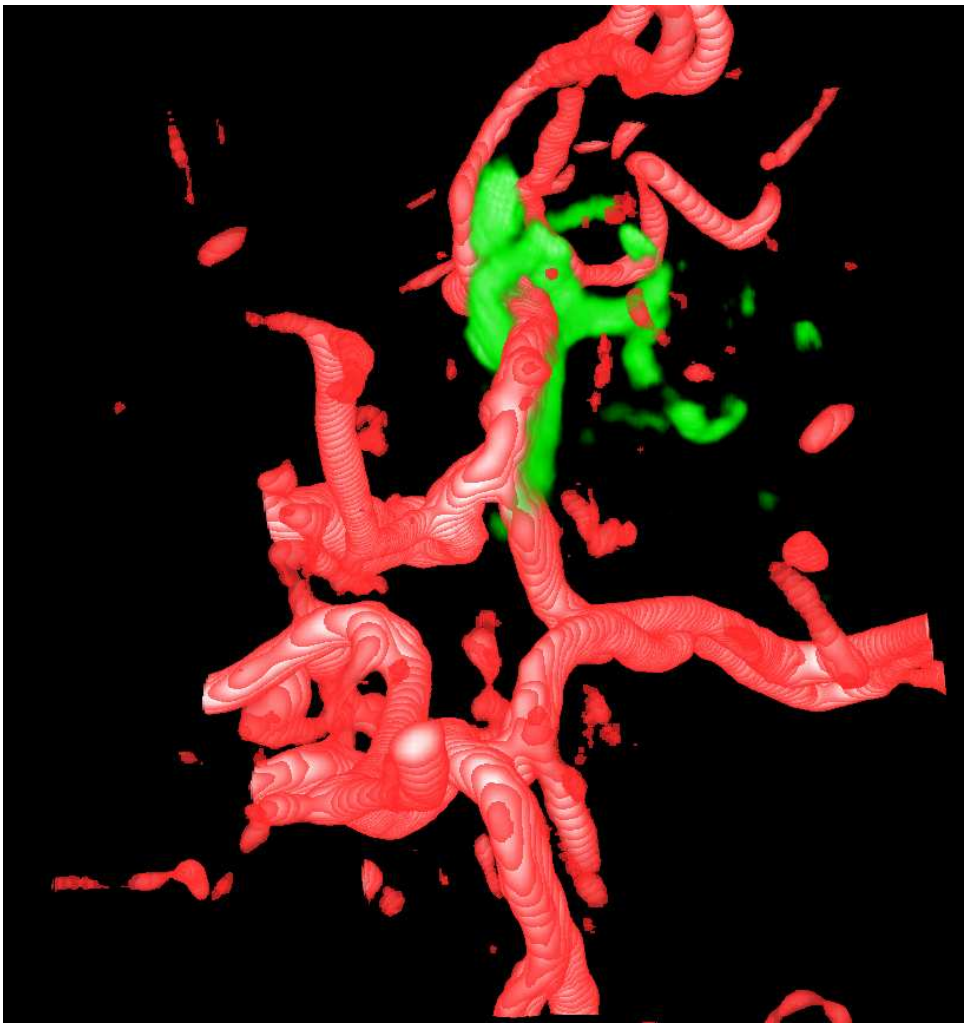

Figure 53: **Registration #7 - View 2 before registration - MRA (*red*) and USA (*green*)**

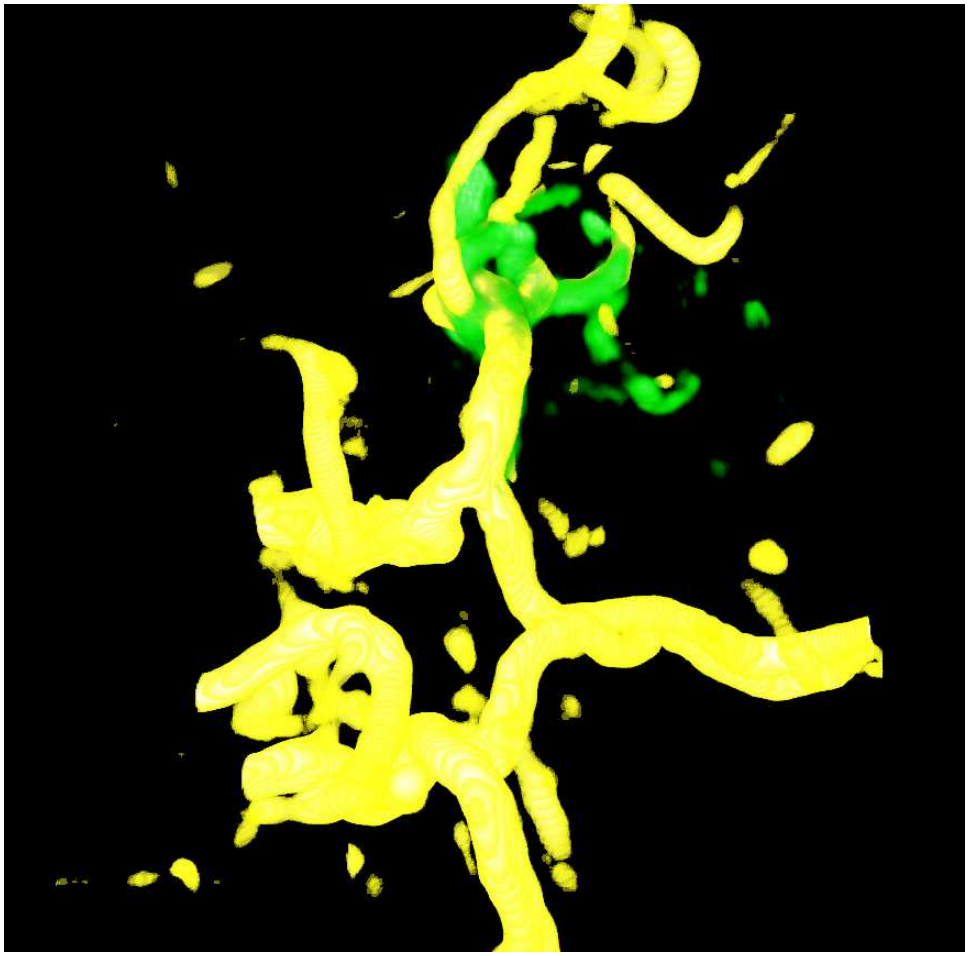

Figure 54: **Registration #7 - View 2 after registration - MRA (*yellow*) and USA (*green*)**

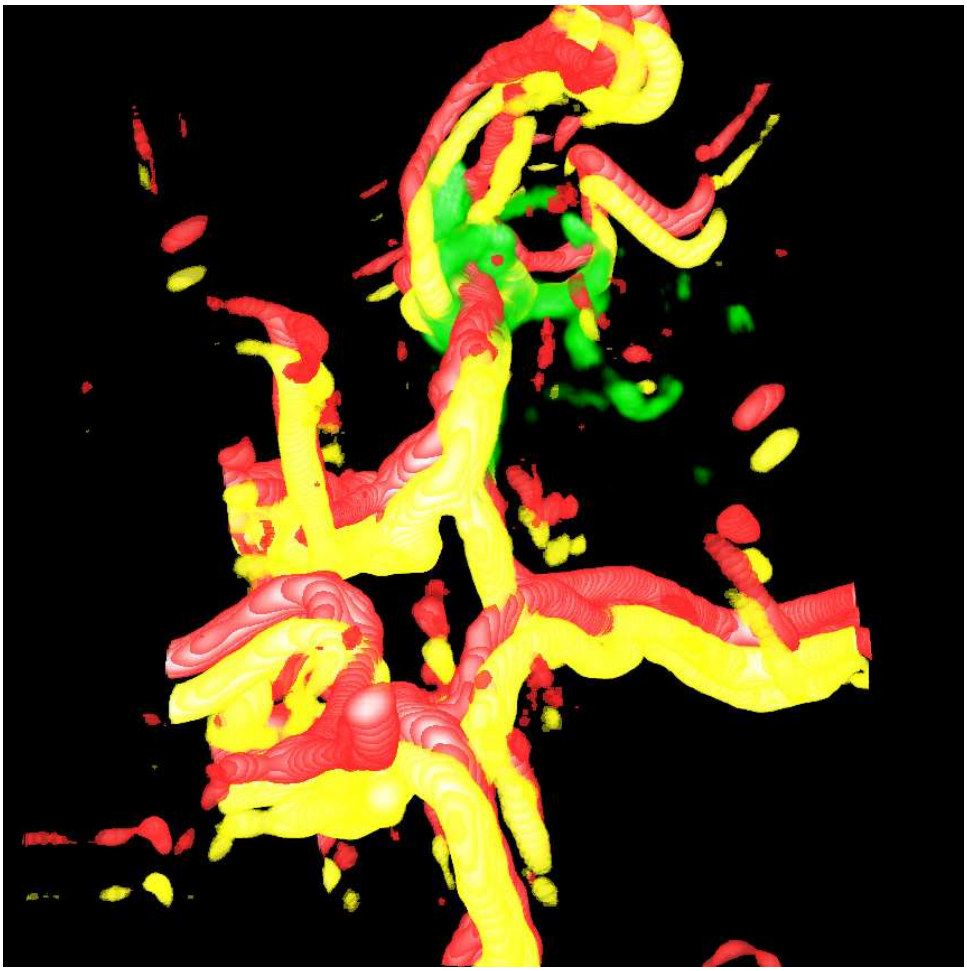

Figure 55: **Registration #7 - View 2 combined - MRA before (*red*), MRA after (*yellow*) and USA (*green*)**

C Questionnaire

This appendix presents the questionnaire used to evaluate the registration results.

Volume-to-Volume registration

evaluation of results
for
Tommy Ryen

A presentation of volumes from three data sets will be performed; including preoperative MRI and intraoperative 3D ultrasound. Automatic programs for volume-to-volume registration have been run on these volumes, to register MRI- and US angio volumes, from the same patient.

You are kindly requested to answer the following question for each registered volume pair:
"Is the registered volume sufficiently adapted to the reference volume, to be used for clinical purposes?"

- reference volume refers to the volume that remains unchanged
- registered volume refers to the volume that is changed by registration.
- clinical purposes primarily refers to planning of, and navigation during, neurosurgery

You will find the answer form in the next page. Other comments may be added at the last page.

Figure 56: **Questionnaire - Page 1**

Profession:

First, please indicate your profession:

Clinician/Surgeon	Tech/Researcher	Student

Tumor 1:

	Not sufficient	Possibly sufficient	Sufficient
RegApp4:			
RegApp5:			

Tumor 3:

	Not sufficient	Possibly sufficient	Sufficient
RegApp4:			
RegApp5:			

Aneurism 1:

	Not sufficient	Possibly sufficient	Sufficient
RegApp4:			
RegApp5:			
RegApp6:			

Figure 57: **Questionnaire - Page 2**

Comments:

Figure 58: **Questionnaire - Page 3**

D Calculations on Consistency

This appendix presents calculations of standard deviations for continuous registrations, of registration #4 and registration #5, in figures 59 60, respectively.

	x-translation	y-translation	z-translation	Mattes' MI	distance
1	-3,95432	-0,200657	1,97271	-0,0315268	4,423629125
2	-3,94792	0,38535	2,76638	-0,033505	4,83605472
3	-2,97596	-0,113013	2,38756	-0,0315892	3,817008333
4	-3,58575	0,685303	0,933706	-0,0304752	3,768162703
5	-2,6491	1,01111	1,77471	-0,0317742	3,345096385
6	-3,66894	1,03926	3,30143	-0,0296416	5,043869756
7	-3,39749	-0,849825	3,32557	-0,0311321	4,829550357
8	-3,22711	-0,257877	2,13569	-0,0310733	3,878390294
9	-4,31729	1,03756	1,90863	-0,0289403	4,833052056
10	-3,74937	0,507881	1,74091	-0,0318742	4,1649113
11	-2,30845	-0,499875	3,14201	-0,0302123	3,930781507
12	-2,10214	0,538951	2,64409	-0,0305536	3,420624605
13	-2,20054	0,405359	2,61878	-0,0303231	3,444517513
14	-3,60385	0,409877	2,54498	-0,0316951	4,430875441
15	-3,23794	0,430787	2,3834	-0,0310727	4,043566303
16	-3,90137	-0,42942	2,45916	-0,032441	4,631690547
17	-3,27591	-0,571321	2,81141	-0,0338742	4,354540183
18	-3,24785	1,0455	2,6352	-0,030455	4,311134295
19	-3,19931	0,451792	1,53422	-0,0334438	3,576804649
20	-3,40752	0,673927	2,502	-0,0308965	4,28081466
mean	-3,2979065	0,28503345	2,3761273	-0,03132496	4,168253737
st,dev	0,605048621	0,589034855	0,603886861	0,001275704	0,515968233

Figure 59: **Standard deviations for Registration #4**

	x-translation	y-translation	z-translation	Mattes' MI	distance
1	3,64268	-2,51212	-1,94685	-0,0233139	4,834262033
2	4,43089	-1,94509	-1,53798	-0,0263171	5,077552932
3	4,00885	-1,48236	-2,56297	-0,0260356	4,983681843
4	4,72829	-2,1436	-2,21164	-0,0242926	5,642968968
5	4,83465	-3,0976	-2,83056	-0,0225236	6,40164325
6	4,90783	-1,24682	-2,552	-0,0214519	5,670454957
7	2,92201	-1,66697	-2,30297	-0,0254321	4,076837284
8	3,88214	-3,2231	-2,3012	-0,0218526	5,545710597
9	3,66902	-1,96558	-1,37951	-0,0244805	4,385004029
10	2,91983	-1,57998	-2,56511	-0,0245914	4,195418137
11	5,02851	-2,1901	-2,32548	-0,0226921	5,957374259
12	4,69234	-1,57489	-2,6441	-0,0252694	5,61155932
13	5,04712	-2,90195	-1,82748	-0,0240285	6,102001085
14	4,0757	-2,58838	-2,6436	-0,0235879	5,504512919
15	4,56243	-2,22182	-1,32922	-0,0240784	5,245862887
16	5,20655	-1,30506	-1,14805	-0,0247773	5,489022072
17	4,32302	-1,53161	-2,28945	-0,0251803	5,126003552
18	4,31851	-1,99739	-1,21231	-0,0251792	4,910070363
19	3,93584	-1,259	-1,78995	-0,0240817	4,503314169
20	3,91476	-1,71871	-2,52315	-0,0253102	4,964433084
mean	4,2525485	-2,0076065	-2,096179	-0,024223815	5,211384387
st,dev	0,655739817	0,601117166	0,534937476	0,00132967	0,627200715

Figure 60: **Standard deviations for Registration #4**